DERAILMENT RISK ASSESSMENT

Simon Wagner

Master of Engineering

James Goldston Faculty of Engineering and Physical Systems
Central Queensland University

2004

ABSTRACT

There is a large quantity of literature available on longitudinal train dynamics and risk assessment but nothing that combines these two topics. This thesis is focused at assessing derailment risks developed due to longitudinal train dynamics. A key focus of this thesis is to identify strategies that can be field implemented to correctly manage these risks. This thesis quantifies derailment risk and allows a datum for comparison. A derailment risk assessment on longitudinal train dynamics was studied for a 107 vehicle train consist travelling along the Monto and North Coast Lines in Queensland, Australia. The train consisted of 103 wagons and 4 locomotives with locomotives positioned in groups of two in lead and mid train positions. The wagons were empty hopper wagons on a track gauge of 1067mm. The scenarios studied include: the effect of longitudinal impacts on wagon dynamics in transition curves; and the effects of longitudinal steady forces on wagon dynamics on curves. Simulation software packages VAMPIRE and CRE-LTS were used.

The effects of longitudinal impacts from in-train forces on wagon dynamics in curves were studied using longitudinal train simulation and detailed wagon dynamics simulation. In-train force impacts were produced using a train control action. The resulting worst-case in-train forces resulting from these simulations were applied to the coupler pin of the wagon dynamics simulation model. The wagon model was used to study the effect of these in-train forces when applied in curves and transitions at an angle to the wagon longitudinal axis. The effects of different levels of coupler impact forces resulting from different levels of coupling slack were also studied. Maximum values for wheel unloading and L/V ratio for various curve radii and coupler slack conditions were identified. The results demonstrated that the derailment criteria for wheel unloading could be exceeded for a coupler slack of 50mm and 75mm on sharper curves, up to 400m radii.

A detailed study of the effect of steady in-train forces on wagon dynamics on curves also was completed. Steady in-train forces were applied to a three wagon model using VAMPIRE. Maximum and minimum values of wheel unloading and L/V ratio were identified to demonstrate the level of vehicle stability for each scenario. The results allowed the worse cases of wheel unloading and L/V ratio to be studied in detail.

Probability density functions were constructed for the occurrence of longitudinal forces and coupler angles for the Monto and North Coast Lines. Data was simulated for a coupler slack of 25, 50 and 75mm and force characteristics were further classified into the occurrences of impact and non-impact forces. These probability density functions were analysed for each track section to investigate the effects of coupler slack, track topography and gradient on wagon dynamics. The possible wagon instability in each of these scenarios was then assessed to give a measure of the potential consequences of the event. Risk assessment techniques were used to categorise levels of risk based on the consequences and likelihood of each event. It was found that for the train configuration simulated, the Monto Line has a higher derailment risk than the North Coast Line for many of the scenarios studies in this thesis. For a coupler slack of 25mm no derailment risks were identified, 50mm coupler slack derailment risks were only identified on the Monto track and the majority of derailment risks were identified for a 75mm coupler slack.

DERAILMENT RISK ASSESSMENT

by

Simon Wagner

BEng Mech

A thesis submitted in partial fulfilment of the requirements for the award of the degree of Master of Engineering

Centre for Railway Engineering

James Goldston Faculty of Engineering and Physical Systems

Central Queensland University

Australia

June 2004

TABLE OF CONTENTS

TABLE OF FIGURES

TABLE OF TABLES

ACKNOWLEDGEMENTS

I would like to sincerely thank my supervisor Colin Cole. Without his commonsense, knowledge and cracking-of-the-whip I would not have been able to complete this thesis. He has always given time generously to discuss ideas, difficulties and provide invaluable advice.

I would also like to extend my gratitude to the director of the CRE, Manicka Dhanasekar for the support that he has given me. The Centre for Railway Engineering (CRE) has been very supportive throughout the time that I have spent working on this thesis. The CRE has provided both financial and personal support. I would like to thank all my friends at CQU for making my time at the university such an enjoyable experience.

I am very lucky to have such supportive and kind hearted friends and family. I am deeply indebted to my parents for their continual support in whatever I do. Without help from all these people I would not have completed this thesis.

STATEMENT OF ORIGINALITY

To the best of my knowledge, this thesis is my own work and has not been published by any other source. Parts of this thesis have been published in papers which have been listed in the publications section.

Simon Wagner

PUBLICATIONS LIST

Wagner, S. and Cole, C. 2003, "Modelling Train-Wagon Interaction on Curves", *Proceedings of the 18th International Association of Vehicle System Dynamics Symposium,* Kanagawa Institute of Technology, Atsugi, Kanagawa, Japan.

Wagner, S. and Cole, C. 2003, "Rollingstock Wheel Unloading Due to Coupler Impacts on Curve Transitions", *Central Region Engineering Conference,* (ed.) Wolfs, P, Central Queensland University, Rockhampton, Australia.

NOMENCLATURE

Notation	Definition
Dn	Step size (m)
H1 and H2	Overhang of wagon 1 and 2 (m)
H3	Coupler length (m)
n	Step
P1, P2, P3 and P4	Position 1,2,3,4 respectively
r	Radius (m)
r_n	Radius for step n (m)
1/r	Curvature (1/m)
X	X axis length (m)
X1 and X2	The X axis height due to coupler angle 1 and 2 respectively
Xn	The total X axis sum for step n (m), (Figure 3-12, p49)
Xn’	The X axis length for step n due to curvature (m), (Figure 3-12, p49)
Xn’’	The X axis length for step n due to error (m), (Figure 3-12, p49)
Y	Y axis length, (m)
Y1 and Y2	The Y axis height due to coupler angle 1 and 2 respectively
Yn	The total Y axis sum for step n (m), (Figure 3-12, p49)
Yn’	The Y axis length for step n due to previous

	angle (m), (Figure 3-12, p49)
Yn''	The Y axis length for step n due to curvature (m), (Figure 3-12, p49)
Yn'''	The Y axis tangent length due to curvature for step n (m), (Figure 3-12, p49)
°	Angle (degrees)
μ	Coefficient of friction
θ1 and θ2	The angle between the overhang and line between both bogie centre pins
θc'	The angle created due to the difference in height of Y1 and Y2
θc1, θc2	Coupler Angle 1 and 2 respectively (degrees)
θn = θn'	Angle at the instant n (degrees), (Figure 3-12, p49)
θn''	Angle between Yn''' and Xn axis (degrees), (Figure 3-12, p49)
θ1'	Angle between the tangent at P2 and the line between P2 and P1 (degrees), Figure 3-15 on page 53.
θ2'	Angle between the tangent at P3 and the line between P3 and P4 (degrees), Figure 3-15 on page 53.
θ1"	Angle between the tangent at P2 and the line between P2 and P3 (degrees), Figure

	3-15 on page 53.
θ2”	Angle between the tangent at P3 and the line between P3 and P2 (degrees), Figure 3-15 on page 53.

GLOSSARY

Term	Definition
AAR	Association of American Railways
Bogie	The primary chassis of a railway vehicle that holds the wheelsets
CABS	Coupler Angling Behaviour Software, developed by the AAR
CRE	Centre for Railway Engineering
CRE-LTS	Centre for Railway Engineering Longitudinal Train Simulator
Degrees Curvature	The angle for a arc of 100ft or 30.3m
DOF	Degrees of Freedom
Kilometridge	The track position based on the survey pegs that are placed along the track
L/V Ratio	Lateral/Vertical ratio of the wheelset
NUCARS	New and Untried Car Analytic Regime Simulation, a wagon dynamic simulator developed by the AAR.
pdf	Adobe Acrobat file format
Run-ins	Run-ins are developed due to the slack between couplers. It usually refers to impact forces that are developed during the transition from tensile to compressive forces
Run-outs	Run-ins are developed due to the slack between couplers. It usually refers to impact forces that are developed during the transition from compressive to tensile forces
Slack	The clearance between coupler knuckles once they are joined
Slack Action	Slack action refers to a series of impacts that are developed due to compressive to tensile forces and visa versa.

SRM	Safety Risk Model
WinBatch	Scripting user input utility software
WU	Wheel Unloading
UltraEdit	Text editor software
VAMPIRE	AEA Rail Technology Vehicle Simulator

1 INTRODUCTION

This project was initiated to gain a better understanding of derailment risks developed due to longitudinal train dynamics. It is known that larger trains generate larger in-train forces and that these forces can cause an increase in derailment risks due to jack-knifing/string lining of wagons; and due to bogie and wagon pitch. Analysing in-train wagon behaviour due to longitudinal train dynamics requires a large number of simulations. Continuous user involvement is required to perform these simulations as train and wagon simulation packages are usually separate.

To assess the derailment risks associated with longitudinal train dynamics a number of simulation cases are required that take in the expected train control scenarios, train configuration, inter-wagon connections, track grades and track curvature. The relevance of this research is supported by the need for railway companies to improve methods of assessing risk as operations tend toward increased train length and wagon capacity. Increasing train length and wagon capacity increases in-train forces and hence train-wagon interaction dynamics.

The aim of this thesis is to do fundamental research on quantifying derailment risks, increasing knowledge on derailment modes involving the interaction of train and wagon dynamics and offer some insight into ways these risks should be managed. By quantifying derailment risk it allows a datum for comparison. Different levels of risk can be compared, while high and low levels of risk can be identified. The levels of risk are quantified by levels of wheel unloading, L/V ratio, consequences and the

probability of events occurring. This thesis investigates how parameters such as coupler slack, track gradient and track curvature affect derailment risks.

1.1. Outline of the Thesis

This thesis is arranged as follows:

Chapter 1 presents a brief introduction to the thesis and provides a brief overview of each subsequent chapter.

Chapter 2 presents a review of literature on derailment, derailment criteria, vehicle dynamics and risk assessment.

Chapter 3 discusses a range of software packages and methods which were used in this thesis. This chapter discusses the tools and methods that were necessary to complete this thesis.

Chapter 4 shows how the VAMPIRE wagon model was validated. It discusses the hunting test, wheel unloading due to steady forces test and bogie pitch test.

Chapter 5 investigates the effects of steady longitudinal forces on wagon dynamics on curves and curve transitions. Different force magnitudes and curve radii were analysed.

Chapter 6 shows the effects of longitudinal impact forces on curve transitions. Particular attention was paid to determining the worse case scenarios for different curve radii and longitudinal impact force magnitudes.

Chapter 7 demonstrates how probability density functions can be used to give a graphical representation of probability densities. Two different track sections were studied to show how probability density functions can be used to compare levels of derailment risk.

Chapter 8 shows the levels of risk for the simulations performed in chapter 7. It demonstrates how risk assessment techniques can be used to identify high risk scenarios and potential derailment events. Chapter 5 and 6 are used in the risk assessment process to determine levels of wheel unloading and L/V ratio in a given scenario.

Chapter 9 concludes this thesis.

2 LITERATURE REVIEW

2.1. Introduction

This literature review is focused on existing literature on derailment, derailment criteria, train and vehicle dynamics and risk assessment. A large range of factors can cause derailment these factors are outlined in Section 2.2. To simplify the analysis of derailment, various derailment criteria have been defined. These include L/V ratio, wheel unloading and flange climb. These criteria are presented in Section 2.3.

The dynamic behaviour of vehicles and trains is an area of study when considering derailments. There are a large number of papers and texts published such as (Duncan and Webb, 1989; El-Sibaie, 1993; Elkins and Wu, 1999; Elkins and Wu, 2000a; 2000b; Garg and Dukkipati, 1984; Hay, 1982; McClanachan *et al*, 2000; Wagner and Cole, 2003a; 2003b) that further improve the understanding of the behaviour of train and vehicle dynamics. Another area of study is the interactive dynamic behaviour between vehicles within a train (longitudinal train dynamics) due to in-train forces. A review of train and vehicle dynamics is included in Section 2.4.

An important issue is the problem of connecting risk assessment techniques with the whole spectrum of factors that can cause derailment. Risk assessment can be used to categorise levels of risk by combining the consequences and likelihood of the event. A brief review of risk assessment is covered in Section 2.5.

2.2. Derailment

Derailment is a large issue that affects railway companies. Table 2-1 shows the number of derailment within each state of Australia published by (ATSB, 2003).

Table 2-1: Running Line Derailments, (ATSB, 2003)

		NSW	NT	Qld	SA	Tas	Vic	WA	Australia
2001	**Jan-Jun**	34	0	21	17	17	39	9	137
	Jul-Dec	29	0	17	12	16	41	10	125
2002	**Jan-Jun**	47	0	21	18	12	43	18	159

Derailments can be extremely costly to a railway company. Costs of derailment accidents can range from very low (i.e., shunting or minor yard incident) to tens of millions of dollars per accident (i.e., multiple wagon derailment at running speed). Derailment of passenger trains can also cause loss of human life and injury which can lead to further costs. There can also be damage to surrounding infrastructure, vehicles and property.

Some of the main contributing factors and indicators of derailment are:

1. Poor maintenance, component failure or poor design, (Wolf, 1998)
2. Poor loading, moving loads (cattle, liquids, etc.) and poor securing of loads
3. Human factors
4. Derailment criteria
    a. Wheel unloading, (Garg and Dukkipati, 1984)
    b. Lateral/Vertical force ratio, (Elkins and Wu, 1999)
    c. Flange climb, (Elkins and Wu, 1999)
5. Train-wagon dynamics
    a. Steady state forces, (Duncan and Webb, 1989)

   b. Forces due to longitudinal vibration, (Duncan and Webb, 1989)
   c. Impacts, (Duncan and Webb, 1989)
      i. Bogie pitch, (McClanachan *et al*, 2000)
      ii. Wagon pitch, (McClanachan *et al*, 2000)
      iii. Vertical and lateral jack knifing, (El-Sibaie, 1993)
6. Wagon-track dynamics
   a. Wagon bounce, (McClanachan *et al*, 2000)
   b. Roll and sway, (Garg and Dukkipati, 1984)
   c. Hunting, (Hay, 1982)
7. A combination of these factors

The scope of this thesis is restricted to the study of the interaction of train and vehicle dynamics, derailment indicators and risk management. Component failure, rollingstock and track maintenance therefore will not be included in this review.

2.3. Derailment Criteria

A large number of publications for derailment criteria were located, so only the more recent and important articles were reviewed in detail, (El-Sibaie, 1993; Elkins and Wu, 1999; Elkins and Wu, 2000a; 2000b; Guangxiong and Xincan, 2000; Guangxiong *et al*, 2000; McClanachan and Cole, 1997; McClanachan *et al*, 2000; McClanachan and Roach, 2000; Miyamoto, 1996; Miyamoto and Fujimoto, 1990; Nadal, 1960; Parena *et al*, 2000; Wu and Zeng, 1998). Derailment indicators such as L/V ratio, Nadal's Criteria, flange climb and wheel unloading are of particular

interest for this thesis, as they can be used to analyse derailment risk and the degree of vehicle instability.

2.3.1. Wheel Unloading

Wheel unloading is a common means of measuring vertical dynamic stability and the final point of wheel lift-off, (Cole, 1999; El-Sibaie, 1993; Guangxiong *et al*, 2000; Iwnicki, 2000; McClanachan and Cole, 1997; McClanachan *et al*, 2000; McClanachan and Roach, 2000; Miyamoto and Fujimoto, 1990; Takai *et al*, 2002). Wheel unloading refers to the amount of static load that has been removed from the rail and wheel interface due to vehicle dynamic behaviour as shown in Figure 2-1, (Elkins and Wu, 1999). When wheel unloading is at 100%, there is no downward force at the rail and when wheel unloading is at -100% there is double the static load at the rail. Wheel unloading can be produced from track geometry changes, coupler forces, irregularities in surface alignment and superelevation. These inputs result in wagon responses such as pitch, bounce, twist and roll. A wheel lift-off of 100 percent is commonly assumed as derailment, but vehicle acceptance does not accept wheel unloading beyond 90%, (AAR, 1993).

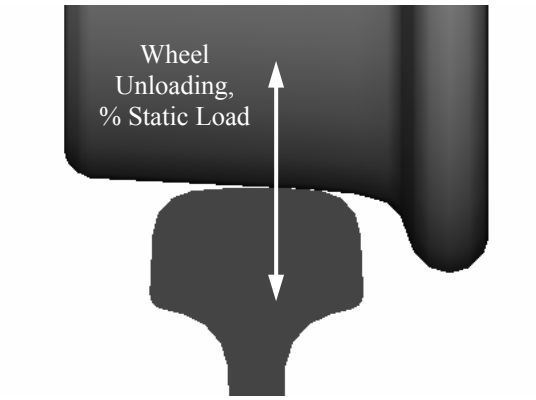

Figure 2-1: Wheel Unloading

2.3.2. Lateral/Vertical Force Ratio

The Lateral/Vertical force ratio (L/V ratio) is used extensively to monitor and predict derailment, (El-Sibaie, 1993; Elkins and Wu, 1999; Elkins and Wu, 2000a; 2000b; Guangxiong and Xincan, 2000; Guangxiong *et al*, 2000; Iwnicki, 2000; Miyamoto, 1996; Parena *et al*, 2000; Wu and Zeng, 1998). The L/V ratio is the lateral force at the rail divided by the vertical force. A paper which discusses the L/V ratio in detail is (Elkins and Wu, 1999). Figure 2-2 shows the direction of the lateral and vertical forces on a wheel set.

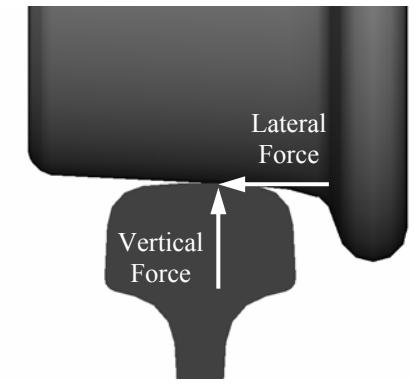

Figure 2-2: Lateral and Vertical Wheelset Forces

Many of these authors use the L/V ratio as their primary tool to analyse derailment. Nadal's Criteria gives a useful method of calculating the L/V ratio, requiring only flange angle and the coefficient of friction between the rail and the wheel, refer to Section 2.3.4 on page 12. It is quite difficult to measure the L/V ratio in the field, so special wheel sets and rail mounted measuring devices have been designed to measure the L/V ratio, (Iwnicki, 2000). Many of the commercial railway vehicle software packages such as VAMPIRE, NUCARS and GENSYS give the L/V ratio as an output, (Iwnicki, 2000). For situations where the friction between the rail and the wheelset is not taken into account, equation (2.1) should be used to give an approximation of limiting the L/V ratio, (Parena *et al*, 2000). In situations where frictional components are considered Nadal's Criteria should be used, as discussed in detail in Section 2.3.4 on Page 12.

$$\frac{LateralForce}{VerticalForce} = \tan\phi \qquad (2.1)$$

Where ϕ is the angle between the vertical side of the rail and the flange, (Parena *et al*, 2000).

Nadal's Criteria can calculate the L/V ratio for flange climb. Flange climb derailment is first introduced to ensure that a clear understanding of the topic is obtained. Nadal's Criteria is then discussed in detail in Section 2.3.4 on page 12.

2.3.3. Flange Climb

The L/V ratio is used when investigating flange climb or for analysing derailment, (Elkins and Wu, 1999; Elkins and Wu, 2000a; 2000b; Guangxiong and Xincan, 2000; Guangxiong *et al*, 2000; Miyamoto, 1996; Parena *et al*, 2000). These papers discuss the angle of attack, L/V ratio, distance to derailment, L/V ratio time duration, speed, longitudinal forces and the coefficient of friction between the rail and the wheel. Many of these papers present equations that can be used to analyse and predict derailment. A paper which discusses flange climb derailment in detail is (Parena *et al*, 2000). The paper published by (Parena *et al*, 2000) investigates the distance that the wheel takes to climb the rail and derail.

While flange climb is primarily the result of lateral and vertical wheel/rail contact forces, it is also influenced by the angle of attack of the wheel and the effects of the traction forces, (Elkins and Wu, 1999). When the L/V ratio is high, the rotating wheel can cause the flange to climb the rail. The flange climb L/V ratio and the L/V distance limit is largely dependant on the angle of attack, (Elkins and Wu, 1999). Flange climb derailment occurs when there is a reduced vertical force component, a large lateral force component and a high angle of attack. Adverse combinations of forces and angles are therefore generated while negotiating track geometry such as curves and turnouts. Further increases in L/V ratio can occur if track surface irregularities are also present.

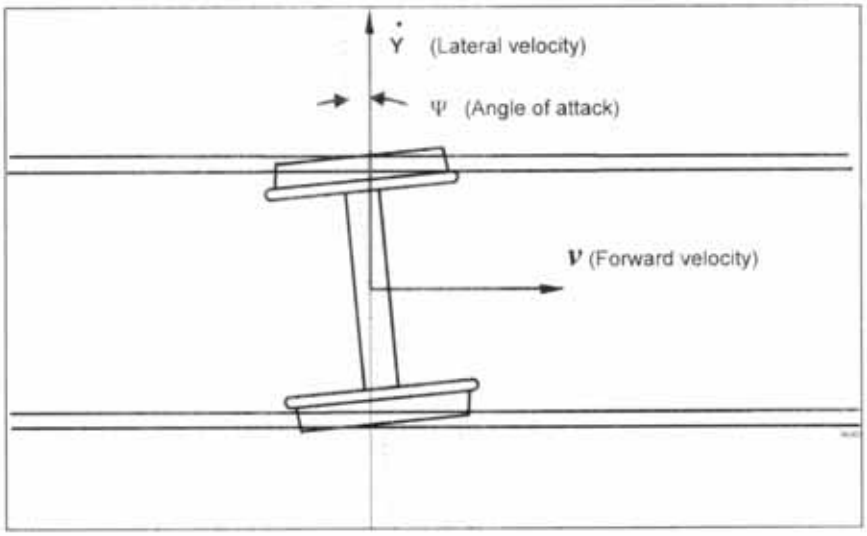

Figure 2-3: Flange Climb Angle of Attack, (Elkins and Wu, 1999)

The lateral velocity component of the sliding velocity at the wheel/rail contact of a wheelset is due to its rotational velocity and angle of attack, it is given by equation (2.2), (Elkins and Wu, 1999).

$$V_t = -\omega r \sin(\psi) \tag{2.2}$$

Where V_t is shown as Ẏ in Figure 2-3, ω is the angular velocity, r is the radius of the wheelset and ψ is the angle of attack of the wheelset.

A more general equation including lateral velocity due to wagon motion and angle of attack is given by equation (2.3), (Elkins and Wu, 1999).

$$V_y = \dot{y} - \omega r \psi \tag{2.3}$$

Where $\psi \cong \sin\psi$ for small angles of attack.

2.3.4. Nadal's Criteria

Nadal's Criteria is used to calculate the L/V ratio for flange climb by many papers, (Elkins and Wu, 1999; Elkins and Wu, 2000a; 2000b; Guangxiong and Xincan, 2000; Guangxiong *et al*, 2000; Parena *et al*, 2000). It is accepted as a way to calculate the L/V ratio for derailment. Many of the papers such as (Elkins and Wu, 1999; Elkins and Wu, 2000a; 2000b; Guangxiong and Xincan, 2000; Guangxiong *et al*, 2000; Parena *et al*, 2000) include the famous formulas developed by (Nadal, 1960).

Nadal's criteria is given by equations (2.4) and (2.5), (Elkins and Wu, 1999).

Minimum L/V ratio for flange climb derailment, refer to Figure 2-4(a):

$$\frac{LateralForce}{VerticalForce} = \frac{\tan\phi - \mu}{1 + \mu\tan\phi} \qquad (2.4)$$

Minimum L/V ratio for derailment without flange climb, refer to Figure 2-4(b).

$$\frac{LateralForce}{VerticalForce} = \frac{\tan\phi + \mu}{1 + \mu\tan\phi} \qquad (2.5)$$

For the condition where μ is the coefficient of friction, ϕ is the angle between the rail and the flange and $\mu = \frac{F_2}{F_3}$ at the limit, (Elkins and Wu, 1999). F_2 is the force acting at the flange angle and F_3 is the force acting into the flange, at right angles to the flange angle as shown in Figure 2-4(a) and Figure 2-4(b). Figure 2-4 defines the orientation of the forces and the angle for Equations (2.4) and (2.5). L is the lateral force and V is the vertical force in Figure 2-4. Equation (2.4) corresponds to a

saturated lateral creep force F_2 acting up the flange for a specified contact angle, (Elkins and Wu, 1999) as shown in Figure 2-4(a). The maximum contact angle between the rail and the flange gives the minimum wheel L/V ratio at which flange climb derailment may occur. Below this L/V ratio, flange climb cannot occur, (Elkins and Wu, 1999).

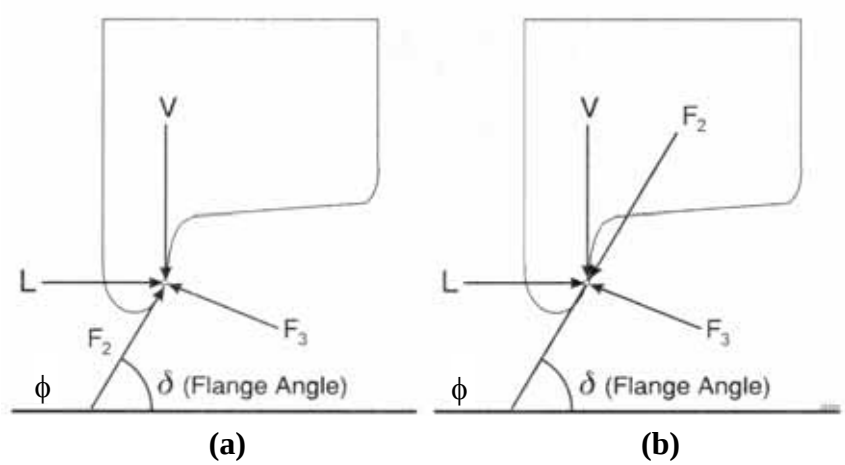

Figure 2-4: Nadal's Criteria Wheel Profile Diagram, (Elkins and Wu, 1999)

Equation (2.5) corresponds to a saturated lateral creep force acting down the flange. Equation (2.5) gives the minimum L/V ratio where derailment may occur, (Elkins and Wu, 1999). Derailment criteria can therefore be used to predict limits of rollingstock stability. There is however, an absence of literature that relates values of Nadal's Criteria approaching derailment levels to levels of risk.

2.4. Train and Vehicle Dynamics

Train and railway vehicle dynamics has historically been divided into two separate fields to reduce complexity. The simulators today also follow this trend some examples of wagon simulation packages used for wagon dynamics are CABS,

NUCARS and VAMPIRE. Railway vehicle dynamics or wagon dynamics is the study of a single or small number of railway vehicles. Section 2.4.2 discusses railway vehicle dynamics.

Train dynamics is simulated in packages such as TOES(AAR), DDTS(Sydac) and The Centre for Railway Engineering Longitudinal Train Simulator (CRE-LTS). Train dynamics refers to a train with a number of vehicles making up a train. These vehicles are typically modelled as independent masses and generally do not include the complexity or the advanced modelling of a vehicle simulator. Train dynamics is concerned with speed control, traction and braking issues, and longitudinal train dynamics. Section 2.4.1 discusses a number of dynamic effects experienced in the train due to train dynamics.

2.4.1. Train Dynamics

Train dynamics refers to the dynamics of the whole train. Excessive longitudinal dynamic forces in trains can cause serious damage to vehicles, the goods being transported and can decrease vehicle stability. The papers reviewed on train dynamics are (Cole, 1998b, 1999; Duncan and Webb, 1989; El-Sibaie, 1990, 1993; Fukazawa, 1992; Mayville and Rancatore, 1999; McClanachan and Cole, 1997; McClanachan *et al*, 2000; McClanachan *et al*, 2002; McClanachan and Roach, 2000; Xiang, 1993). Three categories of longitudinal forces experienced within trains were identified in field testing by (Duncan and Webb, 1989). They are steady state forces, impact forces and forces due to longitudinal vibration.

Steady state forces are due to various external forces acting on the train, such as track gradient, rolling and curving resistance; tractive effort and braking, (Duncan and Webb, 1989). Impact forces arise due to slack in wagon connections usually known as coupler slack. Two types of longitudinal vibration were identified. One is due to a fully compressed or stretched train with locked draft gears. The force magnitudes fluctuate throughout the train at approximately 0.1Hz in a loaded train for the case presented in the paper. Vibration is undamped and sinusoidal. The other type of longitudinal vibration is due to the train trying to reach equilibrium. The wagons impact against each other due to coupler slop or slack, (Duncan and Webb, 1989). The measured force approximates to a square wave and includes damping contributions from draft gears.

The draft gear, coupler and knuckle characteristics are extremely important when investigating coupler impacts. Draft gear behaviour cannot be effectively modelled by using linear springs and dampers because the stiffness is dependent on the impact conditions, (Cole, 1999). It was also found that the draft gear sometimes locks and starts responding in the form of a linear spring, (Cole, 1999; Duncan and Webb, 1989).

Typically draft gears consist of a polymer spring and an arrangement of friction wedges. There are also draft gears based on hydraulic damping and slackless draft gears without spring components. The frictional force produced by the wedges is dependent on the geometry of the friction wedges and the static and kinetic friction coefficients. "A comprehensive model of the draft gear will therefore have to

mathematically relate longitudinal force to both deflection and rod velocity and correctly model wedge locking", (Cole, 1999).

2.4.2. Vehicle Dynamics

The papers which were reviewed for railway vehicle dynamics are (Cole, 1996; Cole, 1998a, 1999; Gilchrist, 1998; McClanachan and Cole, 1997; McClanachan *et al*, 2000; McClanachan *et al*, 2002; Miyamoto, 1996; Miyamoto and Fujimoto, 1990; Parkinson, 1999; Schupp and Jaschinski, 1996; Sun and Dhanasekar, 2000; Wu and Zeng, 1998).

Vehicle dynamics in rail vehicles is fundamentally related to the behaviour of the wheelset. A wheelset travelling down a tangent track in an equilibrium condition will follow a sinusoidal lateral path, (Hay, 1982). This phenomena is called hunting and is developed due to the solid axle and the cone shape of the wheel and has the consequence of cyclic dynamic behaviour, (Ahmadian and Yang, 1998; Gilchrist, 1998). Any minute disturbance from the desired straight line causes lateral oscillations. These oscillations are the result of the wheelset trying to reach equilibrium, and are limited by the flange, (Gilchrist, 1998). Hunting is speed related and it becomes more severe at critical speeds, (Hay, 1982). The study of hunting is outside the scope of this thesis so it will not be discussed further in this review.

Since each wheelset is joined by a solid axle, the cone shape of the wheel has the consequence of self steering on curves. This is due to the difference in diameter of each wheel as the wheelset moves in the lateral direction. On a curve, the outside

wheel must travel further than the inner wheel. The difference in rolling diameter of each wheel allows the wheelset to travel around curves smoothly.

Wagon bounce is when wheel unloading is synchronised across all wheel sets, as shown in Figure 2-5. Examples of bounce were measured and published by (McClanachan and Roach, 2000). If the inputs to the bogies from the track become unsynchronised, pitch motion occurs. Irregularities that are unsynchronised between rails result in wagon roll. Wagon roll can also occur due to track inputs such as curve transitions and turnouts.

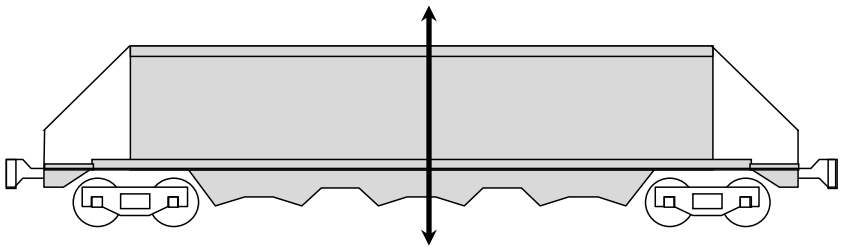

Figure 2-5: Wagon Bounce

Railway vehicle simulators can be used to simulate a wagon model or small number of vehicles. Wagon models can be very complex, as non-linear elements can be included. Simulation software such as VAMPIRE includes a large range of elements including linear and non-linear elements such as springs, dampers, friction wedges and bumpstops, (AEA-Technology, 2002). A bumpstop is a term used in VAMPIRE to describe a non-linear element that has a piecewise definable force and displacement relationship. VAMPIRE also has a large number of outputs available, some examples are wheel unloading, L/V ratio and the velocity, displacement and acceleration of each mass, (AEA-Technology, 2002).

2.4.3. Interaction of Train and Vehicle Dynamics

There were a number of papers reviewed with the view to find what research had been completed on the interaction of train and vehicle dynamics, (Ahmed and Bayoumi, 1983; Cole, 1996; Cole, 1998b, 1999; Duncan and Webb, 1989; El-Sibaie, 1990, 1993; Fukazawa, 1992; Mayville and Rancatore, 1999; McClanachan and Cole, 1997; McClanachan *et al*, 2000; McClanachan and Roach, 2000). Longitudinal train and wagon dynamic interaction can be divided up into longitudinal-rotational dynamics, longitudinal-lateral dynamics and longitudinal-vertical dynamics. Longitudinal-rotational dynamics is when rotations such as bogie pitch and wagon pitch are created due to longitudinal forces and impacts, (McClanachan *et al*, 2000). Longitudinal-lateral dynamics is defined as when a lateral component is generated due to coupler angles. Longitudinal-lateral dynamics increases wheel unloading and L/V ratio of some wheel sets. These effects were demonstrated by (El-Sibaie, 1993). Longitudinal-vertical dynamics is defined as when vertical force components are generated due to the combination of coupler forces and the change of grade. The change of grade creates angles between vehicles in the vertical plane.

The effects of coupler forces and wheel unloading due to bogie and wagon pitch are demonstrated by (McClanachan *et al*, 2000). Data was collected during the normal operation of a unit coal train, (McClanachan and Cole, 1997). Six wagons and two locomotives were equipped with various types of measuring devices. The data that was recorded was analysed by a computer search and then was sorted by the magnitude of events. The worst scenarios in the data collection process where then

identified. The data presented in this paper was from wagon 50 which was positioned in front of the remote locomotive, (McClanachan *et al*, 2000). Figure 2-6 shows the positioning of the wagon, the axle numbering and the sign convention.

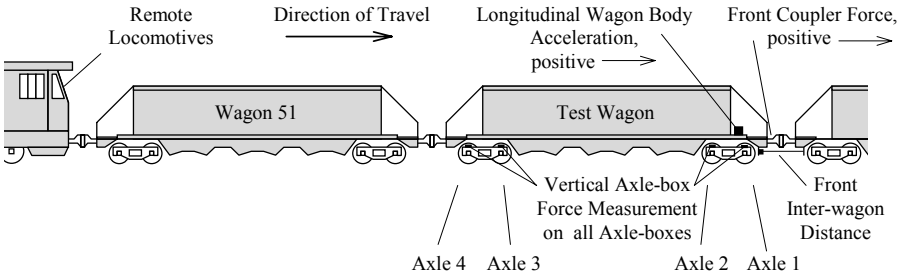

Figure 2-6: Experimental Test Wagon Location, (McClanachan and Roach, 2000)

The information that was collected in (McClanachan and Cole, 1997) was used to validate the various simulations in (McClanachan *et al*, 2000). The paper published by (McClanachan *et al*, 2000) presented wheel unloading due to wagon body and bogie pitch resulting from coupler impact forces applied to the wagon.

2.4.3.1. Longitudinal-Rotational Dynamics

Longitudinal rotational dynamics is defined for the purpose of this thesis as when a rotation is generated about the lateral axes due to longitudinal forces or impacts. The rotation of masses causes wheel unloading on certain wheel sets. Bogie pitch and wagon pitch is covered in this section. Bogie pitch can result from longitudinal forces or impacts. It is due to the bolster centre bowl connection being above the centre of mass of the side frames and the wheelsets. Figure 2-7 is an exaggerated diagram of these effects.

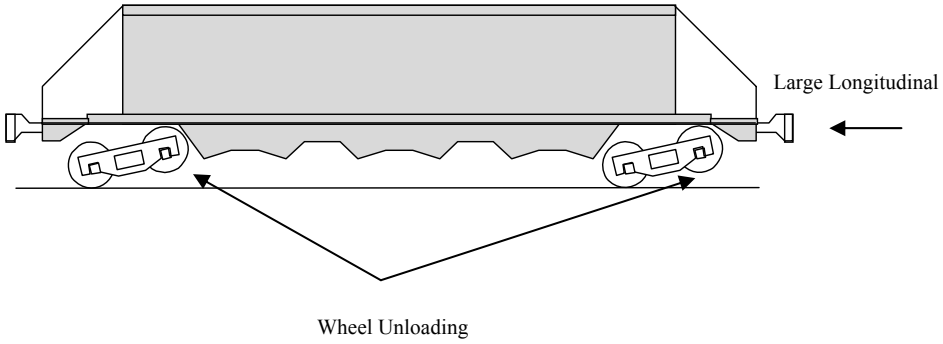

Figure 2-7: Bogie Pitch Wheel Unloading

Wagon pitch can also result from longitudinal forces or impacts. It causes the wagon to rotate about its centre of mass, which creates wheel unloading at some wheelsets. The coupler force is below the centre of mass and therefore creates a moment, which causes the wagon body to pitch. Figure 2-8 is an exaggerated diagram of these effects.

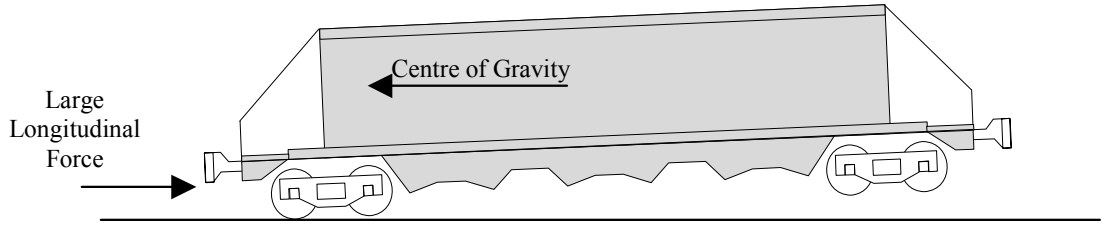

Figure 2-8: Wagon Pitch Wheel Unloading

2.4.3.2. Longitudinal-Lateral Dynamics

Longitudinal-lateral dynamics are developed due to the combinations of coupler angles and in-train forces, (El-Sibaie, 1993). Although the angles between vehicles are not large, impacts forces and larger steady in-train forces (for example 1MN) can cause the Lateral/Vertical ratio to be increased enough to cause derailment. Obviously on tighter curves, larger coupler angles exist allowing larger lateral

coupler force components to be applied to the wagon. These lateral force components increase the magnitude of the lateral forces at the rail. Lateral forces can be generated due to either tensile or compressive forces, (El-Sibaie, 1993). Coupler angles and therefore lateral coupler force components can also be increased by short-long wagon combinations, (El-Sibaie, 1993).

Mixed freight trains are of particular interest as the train consist could be made up of a mixture of wagon types, (El-Sibaie, 1993). Wagons in a mixed freight train can have a variety of bogie centre-to-centre lengths, overhangs and masses. Empty wagons can be scatted throughout a mostly loaded train and wagons can also be partially loaded. Indicating some recognition of this problem in North America, AAR currently sell a software package that will calculate horizontal coupler angles, this package is called AAR CABS.

To allow the simulation of vehicles using coupler force data, coupler angles are required at each instant in time so that longitudinal and lateral forces can be calculated. These coupler angles are due to track curvature. In order to calculate lateral and vertical forces due to coupler angles, it is necessary to calculate these angles from the details of the wagons. The main variables are distance between bogies, overhang, coupler slack and curve radius.

Railway tracks are made up of straights, transitions and curves. The transition of the curve is very important so that a section of track can gradually change into a different curvature. The transition of the curve is included in the track so that the increase in lateral acceleration is applied over time. If transitions were not included there would

be a sudden lateral acceleration at the beginning of the curve. Figure 2-9(a) and (b) shows this transition.

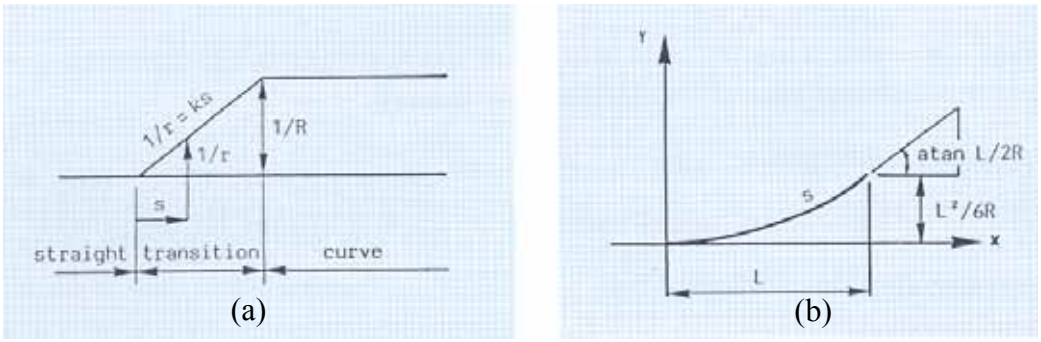

Figure 2-9: Railway Track Curvature, (Esveld, 1989)

If railway track is specified by 1/r (curvature) which is shown in Figure 2-9(a). When 1/r=0 the track is straight, i.e. infinite radius, and when 1/r=0.002, the radius is 500 metres.

A clothoid is a specific type of spiral where its curvature increases linearly with the distance along the spiral. The clothoid makes a perfect transition spiral or transition curve and is specified by Equation (2.6). The transition curve is shown in Figure 2-9(a).

$$\frac{1}{r} = ks \qquad (2.6)$$

Where r is the radius, k is a constant and s is the curve length from the origin, (Esveld, 1989). A clothoid can be approximated by a cubic parabola as shown in Equation (2.7), (Esveld, 1989).

$$y = \frac{x^3}{6RL} \qquad (2.7)$$

Where y is the y-axis coordinates, x is the x-axis coordinates, R is the radius and L is the length of the curve projected onto the x-axis. Figure 2-10 shows how this can be used to find transition coordinates. No method was located in literature that allowed calculation of coupler angles in a moving coordinate system referenced to the track centreline.

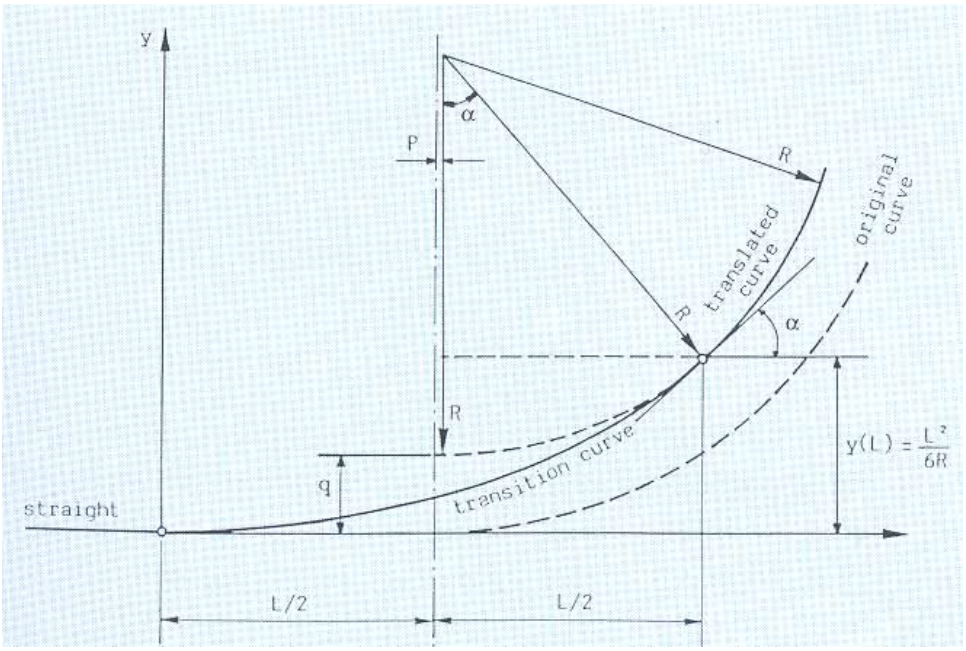

Figure 2-10: Curve Transition, (Esveld, 1989)

2.4.3.3. Longitudinal-Vertical Dynamics

Longitudinal-vertical dynamics can be generated through vertical coupler angles. This is due to the change of grade. If a wagon is travelling over a hill or through a dip there is a small angle measured in the vertical plane between vehicles. If there is a large impact or forces developed between two vehicles, a vertical component will be produced. Although the angles between these wagons are very small, the magnitude of the vertical force components that are experienced between wagons

could be significant for large coupler forces. A paper published by (Cole, 1999) mentions that these angles are developed due to changes of grade, but no published results exploring this problem were found.

2.5. Managing Derailment Risks

The papers which were reviewed for this section are (Anderson and Francis, 2002; DiBartolomeis *et al*, 1994; Iwnicki and Stow, 1999; Muttram, 2002; Novosyolov, 2002; Waters *et al*, 2002). Only two references were found which combined derailment with risk management, (Muttram, 2002; Waters *et al*, 2002). The paper published by (Muttram, 2002) is focused on a Safety Risk Model (SRM) for railway application. The SRM is focused on cumulative risk and the reduction of risks in key areas from previous incidents. Data is collected when an incident occurs and it is categorised into a hazardous event number. This information can then be sorted by a hazardous event number to find the area of highest cumulative risk. Cumulative risk not only takes into account the risk factor but also the level of injury that could result from an incident. This helps railway companies focus funding into the correct areas, (Muttram, 2002). Although this is a good approach of assessing risk from previous events across a railway company, this strategy is different to what is required for this thesis. This thesis is concentrated on derailment risks due to longitudinal dynamics. No literature could be found on this topic. The following sections review principles of generic risk management.

2.5.1. The Risk Management Process

Risk Management has been documented by (Standards Association of Australia, 1999). It demonstrates the process to follow and gives a range of examples that can be used, (Standards Association of Australia, 1999). Risk Management theory allows risks to be categorised by their consequences and likelihood of occurring. From this information the level of risk can be found. Risk Management allows appropriate action to be made towards implementing methods of control or risk reduction techniques. Figure 2-11 shows the risk management process and an overview of the steps that should be taken.

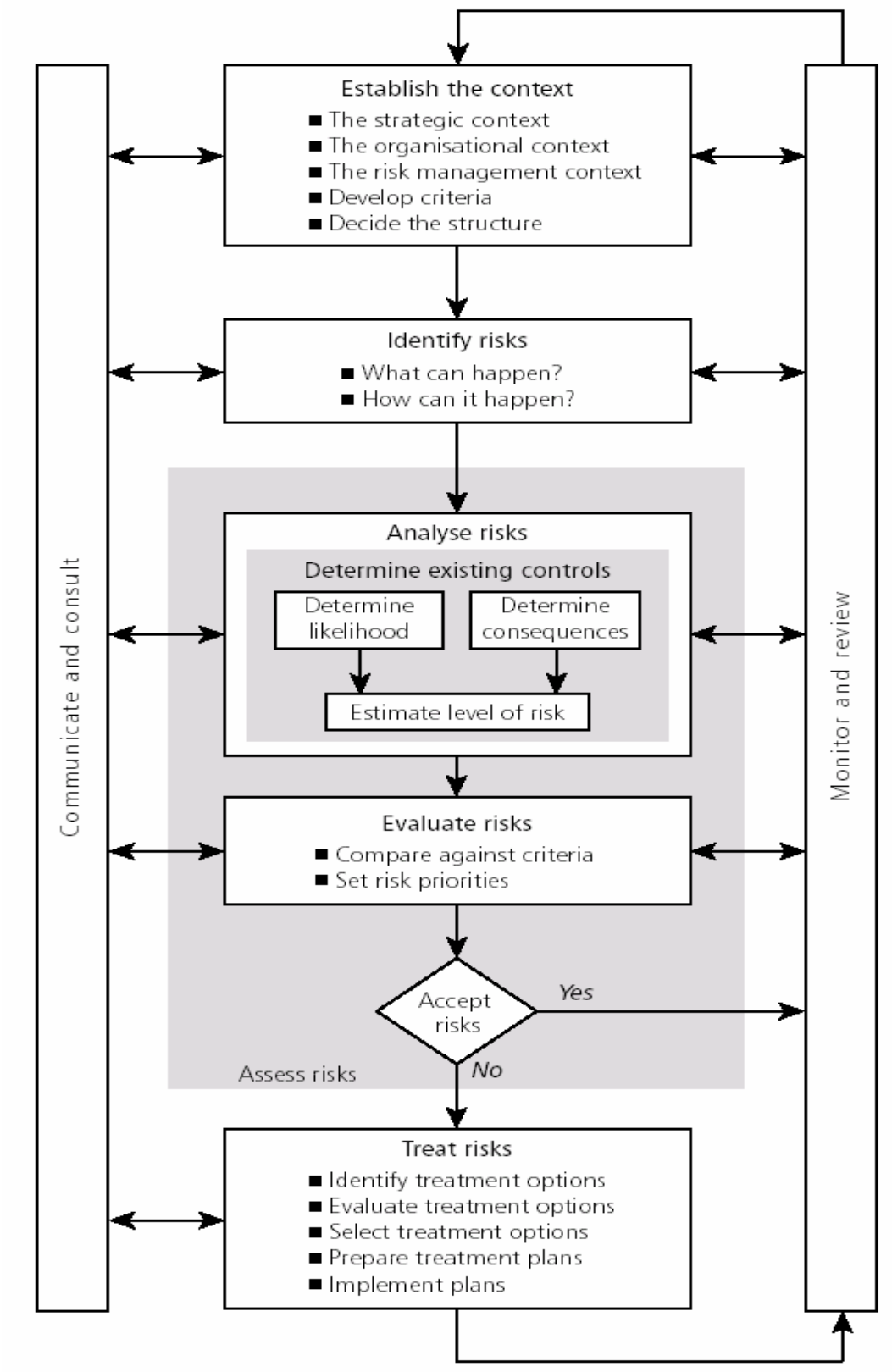

Figure 2-11: Risk Management Process, (Standards Association of Australia, 1999)

2.5.2. Risk Assessment

Risk assessment is an important part of the risk management process. It consists of risk analysis and risk evaluation. It determines the likelihood of an event, the severity of the outcome and the evaluation of these risks. This allows appropriate steps to be made towards decision-making. An important part of the risk assessment process is to separate minor acceptable risks from major risks, and to provide data to assist in the evaluation and treatment of these problems, (Standards Association of Australia, 1999). The risk assessment process can sometimes be overlooked by the haste of moving from the risk identification or treatment of risks to the solution. This can result in efforts being focused into the incorrect areas, while some major risks are left unattended, (Standards Association of Australia, 1999).

When risk assessment is focused on derailment, the terms likelihood and consequences must be defined in derailment terms. The likelihood of a derailment happening would depend on a large range of factors. Derailment criteria must be used to analyse derailment. For derailment, the likelihood of a derailment would take into account the wheel unloading and the L/V ratio. The consequences could be the uncontrolled kinetic energy of the train or railway vehicle.

2.5.3. Risk Analysis

The risk analysis process determines the existing control measures that are implemented, and analyses risks in terms of consequence and likelihood, (Standards Association of Australia, 1999). The analysis should consider the range of potential

consequences and how likely those consequences are to occur. It is also important to consider multiple event scenarios, the likelihood of the event occurring and the chances of the existing controls not working properly or failing completely. Data and information should be produced and recorded to enforce any decisions that are made during the risk management process, (Standards Association of Australia, 1999). This information can later be reviewed and compared to any new data. A similar table to Table 2-2 is commonly used for risk analysis and is advised by the Australian standards, (Standards Association of Australia, 1999). Table 2-3,
Table 2-4 and Table 2-5 are used as definitions. The tables are used so that it is easy to identify dangerous scenarios.

Table 2-2: Risk Table, (Standards Association of Australia, 1999)

Likelihood	Consequences				
	Insignificant	Minor	Moderate	Major	Catastrophic
Almost Certain	High Risk	High Risk	Extreme Risk	Extreme Risk	Extreme Risk
Likely	Moderate Risk	High Risk	High Risk	Extreme Risk	Extreme Risk
Moderate	Low Risk	Moderate Risk	High Risk	Extreme Risk	Extreme Risk
Unlikely	Low Risk	Low Risk	Moderate Risk	High Risk	Extreme Risk
Rare	Low Risk	Low Risk	Moderate Risk	High Risk	High Risk
Very rare	Trivial Risk	Trivial Risk	Low Risk	Moderate Risk	High Risk
Almost incredible	Trivial Risk	Trivial Risk	Low Risk	Moderate Risk	Moderate Risk

Table 2-3: Consequences, (Standards Association of Australia, 1999)

Consequences	Definition
Catastrophic	The consequences would threaten the survival of not only the programme, but also the Organisation, possibly causing major problems for clients, the administration of the programme or for a large part of the Public Sector. Revenue loss greater than x% of total revenue being managed would have extreme consequences for the Organisation both financially and politically.
Major	The consequences would threaten the survival or continued effective function of the programme, or require the intervention of top level management or by the Elected Representatives. Revenue loss greater than y% of total revenue being managed would have very high consequences for the Organisation both financially and politically.
Moderate	The consequences would not threaten the programme, but would mean that the administration of the programme could be subject to significant review or changed ways of operating. Revenue loss greater than z% of total revenue being managed would have medium consequences for the Organisation both financially and politically.
Minor	The consequences would threaten the efficiency or effectiveness of some aspects of the programme, but would be dealt with internally. A loss of revenue below the tolerance level of 5% (Audit materiality) applied to clients would be of low consequence.
Insignificant	The consequences are dealt with by routine operations. A loss of revenue below the programme tolerance level of w% (less than Audit materiality) applied to clients would be of negligible consequence.

Table 2-4: Likelihood, (Standards Association of Australia, 1999)

Likelihood	Definition	Probability
Almost certain	The event will occur on an annual basis	Will occur once a year or more frequently
Likely	The event has occurred several times or more in your career	Will occur once every three years
Moderate	The event could occur in your career or could occur at any time	Will occur once every ten years
Unlikely	The event has not yet occurred but could occur at some time	Will occur once every 30 years
Rare	Heard of something like this occurring elsewhere	Will occur once every 100 years
Very rare	Have heard of this happening	One in 300 years
Almost Incredible	One off event in exceptional circumstances	One in 1000 years

Table 2-5: Impact and Action, (Standards Association of Australia, 1999)

Level of Risk	Impact and Action
Extreme Risk	Almost certain to threaten the survival of the program, its administration and the Organisation either financially or politically. Must be managed by senior management with a detailed plan
High Risk	Likely to cause some damage, disruption or breach of controls. Detailed research and management planning required at senior level
Moderate Risk	Unlikely to be a threat to the efficiency and effectiveness of the program. Manage by specific monitoring or response procedures
Low Risk	Unlikely to threaten some aspects of the program. Manage by routine procedures
Trivial Risk	Risks have negligible impact on the program. Unlikely to need specific application of resources

3 SOFTWARE AND METHODS

3.1. Introduction

The method adopted for quantifying derailment risks was to first perform train and detailed wagon dynamics simulations. These simulations can be used to give data describing the dynamic behaviour of trains and vehicles. The levels of wheel unloading and L/V ratio can be used to indicate if a vehicle will derail in a given situation. If an extensive database of simulated results is available, event probabilities can be calculated by determining how often a dynamic event occurs. Likelihood, as defined in the risk matrix, can therefore be determined from wheel unloading and L/V ratio simulation data. The running speed being proportional to the kinetic energy of the system, gives an indication of the consequences. A similar table to Table 2-2 can be used to determine the level of risk by combining the likelihood and consequences of a given event.

3.2. Method of Research

A variety of software packages, computer code and other computer methods were used to complete this thesis. Simulation software such as VAMPIRE and CRE-LTS (The Centre for Railway Engineering Longitudinal Train Simulator) were used to simulate vehicle dynamics and longitudinal train dynamics. VAMPIRE was chosen as the vehicle simulator software package as it is a rail industry specific package for modelling railway vehicle behaviour. The longitudinal train simulator package used for simulation was CRE-LTS. This software package was chosen because the source

code was available and could be easily modified to incorporate calculations of coupler angles.

Programming software packages utilising C such as Microsoft Visual Studio and National Instruments Measurement Studio were used to create computer utility applications. Both these software packages were chosen because they are common packages used for C programming and the development of software. Utility application software, both purchased and developed were extremely useful in developing batching and reporting systems for simulation studies. The packages used for batching were WinBatch and UltraEdit. WinBatch was chosen because it is effective in recording and simulating user inputs. UltraEdit is one of the most effective text editing packages available and includes many useful features and tools; such as macro tools and advanced searching and replacement text functions.

A flow chart of the method used for the research performed in this thesis is shown in Figure 3-1. The step number is shown in front of each description in Figure 3-1. The basic process used to perform the research in this thesis was to first develop the mathematical models needed for simulation, validate each model, perform the simulations, analyse the simulations and then use this information to determine levels of risk. Step 1 in Figure 3-1 was to prepare the wagon model for vehicle simulations. The model used was a VAMPIRE wagon model of a VAMB coal hopper wagon and it is covered in detail in Section 3.3.1 on page 35. The model then needed to be validated, as shown in step 5 in Figure 3-1. The model was validated for hunting, steady forces on curves and bogie pitch, as covered in chapter 4 on page 75. The VAMPIRE wagon model was used to simulate steady forces on curves and curve

transitions, as shown in step 9 in Figure 3-1. This study was performed to identify the effects of steady in-train forces on curves, as discussed in Chapter 5 on page 88.

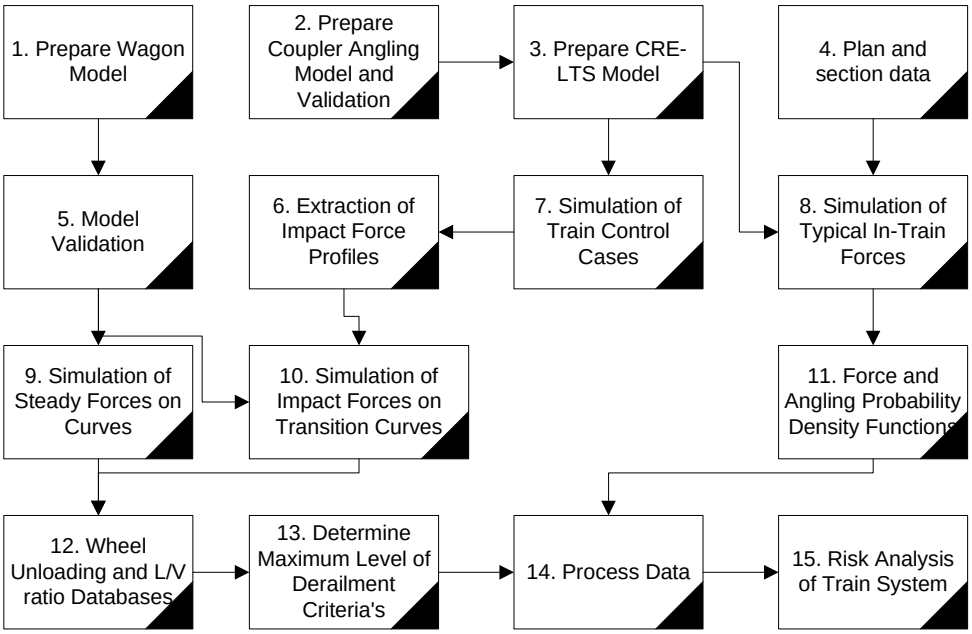

Figure 3-1: Flowchart of Method of Research

The models used for longitudinal simulations consisted of a coupler angling model (step 2, Figure 3-1) and an existing train model developed by the Centre for Railway Engineering. The existing train model and simulator used for simulation was CRE-LTS. It was necessary to combine the coupler angling model and CRE-LTS for longitudinal train simulation on curves, (step 3, Figure 3-1). The coupler model, CRE-LTS and the implementation of the coupler angling code into CRE-LTS is covered in Sections 3.3.2, 3.3.3 and 3.3.4 on page 43, 45 and 57 respectively. Longitudinal train simulations of impact forces allowed the identification of the worse case impact forces in a train simulation, (step 6 and 7, Figure 3-1). These worse case impact forces were applied to the coupler pin of the VAMPIRE model so

that the effect of impact forces on curve transitions could be studied as shown in (step 10, Figure 3-1), it is also covered in detail in Chapter 6 on page 95.

Maximum levels of wheel unloading and L/V ratio were determined from the simulations of impact and steady forces on curves and curve transitions, (step 12 and 13, Figure 3-1). The maximum level of wheel unloading and L/V ratio determined for each scenario was used to indicate if a vehicle would derail, (step 14, Figure 3-1). These levels of wheel unloading and L/V ratio were used in the risk analysis process combined with event probabilities to determine the level of risk, (step 15, Figure 3-1) and are covered in detail in Chapter 8 on page 122.

To determine the probability of an event occurring, it was necessary to perform simulations of typical train operations. These simulations were performed with the combination of the coupler angling model, CRE-LTS, plan and section data; and a driver action model, (step 4 and 8, Figure 3-1). The longitudinal train simulations of typical train operations gave in-train forces along each chosen track section. These in-train forces were used to determine the probability of events occurring in typical train operations using probability density functions, (step 11, Figure 3-1). The combination of the probability of an event occurring and if a vehicle would derail were used to determine the likelihood of each event. The consequences were dependent on running speed. The level of risk could then be determined from the likelihood and consequences of each event, (step 15, Figure 3-1). The risk assessment process is covered in detail in chapter 8 on page 122.

3.3. Mathematical Modelling

This section of the thesis discusses in detail the mathematical models developed and used in this thesis.

3.3.1. VAMPIRE

VAMPIRE is a railway vehicle simulator developed by AEA Technology Rail. It allows the analysis of vehicle models which are created by defining the parameters for the model. Model parameters are defined in text based files. A large range of dampers, springs and non-linear elements can be specified. VAMPIRE also allows a large selection of output channels to be plotted for a given simulation. Output channels can include wheel unloading, L/V ratio and acceleration of all masses in six DOF, (AEA-Technology, 2002).

VAMPIRE was used throughout this project to simulate the dynamic behaviour of railway vehicles. A wagon model was created for VAMPIRE so that lateral and longitudinal forces could be applied to the model. The centre bowl connections were modelled to allow bogie pitch. This allowed the simulation of wagon dynamics adding longitudinal and lateral forces provided from the longitudinal train simulator (CRE-LTS). Forces from longitudinal train simulations were applied at the coupler pin of the wagon model.

3.3.1.1. The Wagon Model

A vehicle model representative of a coal hopper wagon was created in VAMPIRE. The vehicle model was created by first defining the masses. These masses are then joined together with springs, dampers, non-linear elements and other connection types that can be defined in VAMPIRE refer to (AEA-Technology, 2002). The process of defining the model was achieved by creating a text document that contains all the necessary data to create the desired model. Testing and validation was performed on the model to ensure that it had the correct dynamic behaviour.

The wagon model that was developed for this thesis was based on a four-axle wagon with three-piece narrow (1067mm) gauge bogies. The wagon mass was 15 tonne (empty) and the coupler height taken as 785mm. This wagon is known as a VAMB wagon at Queensland Rail and has a gross mass of 70 tonnes. Two different models were created for simulations as follows:

1. A single empty vehicle model, as shown in Figure 3-2.
2. An empty vehicle model with dummy wagons attached at the front and rear, as shown in Figure 3-3.

The single vehicle model was primarily used for simulations where external forces were added to the coupler pin to simulate the effects of coupler angling and longitudinal in-train forces. The model with the dummy wagons attached could not be used in impact conditions, as it was desired to use the fully detailed coupler and draft gear model available from CRE-LTS. Train simulations could be first performed to determine in-train forces. Coupler angles and coupler forces were

recorded to data files with resolution of 100 samples a second. The force data obtained from CRE-LTS for a specific vehicle can be applied to the coupler pin on the single vehicle model for a detailed analysis. This process allows detailed analyses of any vehicle in the simulated train consist.

The model with the dummy wagons added at the front and rear was used for steady in-train forces where the dynamic effects of the draft gear and coupler slack would have little effect on the forces applied to the wagon. Simulations were therefore simpler as the angle between vehicles was provided by VAMPIRE.

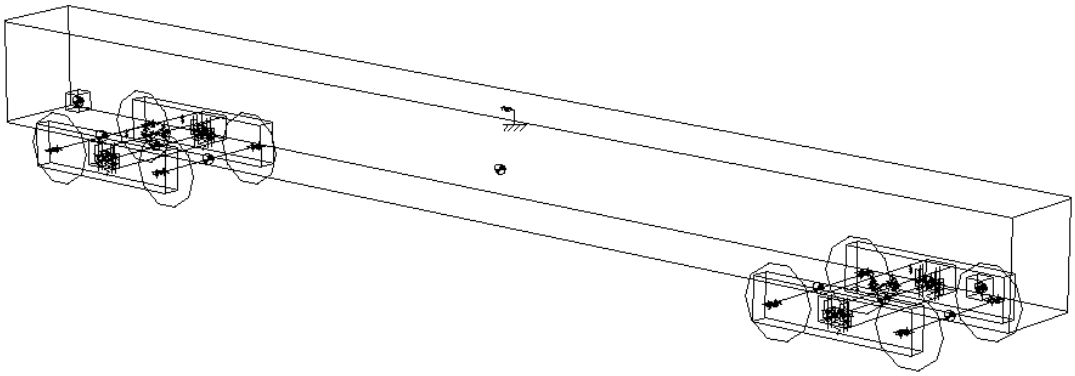

Figure 3-2: Isometric View of the Wagon Model

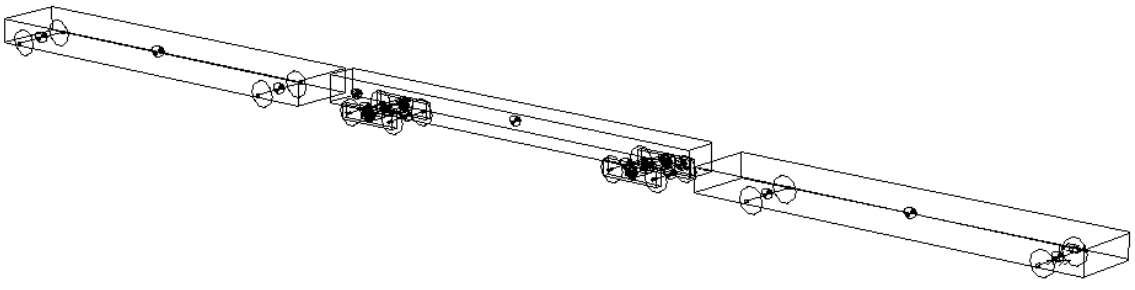

Figure 3-3: Isometric View of Wagon Model with Dummy Wagons

A number of assumptions were made to reduce the complexity of the models. The following assumptions were made:

- Coupler connections to the wagon model were modelled as a steel on steel connection representing a force input at the draft gear pocket.
- The bogie model was a typical three-piece freight bogie.
- The secondary suspension includes both vertical and torsional stiffness and friction damping elements.
- The friction in the constant force wedge dampers (snubbers) is modelled by vertical and horizontal components.
- Minimal damping in many components modelled as steel on steel connections. These include side frame to wheel set connections.

3.3.1.2. VAMPIRE Model Connections and Elements

A large range of different connections and eleven masses were used to create the vehicle models used for the VAMPIRE simulations. It is important to choose the correct type of connections with the correct values. Table 3-1 gives an overview of connections in the VAMPIRE model. The axis system that is used in VAMPIRE is shown in Figure 3-4 and Table 3-1.

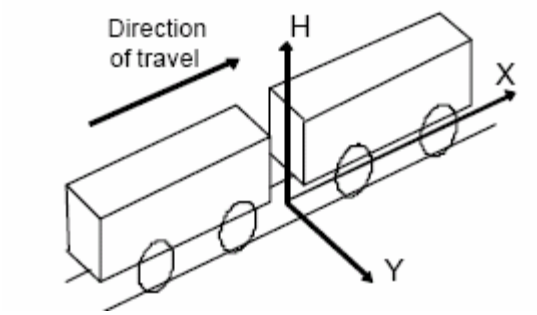

Figure 3-4: Vehicle Axis, (AEA-Technology, 2002)

Table 3-1: VAMPIRE Model Mass Connections

Connection	DoF	Description	Stiffness	Damping	Comments
Centre Plate-Bolster	Vertical	Steel-on-steel and lift-off Bumpstop*	450MN/m	None	4 springs allowing roll and pitch
Centre Plate-Bolster	Vertical	Vertical Friction	None	μ=0.30	
Centre Plate-Bolster	Yaw Rotation	Friction Torque	None	μ=0.30	
Centre Plate-Bolster	Longitudinal and Lateral	Steel on Steel Spring Connection	450MN/m	None	
Side Bearers	Vertical	Lift-off Bumpstop*	20kN/m	None	
Bolster to Side Frame	All	Spring nest with stiffness in all planes	4, 4, 6, 0.4, 0.4, 2.0MN/m**	None	
Bolster to Side Frame	Vertical and Lateral	Vertical and Lateral Friction elements	None	μ=0.2, μ=0.13	
Bolster to Side Frame	Yaw Rotation	Torsional Damping	None	0.53MNs/m	
Side Frame to Axle Box	Vertical	Steel-on-steel and lift-off Bumpstop* and Damping	450MN/m	0.33MNs/m	2 Springs for Pitch
Side Frame to Axle Box	Lateral	Spring Connection and Damping	6.44MN/m	0.33MNs/m	2 Springs for Roll
Side Frame to Axle Box	Longitudinal	Spring Connection and Friction	440MN/m	μ=0.5	2 Springs for Yaw
Side Frame to Axle Box	Yaw Rotation	Friction Elements	None	μ=0.5	
Coupler Pin to Wagon Body	All	Steel on Steel Spring	440MN/m	None	

*Bumpstop is a non-linear element modelling facility provided by VAMPIRE.

** List is in the following order X Axis, Y Axis, Z Axis, Roll, Pitch, Yaw.

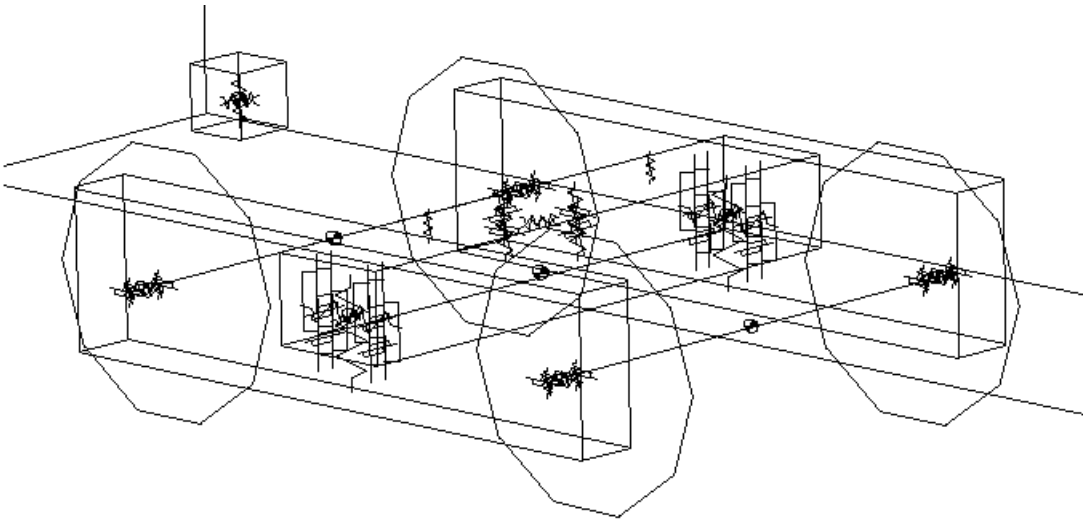

Figure 3-5: Centre Bowl Connection Diagram

The centre plate to bolster connections were modelled using bumpstops to model lift off of the centre plate and bogie pitch. A bump stop is a non-linear element in VAMPIRE which allows a user to define a force and displacement relationship. The centre-plate to bolster vertical connections are modelled as bumpstops with line and rotational friction across each element. The line and rotational friction at the centre plate to bolster connection is added for damping. By defining the centre plate to bolster vertical connections as a bumpstop it allows bogie pitch and wagon pitch to occur and reflects the looseness of the actual centre bowl connection. The bumpstop (non-linear element) is shown in Figure 3-6 and the positioning of these elements is shown in Table I-3 elements 1-8. The connection began acting as a steel on steel connection if the wagon body reached the hard limit of the centre pin. The longitudinal and lateral connections were steel on steel with a stiffness of (440MN/m), as shown in Table I-3 elements 1-4. Frictional elements were also added in the vertical and rotational planes across each of the bump stops. A coefficient of friction of 0.26 was applied to these friction elements, as shown in Table I-5 elements 1-8.

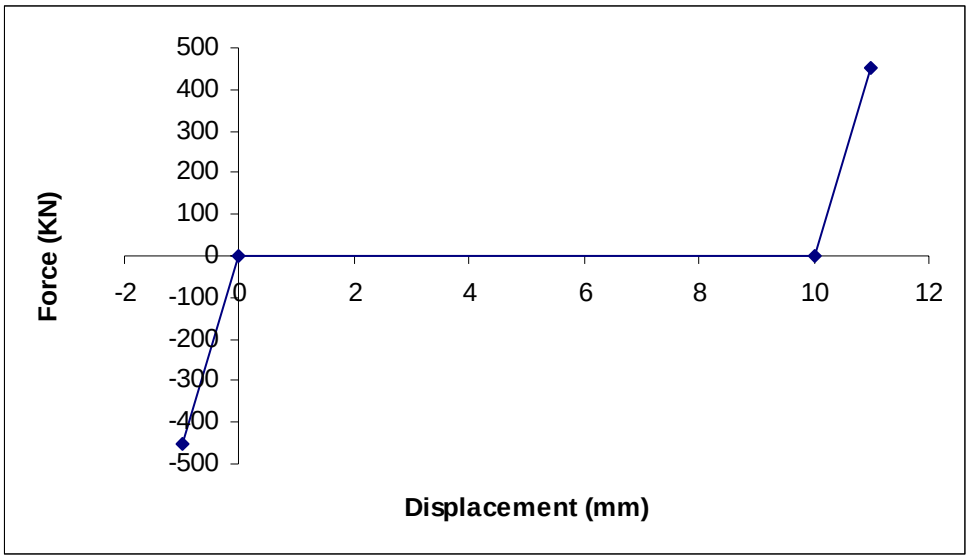

Figure 3-6: Centre Plate to Bolster Vertical Non-Linear Connections (bumpstop)

Each bolster to side frame spring connection was modelled as a spring nest with six degrees of freedom and a spring stiffness value applied to each of the degrees of freedom, as shown in Table 3-1 and in Appendix I (Table I-4 on page 143). Frictional elements were added to model the friction wedges in the vertical and lateral planes. Friction was also added for the Z axis and rotational about the Z axis, as shown in Appendix I in Table I-5 elements 9-24 on page 144. Rotational damping was added around the Y axis, as shown in Table I-5 elements 26-32. Spring connections were also added in the longitudinal plane, Table I-2 elements 21-24. The side bearer connections were modelled as non-linear elements shown in Figure 3-7. This allowed the side bearers to act as a spring with a stiffness of zero until the side bearers came in contact with the bolster, the connection then began acting as an steel on steel spring connection. Full details of these connections are in Appendix I, Table I-3 connections 9-12 on page 143.

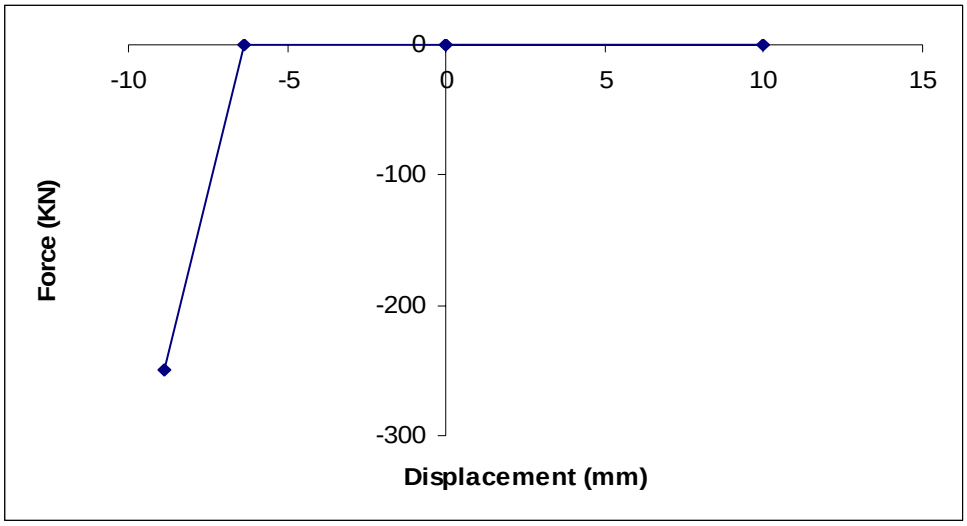

Figure 3-7: Side Bearer Non-Linear Elements

The side frame to axle box vertical connections were modelled as non-linear elements to allow the side frame to lift off the axle box, as shown in Figure 3-8, connection data and parameters are listed in Appendix I (Table I-3 connections 13-28 on page 143). The longitudinal connections were modelled as spring elements with frictional elements added in the longitudinal and longitudinal rotational planes, are shown in Table I-2 connections 13-20, Table I-5 connections 26-42. The lateral connections were modelled as spring elements with damping, these elements are shown in Appendix I in Table I-2 connections 5-12 on page 142 and Table I-6 connections 1-8 on page 145 respectively.

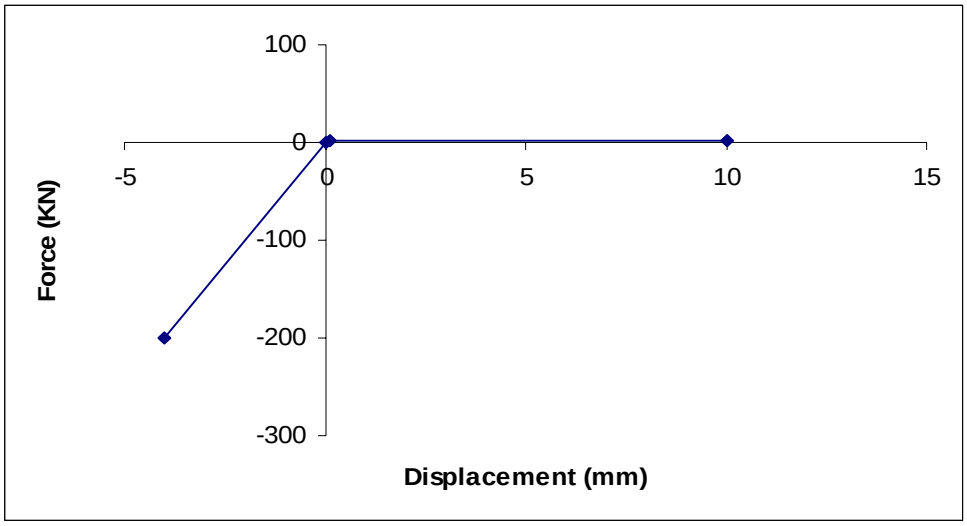

Figure 3-8: Side Frame to Axle Box Non-Linear Elements

The coupler pin masses were modelled to allow coupler forces to be applied to the vehicle model. Small coupler pin masses were added to the front and rear of the wagon. These masses were connected to the wagon with spring connections with a stiffness of 440MN/m, as shown in Table I-2 elements 26-31.

3.3.2. The Centre for Railway Engineering Longitudinal Train Simulator

CRE-LTS (The Centre for Railway Engineering Longitudinal Train Simulator) is a longitudinal train simulator that has been developed by The Centre for Railway Engineering and was written in the C programming language. The train simulator model consists of a number of independent masses joined together by wagon connection models. The wagon connection model includes the coupler and draft gear, as shown in Figure 3-9. The paper published by (Cole, 1998b) makes the case that models using linear springs and dampers are not representative of observed train dynamics. The paper goes on to discuss the more complex wagon connection model

that has been implemented in CRE-LTS. The advantage of using the more complex wagon connection model offered in CRE-LTS is that simulations give a closer representation of what would be experienced by a draft gear. The simulator does not take into account the effects of curvature other than curve drag forces. All forces between vehicles are applied as longitudinal forces with no lateral component. It was not necessary to validate CRE-LTS as it had been previously validated with recorded track data. Publications such as (Cole, 1998a; 1998b, 1999) also mention validation that was performed on CRE-LTS.

The wagon connection modelling used in CRELTS includes modelling for free slack and friction wedge type draft gears typical of auto-coupler systems used by Australian mineral unit train operators. The model includes friction damping that is proportional to the longitudinal force and includes a function relating friction coefficient to static, kinetic and transitional conditions reflecting differing impact conditions, (Cole, 1998b). To model the effects of coupler angles on curves an algorithm was developed and added to CRE-LTS to calculate the angles between vehicles. Details of the algorithm are given in the next section. Using the angles calculated, coupler forces could be broken up into longitudinal and lateral force components at the coupler pin.

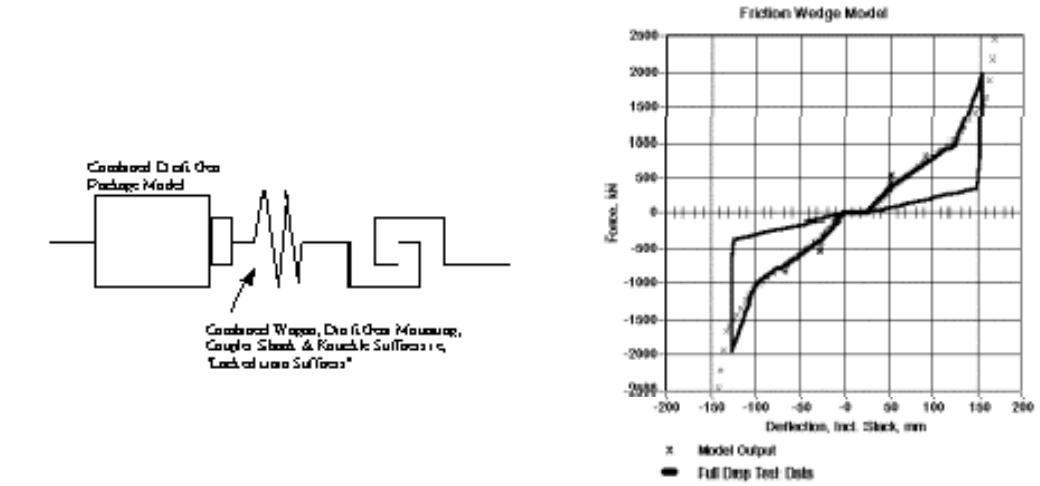

Figure 3-9: Draft Gear Model and Response Curve, 10Hz Sinusoid Input

The simulator has the following assumptions:

- The connection of the two coupler-shanks between vehicles remains straight. It is modelled as a drawbar that varies in length due to coupler slop.
- Vehicles are modelled as a single mass with one degree of freedom.
- Grade and curve forces are added as longitudinal components.

3.3.3. Coupler Angling Code Development

In order to determine longitudinal and lateral forces it is necessary to calculate the coupler angles at any point in time. Railway track curvature becomes extremely complex when considering the combinations that are possible. It is possible to have any combination of straights, curves, transitions and also irregularities. A good solution to the problem should be able to analyse any section of track and must be compatible with a moving co-ordinate system. After many ideas were explored the preferred solution to the problem was decided upon. The algorithm consisted of

adding up the X and Y displacements while stepping along the track, as shown in Figure 3-10 and Figure 3-11.

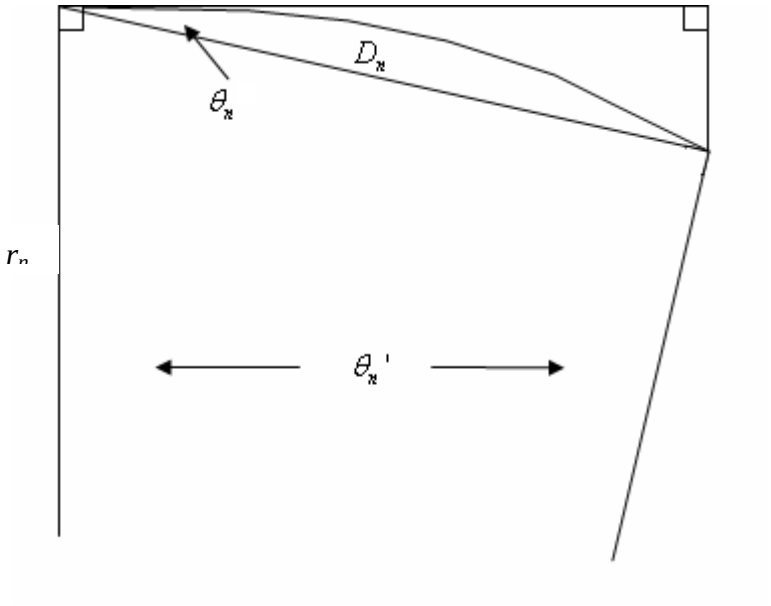

Figure 3-10: Coupler Angling Algorithm Trigonometry Diagram

$$\theta_n = \theta_n' = \sin^{-1}\left(D_n\left(\frac{1}{r_n}\right)\right) \tag{3.1}$$

Where θ_n' is the angle at that instant for the step size, D_n is the step size and $\frac{1}{r_n}$ is the curvature. The track is broken up into small track sections. The total X and Y axis can be found by adding the X and Y sections of each small section, as shown in Figure 3-11.

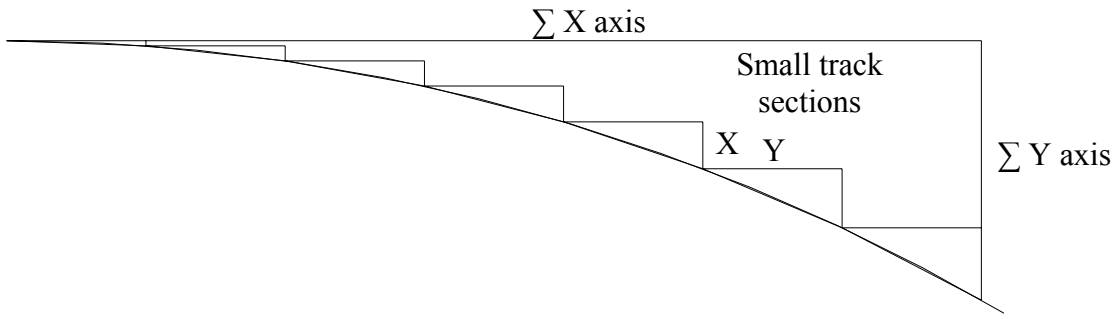

Figure 3-11: Coupler Angling Algorithm Trigonometry Stepping Diagram

3.3.3.1. The Algorithm

An overview of the final procedure is shown below for reference purposes.

To determine coupler angle 1 and coupler angle 2 substitute $\theta 1, \theta 2$, H1, H2 and H3 into equation (3.16) and (3.17). Refer to Figure 3-16 for the diagram.

$$\theta c1 = \theta 1 + \sin^{-1}\left(\frac{(H1)\sin\theta 1 - (H2)\sin\theta 2}{H3}\right) \qquad (3.16)$$

$$\theta c2 = \theta 2 - \sin^{-1}\left(\frac{(H1)\sin\theta 1 - (H2)\sin\theta 2}{H3}\right) \qquad (3.17)$$

To determine $\theta 1$ and $\theta 2$ use equation (3.9) and (3.10), as shown in Figure 3-15.

$$\theta 1 = \theta 1' + \theta 1'' \qquad (3.9)$$

$$\theta 2 = \theta 2' + \theta 2'' \qquad (3.10)$$

To determine each variable the following procedures should be used.

- To calculate $\theta 1'$ start at position P2 using equation (3.2), (3.6), (3.7) and (3.8) iterate back to P1.

- To calculate $\theta 1$" start at position P2 using equation (3.2), (3.6), (3.7) and (3.8) iterate forward to P3.
- To calculate $\theta 2$' start at position P3 using equation (3.2), (3.6), (3.7) and (3.8) iterate back to P4.
- To calculate $\theta 2$" start at position P2 using equation (3.2), (3.6), (3.7) and (3.8) iterate forward to P3.

$$\theta_n = \theta_{n-1} + \sin^{-1}\left(\frac{D_n}{r_n}\right) \tag{3.2}$$

$$Y_n = Y_{n-1} + \frac{D_n \sin\theta_{n-1}}{\cos\left(\sin^{-1}\left(\frac{D_n}{r_n}\right)\right)} + \left(\frac{D_n^2}{r_n}\right)\sin\left(\frac{\pi}{2} - \theta_{n-1} - \sin^{-1}\left(\frac{D_n}{r_n}\right)\right) \tag{3.6}$$

$$X_n = X_{n-1} + \frac{D_n \cos\theta_{n-1}}{\cos\left(\sin^{-1}\left(\frac{D_n}{r_n}\right)\right)} \tag{3.7}$$

Where Y_{n-1}, X_{n-1} and θ_{n-1} are initially zero.

$$\theta = \tan^{-1}\left(\frac{Y_n}{X_n}\right) \qquad \text{The angle for the curve.} \tag{3.8}$$

In order to calculate the coupler angles it is necessary to calculate the angle between the track tangent of the first point and the second point. The algorithm must be able to calculate this on any section of track with any complexity including straights, constant radius curves, transitions, irregularities and any combination of these.

For a small section of track it is assumed that:

- The distance between two points on a curve is straight.
- Xn'≈Xn'' as shown in Figure 3-12. When Xn'-Xn''= 0 there is no error.

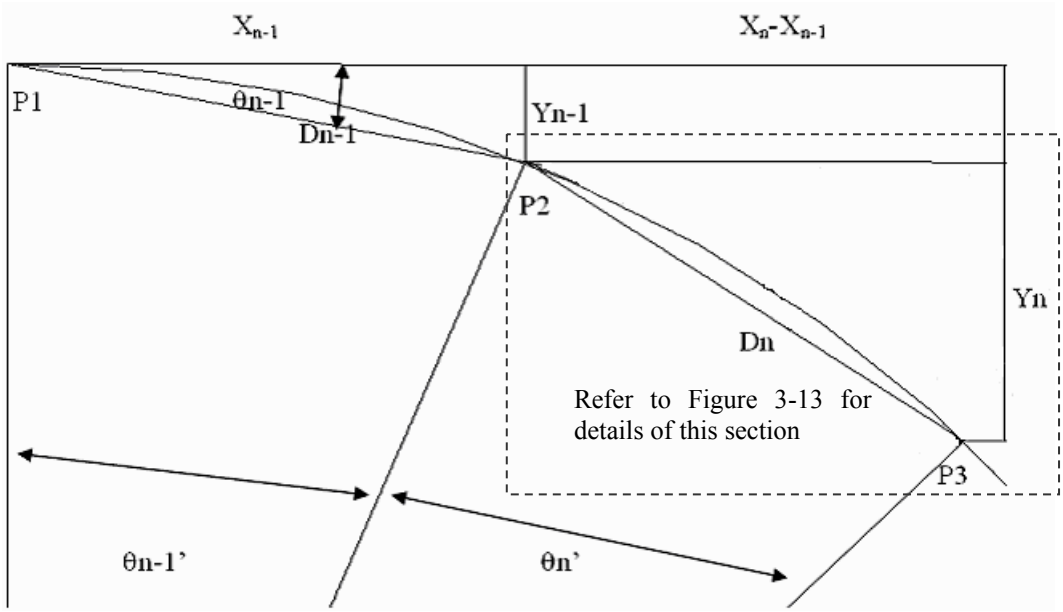

Figure 3-12: Overview of Coupler Angling Algorithm Diagram

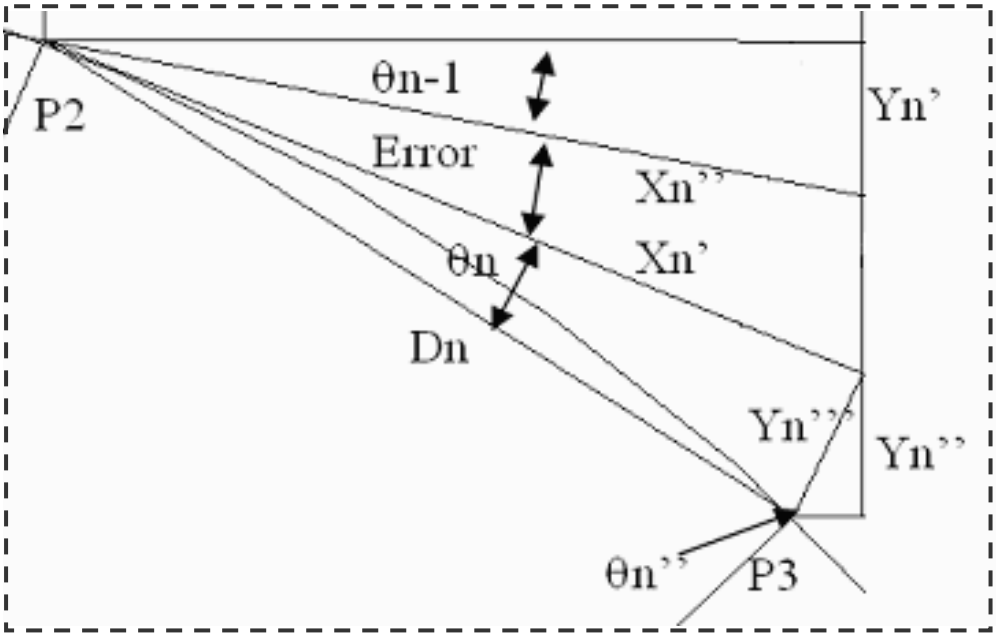

Figure 3-13: Magnified View of Coupler Angling Algorithm Diagram

Please refer to the nomenclature on page xiv for definition of symbols.

Solution for θ_n.

$$\theta_n = \theta_{n-1} + \theta_n' \text{ and } \theta_n = \sin^{-1}\left(\frac{D_n}{r_n}\right)$$

$$\therefore \theta_n = \theta_{n-1} + \sin^{-1}\left(\frac{D_n}{r_n}\right) \tag{3.2}$$

Where θ_{n-1} is initially zero.

Solution for Y_n.

$$Y_n = Y_{n-1} + Y \text{ and } Y = Y_n' + Y_n''$$

Where Y_{n-1} is initially set to zero.

$$\therefore Y_n = Y_{n-1} + Y_n' + Y_n'' \tag{3.3}$$

$$Y_n' = X_n' \sin\theta_{n-1} \text{ and } X_n' = \frac{x}{\cos\theta_n}$$

$$\therefore Y_n' = \left(\frac{D_n}{\cos\theta_n}\right)\sin\theta_{n-1} \tag{3.4}$$

$$Y_n'' = Y_n''' \sin\theta_n'' \text{ and } Y_n''' = X_n \sin\theta_n.$$

$$\therefore Y_n'' = \left(X_n \sin\theta_n\right)\sin\theta_n''$$

$$\theta_n'' = \frac{\pi}{2} - \theta_n \text{ and } \theta_n = \theta_{n-1} + \sin^{-1}\left(\frac{D_n}{r_n}\right)$$

$$\therefore \theta_n'' = \frac{\pi}{2} - \left(\theta_{n-1} + \sin^{-1}\left(\frac{D_n}{r_n}\right)\right)$$

$$\therefore Y_n'' = \left(D_n \sin\theta_n\right)\sin\left(\frac{\pi}{2} - \left(\theta_{n-1} + \sin^{-1}\left(\frac{D_n}{r_n}\right)\right)\right) \tag{3.5}$$

Final equation with (3.3), (3.4) and (3.5).

$$Y_n = Y_{n-1} + Y_n' + Y_n''$$

$$Y_n = Y_{n-1} + \left(\frac{D_n}{\cos\theta_n}\right)\sin\theta_{n-1} + \left(D_n \sin\theta_n\right)\sin\left(\frac{\pi}{2} - \left(\theta_{n-1} + \sin^{-1}\left(\frac{D_n}{r_n}\right)\right)\right)$$

Substitute

$$Y_n = Y_{n-1} + \left(\frac{D_n}{\cos\left(\sin^{-1}\left(\frac{D_n}{r_n}\right)\right)}\right)\sin\theta_{n-1} + \left(D_n \sin\left(\sin^{-1}\left(\frac{D_n}{r_n}\right)\right)\right)\sin\left(\frac{\pi}{2} - \left(\theta_{n-1} + \sin^{-1}\left(\frac{D_n}{r_n}\right)\right)\right)$$

Simplifying

$$Y_n = Y_{n-1} + \frac{D_n \sin\theta_{n-1}}{\cos\left(\sin^{-1}\left(\frac{D_n}{r_n}\right)\right)} + \left(\frac{D_n^2}{r_n}\right)\sin\left(\frac{\pi}{2} - \theta_{n-1} - \sin^{-1}\left(\frac{D_n}{r_n}\right)\right) \qquad (3.6)$$

Where Y_{n-1}, X_{n-1} and θ_{n-1} are initially zero.

Solution for X_n.

$$X_n = D_n'\cos\theta_{n-1} \text{ and } D_n' = \frac{x}{\cos\theta_n}$$

$$\therefore X_n = X_{n-1} + \left(\frac{D_n}{\cos\theta_n}\right)\cos\theta_{n-1}$$

$$\theta_n = \sin^{-1}\left(\frac{D_n}{r_n}\right)$$

$$\therefore X_n = X_{n-1} + \frac{D_n \cos\theta_{n-1}}{\cos\left(\sin^{-1}\left(\frac{D_n}{r_n}\right)\right)} \qquad (3.7)$$

The final equations are:

$$\theta_n = \theta_{n-1} + \sin^{-1}\left(\frac{D_n}{r_n}\right) \tag{3.2}$$

$$Y_n = Y_{n-1} + \frac{D_n \sin\theta_{n-1}}{\cos\left(\sin^{-1}\left(\frac{D_n}{r_n}\right)\right)} + \left(\frac{D_n^2}{r_n}\right)\sin\left(\frac{\pi}{2} - \theta_{n-1} - \sin^{-1}\left(\frac{D_n}{r_n}\right)\right) \tag{3.6}$$

$$X_n = X_{n-1} + \frac{D_n \cos\theta_{n-1}}{\cos\left(\sin^{-1}\left(\frac{D_n}{r_n}\right)\right)} \tag{3.7}$$

Where Y_{n-1}, X_{n-1} and θ_{n-1} are initially zero.

These equations are iterated. The value of D_n should be small. As D_n is decreased the accuracy increases.

Once X_n and Y_n are calculated Figure 3-14 can be constructed and the angle can be calculated.

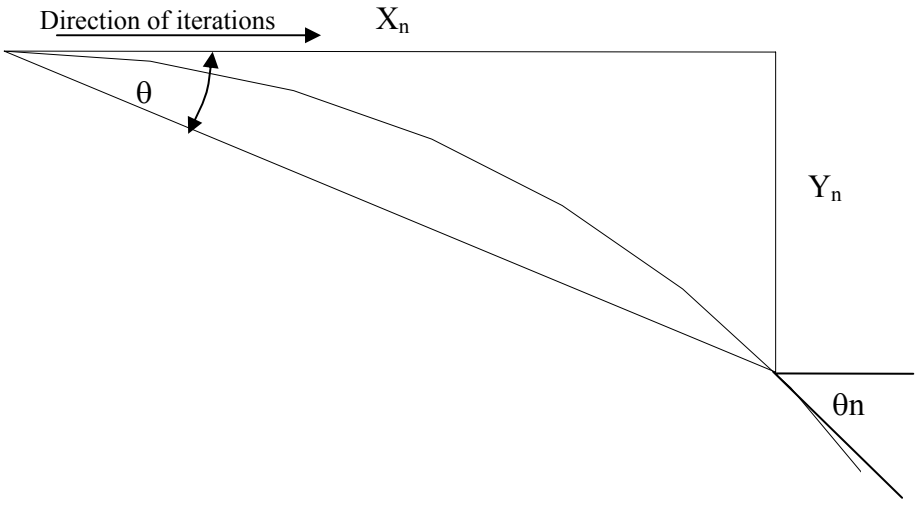

Figure 3-14: Coupler Angling Algorithm Final Angle Diagram

$$\theta = \tan^{-1}\left(\frac{Y_n}{X_n}\right) \qquad \text{The angle for the curve.} \qquad (3.8)$$

The algorithm allows the angle to be calculated between the tangent of the first point and the second point, as shown in Figure 3-14. In order to calculate the coupler angles the calculations must be made from the details of the each vehicle pair, it is shown in, Figure 3-15. The algorithm outlined below shows the method of calculating coupler angles based on vehicle details.

The assumptions for this algorithm are:

- The connection of the two coupler-shanks between vehicles remains straight. It is modelled as a drawbar that varies in length due to coupler slop.
- Wheel sets always remain centred on the track.
- There is minimal or negligible body roll.
- There is no vertical coupler angle.

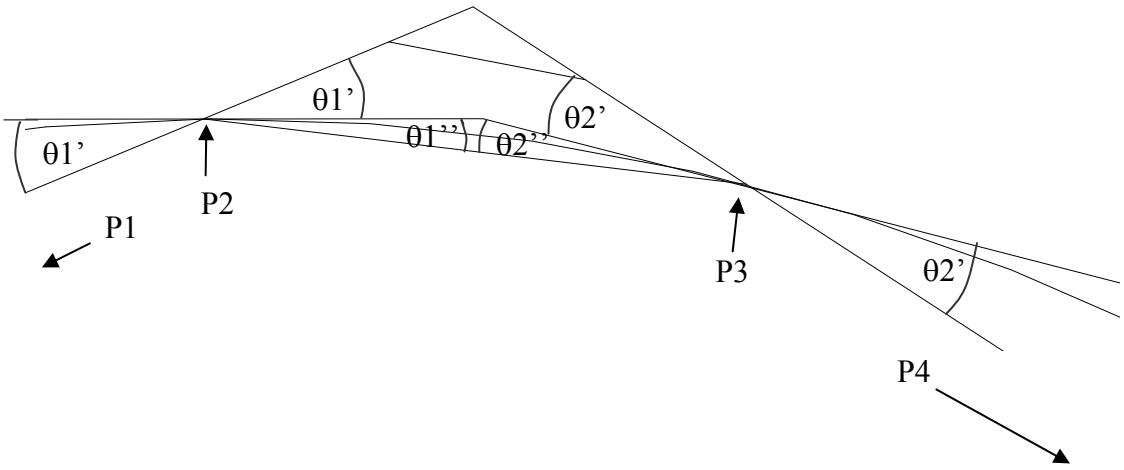

Figure 3-15: Algorithm Angle Calculation Diagram

Please refer to the nomenclature on page xiv for definition of symbols.

$$\theta 1 = \theta 1' + \theta 1'' \tag{3.9}$$

$$\theta 2 = \theta 2' + \theta 2'' \tag{3.10}$$

To calculate the angles use the algorithm using equations (3.2), (3.6), (3.7) and (3.8).

$$\theta_n = \theta_{n-1} + \sin^{-1}\left(\frac{D_n}{r}\right) \tag{3.2}$$

$$Y_n = Y_{n-1} + \left(D_n \sin\theta_{n-1} \tan\left(\frac{D_n}{r}\right)\right) + \frac{D_n^{\,2}}{r}\cos\left(-\theta_{n-1} - \sin^{-1}\left(\frac{D_n}{r}\right)\right) \tag{3.6}$$

$$X_n = X_{n-1} + \left(D_n \tan\left(\frac{D_n}{r}\right)\right)\cos\theta_{n-1} \tag{3.7}$$

Where Y_{n-1}, X_{n-1} and θ_{n-1} are initially zero.

$$\theta = \tan^{-1}\left(\frac{Y_n}{X_n}\right) \qquad \text{The angle for the curve.} \tag{3.8}$$

To determine each variable the following procedures should be used.

- To calculate $\theta 1'$ start at position P2 using equation (3.2), (3.6), (3.7) and (3.8) iterate back to P1.
- To calculate $\theta 1''$ start at position P2 using equation (3.2), (3.6), (3.7) and (3.8) iterate forward to P3.
- To calculate $\theta 2'$ start at position P3 using equation (3.2), (3.6), (3.7) and (3.8) iterate back to P4.
- To calculate $\theta 2''$ start at position P2 using equation (3.2), (3.6), (3.7) and (3.8) iterate forward to P3.

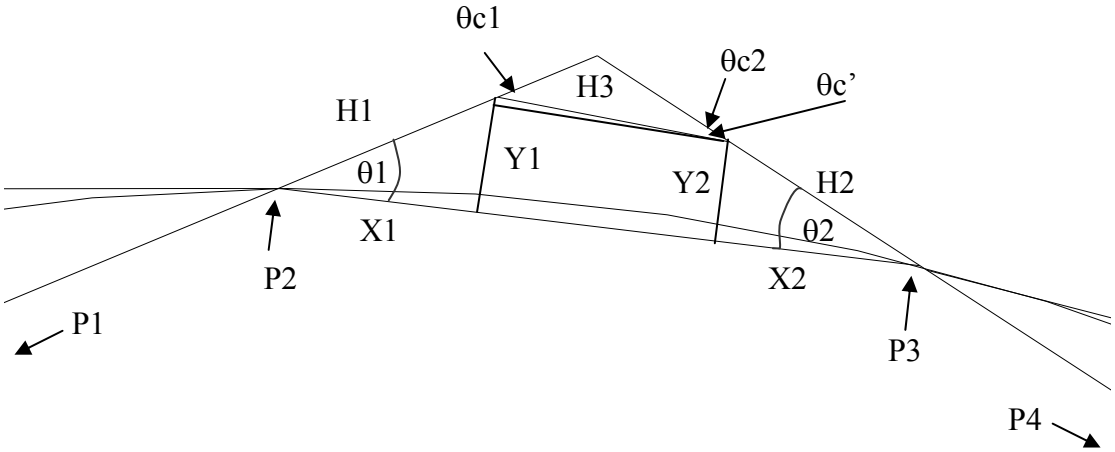

Figure 3-16: Coupler Angling Wagon Diagram

θc1 and θc2 is coupler angles 1 and 2, H1 and H2 is the distance from the bogie centre to coupler pin (overhang) of vehicle 1 and 2, H3 is the coupler slop plus the distance between the centre pin to the knuckles of both couplers, θ1 and θ2 is the angle between the overhang and line between both bogie centres and θc' is the angle created due to the difference in height of Y1 and Y2.

$$Y1 = H1\sin\theta 1 \tag{3.11}$$

$$Y2 = H2\sin\theta 2 \tag{3.12}$$

$$\theta c' = \sin^{-1}\left(\frac{Y1 - Y2}{H3}\right) \tag{3.13}$$

$$\theta c1 = \theta 1 + \theta c' \tag{3.14}$$

$$\theta c2 = \theta 2 - \theta c' \tag{3.15}$$

Substituting equation (3.11), (3.12) and (3.13) into (3.14) and (3.15) gives:

$$\theta c1 = \theta 1 + \sin^{-1}\left(\frac{(H1)\sin\theta 1 - (H2)\sin\theta 2}{H3}\right) \tag{3.16}$$

$$\theta c2 = \theta 2 - \sin^{-1}\left(\frac{(H1)\sin\theta 1 - (H2)\sin\theta 2}{H3}\right) \tag{3.17}$$

3.3.3.2. Error in the Algorithm

The amount of error in the algorithm is dependent on the step size. If a small step size is used the amount of error is small. For Table 3-2 a step size of 0.05m was used. The accuracy was acceptable as shown in Table 3-2 while the processing power was still relatively low. Table 3-2 shows that as the curve radius is increased the accuracy of the algorithm increases. The actual angle shown in Table 3-2 was calculated by hand using trigonometry.

Table 3-2: Algorithm Error

Curve Radius	Actual Angle	Calculated Angle	Error
200	2.14000	2.14022	0.0105%
400	1.00500	1.00761	0.0026%
600	0.39000	0.39042	0.0011%
800	0.05330	0.05332	0.0004%

The only downfall when calculating angles between wagons is that simulation time is increased by 200%. Significant improvements can be made by not using the algorithm when a wagon pair is on straight track sections or on constant radius curve. When the track is straight at the four bogie positions the coupler angle can be assumed to be zero. This would improve the simulation speed considerably as the major proportion of track is straight. When the track curvature is the same at each bogie position and not equal to zero an alternative method of calculating the angle

could be used based on constant radius curves. These features were not incorporated into the algorithm as simulation speed was adequate for the study program.

3.3.4. Implementation of Coupler Angling Code into CRE-LTS

The coupler angling algorithm outlined in the previous section of this thesis was incorporated into the existing CRE-LTS simulator. The algorithm allowed coupler angles to be calculated at every time step in the simulation. The resulting output gave a full database of the coupler angles for every vehicle in the train. Longitudinal and lateral components of in-train forces were then calculated.

3.4. Data Processing and Automation Methods

Data processing was necessary to process the simulation data produced by simulation packages. The simulation software used in this thesis provided little automation and compatibility, so alternative methods were used and developed. The data processing and automation methods used in this thesis are outlined below.

3.4.1. Force Analysis Interface

The coupler angle and longitudinal force databases created by CRE-LTS were too large to be viewed in Excel. A force analysis interface was created in National Instrument Measurement Studio so that the database could be viewed, selected and extracted. Code was added to CRE-LTS to allow selected forces, curvature and

coupler angles to be written to a comma-delimited file. This information was processed using the user interface shown in Figure 3-17.

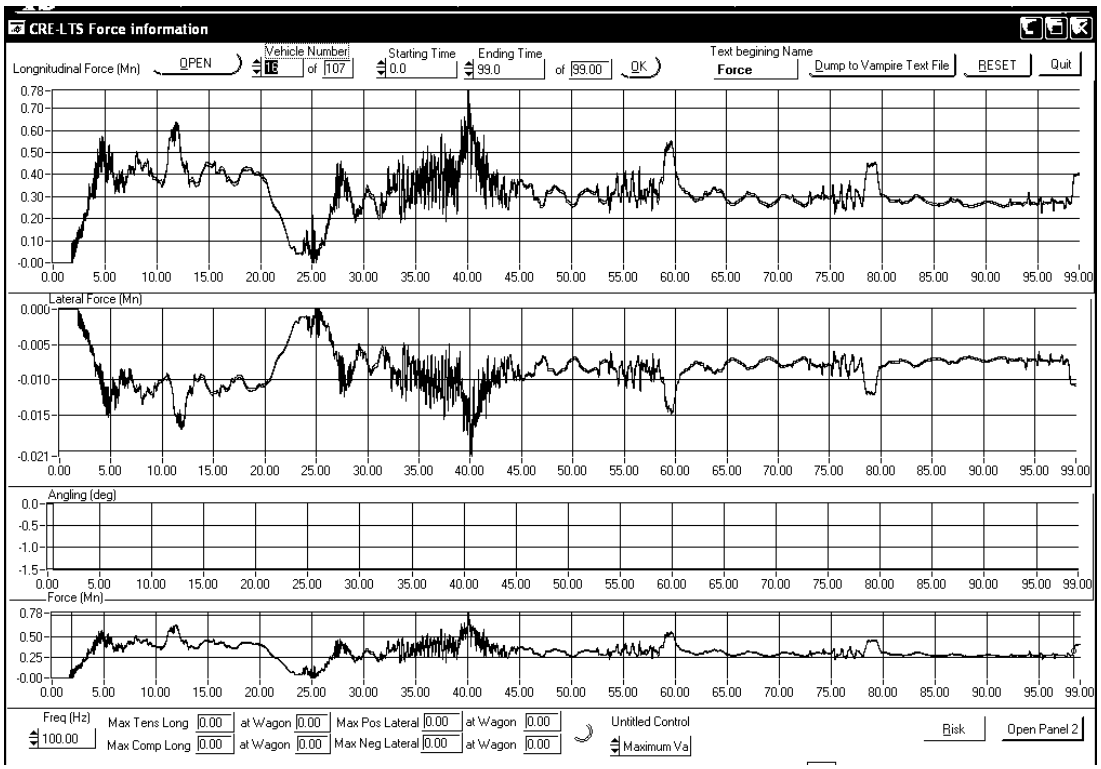

Figure 3-17: Screen Dump of Force Processing Interface

The following functions were added to the interface.

- Viewing and zooming capabilities.
- Search capabilities.
- Filtering capabilities.
- VAMPIRE force file dump.
- Screen dump and printing capabilities.
- Risk assessment processing capabilities.

For the interface to function properly a number of tasks needed to be performed. The interface first needed to read in the files created in CRE-LTS and process them so that they could be plotted. Once the curvature, coupler angling and force files were read into memory, the in-train lateral and longitudinal forces were calculated from the coupler angles and forces at each wagon position. They were then graphed using the graphical user interface library functions.

Navigation functions were also needed. The interface allows a user to specify the wagon position that they wish to view. The user can also zoom in for a more in depth analysis of the data. The zooming abilities of the interface are only restricted by the frequency of the data. The simulations that are produced in CRE-LTS output data at 100 samples/sec. This data sampling rate gives very good resolution and definition to force files when they are viewed using the interface.

The quantity of output data that is produced by CRE-LTS makes it difficult to locate the worse impacts and accelerations in the data. Searching capabilities were added to the interface to speed up the process. A number of searching capabilities were added based on the type of forces that the user is searching for.

3.4.2. Processing of Simulation Data

The following force search capabilities were added:

- Maximum average longitudinal force over a given time which is specified in the interface.

- Maximum average acceleration over a given time which is specified in the interface.
- Largest magnitude impact.

The maximum average longitudinal force was calculated by taking the average magnitude of the force profile over a given time window. The train position of this maximum average was then displayed on the screen for positive and negative forces. The maximum average acceleration over a given time window was calculated in a similar fashion to the maximum average longitudinal force. Instead of using the maximum force magnitude, the maximum difference in front and rear coupler forces was used as an indicator of maximum acceleration. The position of the maximum difference in front and rear coupler forces value was then displayed on screen.

Finding the largest magnitude impact was the most difficult to implement of the three criteria. It involved the application of three Butterworth filters and then locating a force that began at approximately zero and had a high gradient. An impact is defined as "the collision of two bodies and is characterised by the generation of relatively large contact forces that act over a very short interval of time", (Meriam and Kraige, 1993). The three stages of the Butterworth filter were used to filter the data to approximate the 50ms criteria, (AAR, 1993).

The three filter stages were:

1. A 5Hz 1 pole Digital Butterworth Filter
2. A 40Hz 1 pole Digital Butterworth Filter
3. A 8Hz 5 pole Digital Butterworth Filter

These three stage Butterworth filters approximate to the AAR 50ms criteria, (Cole, 2004). As an impact force must be associated with a collision it is required that the force profile begins at approximately zero or passes through zero. As large forces are expected to act over a short time interval the force profile also needs to have a steep gradient.

It was necessary to develop an algorithm to categorise the forces into steady and impact forces. An example of an impact force is shown in Figure 3-18. The coupler slack between vehicles and the design of the coupler makes it possible for an impact to occur for buff and draft forces, so a negative or positive force impact can occur.

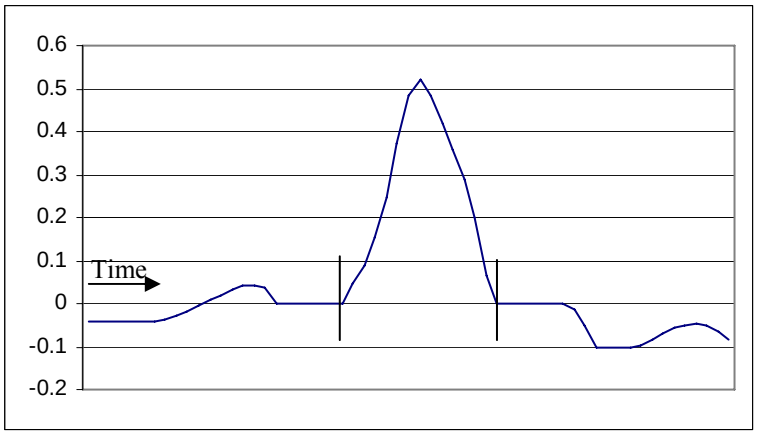

Figure 3-18: Impact Force Profile

When processing the force profiles it was assumed that if the force profile was not an impact force, then it was considered a non-impact force. A non-impact force is defined as a force profile that does not meet the criteria of an impact force. A non-impact force profile consists of steady forces, low frequency transients and high frequency transients. Steady forces, low frequency and high frequency transients all give simular wagon dynamic behaviours as the forces do not create wagon or bogie

pitch. There was some difficulty in determining the point when an impact force became a non-impact force. Figure 3-19 has the characteristics of an impact force but it does not have the characteristics of the initial collision conditions. Some impact type forces are shown in Figure 3-19 and Figure 3-20. It was decided that an impact force needed to be clearly defined.

For the purpose of this thesis an impact is defined as a force that:

- Can be initially positive or negative.
- Begins at approximately zero or passes through zero.
- Has an absolute loading rate gradient value of greater than 200kN/s.
- The maximum absolute value of the impact must occur within 1 second from when the force was approximately zero.
- The force must decrease in magnitude after the initial impact.

The force profiles were processed using computer code which was written in the C programming language. It was designed to extract impact and non-impact forces from the longitudinal force profiles. Force distribution curves and probabilities could then be calculated specifically for non-impact or impact forces. The computer code necessary to extract impact forces and non-impact forces from the force profiles became complex. A flow chart of the process is shown in Figure 3-21.

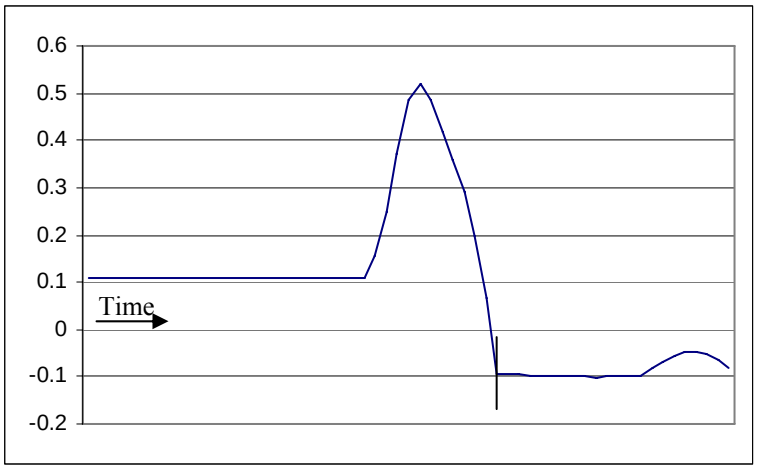

Figure 3-19: Example #1 Impact Type Force

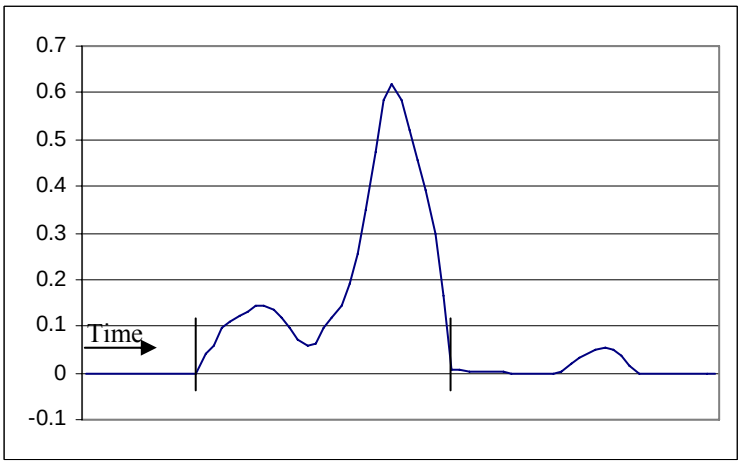

Figure 3-20: Example #2 Impact Type Force

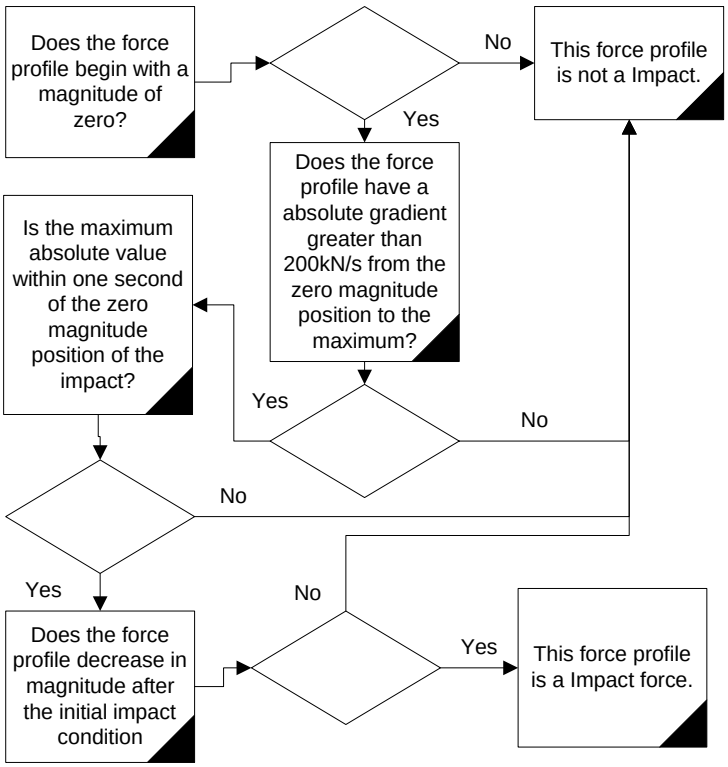

Figure 3-21: Flow Chart of Determining an Impact Force

Figure 3-18, Figure 3-19 and Figure 3-20 shows force profiles of impact type forces. Figure 3-18 is definitely an impact force providing that it has a high enough gradient and the maximum is within one second of the initial zero. The start position and ending position is shown by two lines in Figure 3-18. Following this example through the flowchart in Figure 3-21 the starting position and the maximum is within one second of each other it satisfies all criteria. Figure 3-19 shows an impact type force but there is no zero starting position so it is not an impact force. Figure 3-20 shows another impact type force and in this instant this force profile would be an impact if the maximum is within one second of the starting zero position. The starting and ending positions are indicated by two lines.

The computer code that classified force profiles into non-impact and impact forces began by first finding an absolute magnitude of approximately zero before the absolute value of the magnitude increased. A positive or negative impact could occur so it was necessary to determine the initial gradient. If the gradient was positive then it was a potential positive impact and if it was negative then it could be a negative impact. If the gradient was zero then it was necessary to move the analysis window forward.

Once the gradient was calculated it was necessary to determine a maximum value over a one second time window. A minimum value was also found to ensure that the force profile did not cross the zero axis before the maximum. The end of the impact force was found by determining the minimum value within one second of the maximum value. If the force profile met all the above specifications then the section of data was passed into the impact array. The longitudinal impact and longitudinal non-impact force arrays were used for processing to determine event probabilities and plotting distribution curves. The process used to determine event probabilities and distribution curves is discussed in the next section.

To make the task of extracting data from CRE-LTS easier, a function to produce a text file was added to the interface. Once an appropriate section of data was selected the interface creates force files in the VAMPIRE format to allow coupler forces to be applied to the VAMPIRE model. Each coupler force is broken into longitudinal and lateral forces giving a total of four forces, two for each coupler as shown in Figure 3-22.

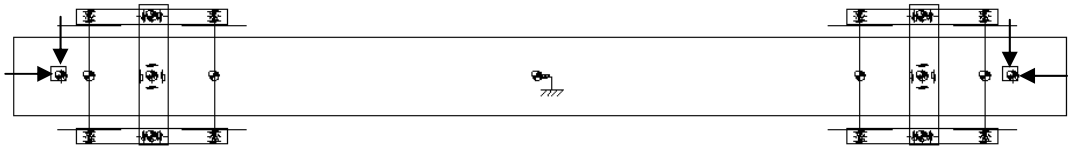

Figure 3-22: Application Positions of Coupler Forces in VAMPIRE

Screen dumping and printing capabilities were added to the interface to save time when presenting graphical data. These functions allowed graphical outputs to be able to be inserted into Microsoft Word and the printing capabilities also allowed the creation of Adobe Acrobat files (PDF's). The interface was also later modified to included risk analysis tools as described in the next section.

3.4.3. Derailment Risk Assessment

In order to assess the risk of an event, it is necessary to determine how often an event occurs. From the event-frequency information, probability information can be deduced. Simulations in CRE-LTS were analysed to determine probability density functions and therefore the probability of an event occurring. Event counting functions were added to the Force Analysis Interface for coupler forces, curvature and coupler angle files.

The force analysis interface can plot event distribution curves and calculate event probabilities for:

- Longitudinal impact forces.
- Longitudinal non-impact forces.
- Longitudinal forces.

- Lateral forces.
- Coupler angles.
- Curvature.
- Rate of change of curvature.

An example of probability distribution curves is shown in Figure 3-23. The process of constructing these distribution curves is outlined in the next section. The tools added to the force analysis interface also allowed probabilities of different scenarios to be calculated. The probability of a longitudinal coupler force between -0.02MN and 0.03MN for a 75mm coupler slack can be easily calculated using the Force Analysis Interface in Figure 3-23, the probability is 50.7%. Calculations can be made to determine the probability of a specific event occurring using the tools in the interface. Probabilities and probability density functions can also be calculated on specific vehicle positions and vehicle position ranges. A screen dump of the Force Analysis Interface is shown in Figure 3-24.

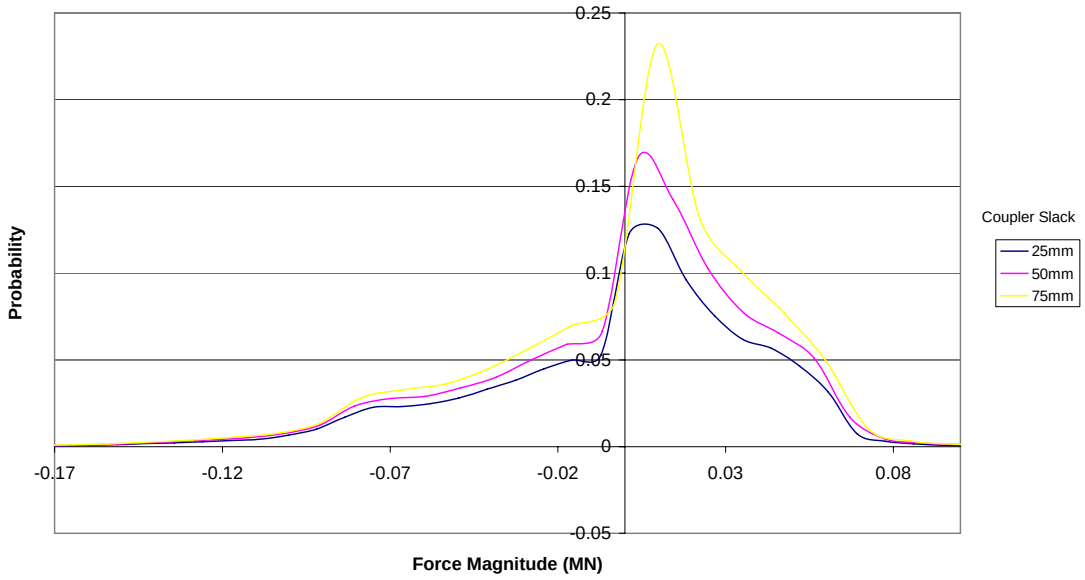

Figure 3-23: Example Probability Distribution Curve for Longitudinal Coupler Forces

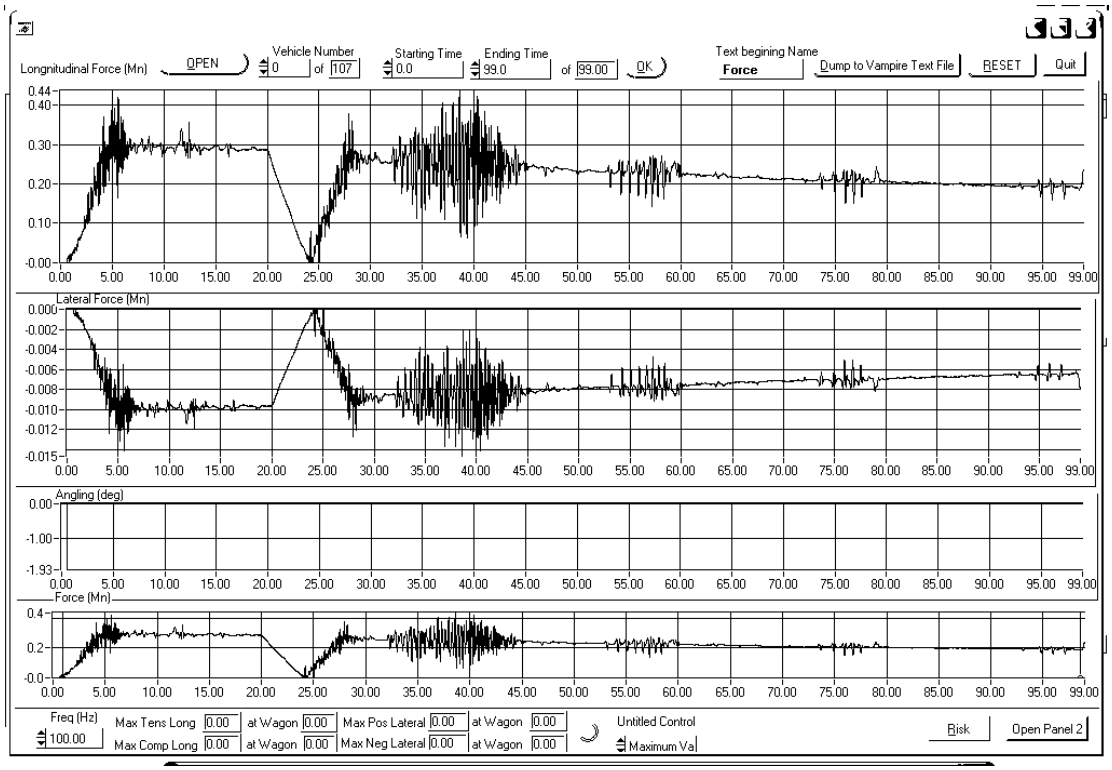

Figure 3-24: Force Analysis Screen Dump

The probability of the vehicle being on the curve transition was also analysed so that it is possible to determine the probability of a non-impact or impact force occurring on a curve transition.

3.4.3.1. Force Probability Distribution Curve

One of the tasks of this thesis was determining the probability of a given event occurring and relating the event to some measure of derailment risk. A program was written based on normal distribution theory and it was found to be unsatisfactory, it was found that the force distribution curve for the simulations completed were not normally distributed. Alternative methods of solving the problem were formulated. The method used to create a force distribution curve consisted of specifying a

number of force ranges and counting the number of force occurrences in each range. A large number of force ranges could be specified to increase the accuracy of the distribution curve. The force distribution curve could then be analysed to determine event probabilities.

The existing Force Analysis Interface covered in Section 3.4.1 included many functions which would be helpful when analysing force, angle and curve profiles, so a new screen linked to the current interface was added. Two simular functions were written in the C programming language for processing the arrays simulated in CRE-LTS. The first function calculated the probability of an event occurring in a given range and the other created an array which could be plotted to show the probability distribution. The probability function calculated event probabilities by iterating through the specified section of the array and determining the number of values in the specified range. The total number of elements in the specified section of the array was also recorded.

After iterating through the selected section of the array the number of values in the specified range is known and the number of total values is also known. The number of values in the specified range divided by the total number of values is the probability of that specified event occurring. The second function collected this information to provide a probability distribution curve. It was simular to the procedure used to calculate event probabilities but it consisted of a number of ranges to find event probabilities.

A large number of ranges were specified. The number of events in each range divided by the total number of events gave the probability for each range. This allowed the creation of a probability distribution curve. The number of ranges specified in the risk section of the Force Analysis Interface was 1000. This allowed a smooth probability distribution curve while not requiring large amounts of processing power. Figure 3-25 shows a screen shot of the risk section of the Force Analysis Interface showing an example of a probability distribution curve.

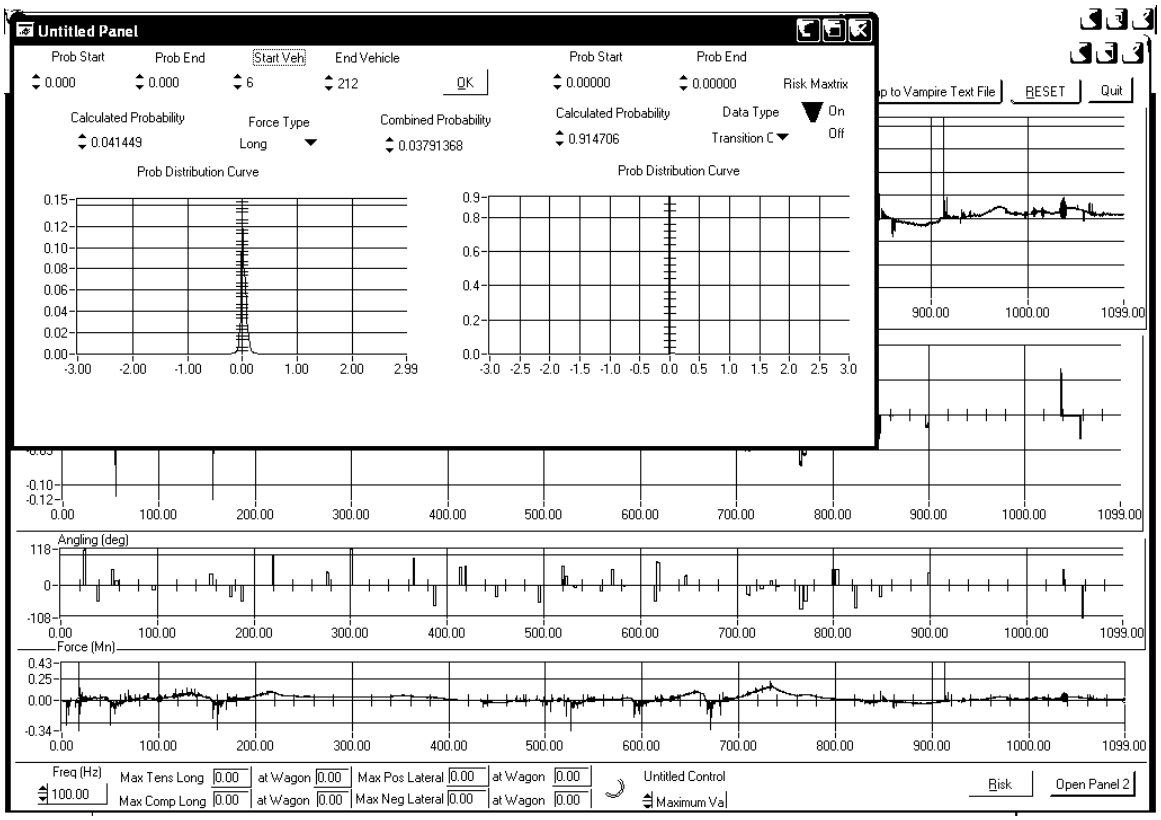

Figure 3-25: Screenshot of the Risk Section of the Force Analysis Interface

3.4.4. Utility Programs

Several utility programs were used during this thesis to simplify tasks, automate tasks and batch simulations. The use of these utility programs reduced the time consuming and repetitive tasks associated with completing large numbers of simulations. UltraEdit was used to create large numbers of text files for VAMPIRE and CRE-LTS.

3.4.5. User Involvement Simulation Package

WinBatch is a user involvement simulation package. It is a small program that can record mouse clicks, keyboard inputs and a range of other input devices. Once the inputs are recorded they can be played back to perform tasks on the computer desktop as though a user was physically controlling the mouse, keyboard etc. WinBatch is therefore very useful for automating batches of jobs on software designed only for keyboard/mouse user input. A flow chart is show in Figure 3-26.

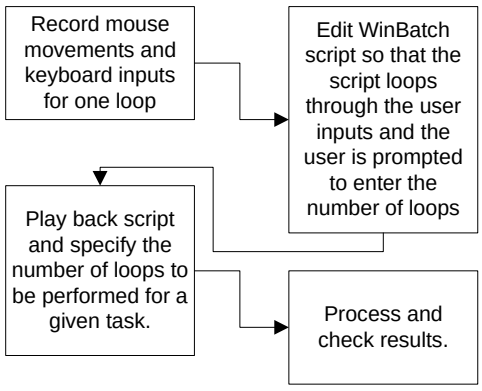

Figure 3-26: Flow Chart for WinBatch Scripts

WinBatch was used to automate the production of graphs and comma-delimited (csv) spreadsheet files from VAMPIRE simulations. The production of 100 sets of graphs and spreadsheet outputs became a simple process of setting up a 100 loops and waiting for simulations to be completed.

3.4.6. Determining the Minimum and Maximum Values from VAMPIRE Export Files.

To make the task of extracting minimum and maximum values for each VAMPIRE simulation easier, a small program was written in the C programming language.

After VAMPIRE was controlled using WinBatch to export the VAMPIRE simulations, the minimum and maximum values for wheel unloading and L/V ratio were needed from each spreadsheet. The program read the VAMPIRE output files and collected the maximum values by compiling a report table as shown Table 3-3.

Table 3-3: Sample of Exported Data

		Wheel Unloading Left 1 (%)	Wheel Unloading Right 1 (%)	Wheel Unloading Left 2 (%)	Wheel Unloading Right 2 (%)
d:\Vampire\ 0200R 25mm slop 6.65.csv	Max	44.22	88.57	44.44	45.77
d:\Vampire\ 0200R 25mm slop 6.75.csv	Max	44.24	81.96	45.98	28.32
d:\Vampire\ 0200R 25mm slop 6.85.csv	Max	44.45	80.68	43.15	25.01
d:\Vampire\ 0200R 25mm slop 6.95.csv	Max	44.19	78.35	40.18	25.91

3.4.7. Creating VAMPIRE Simulation Files.

Creating simulation parameter files for VAMPIRE can be tedious and time consuming. VAMPIRE uses a ten space delimited format for most of its input files. This includes track files, force files, irregularity files, etc. It was found that these files needed to be formatted exactly. A small program was created to convert excel files into the VAMPIRE format. This program converts a number of comma(CSV), space, or tab delimited files to a ten space delimited format. It was used throughout this thesis to create a range of files.

Once the program is executed a small screen is displayed where you can choose a number of files, as shown in Figure 3-27. Once the list of files is selected, files with a .dat extension were created with the VAMPIRE file format. This allowed files to be created in excel using the various functions and formulas available in the software and then convert it into a VAMPIRE format.

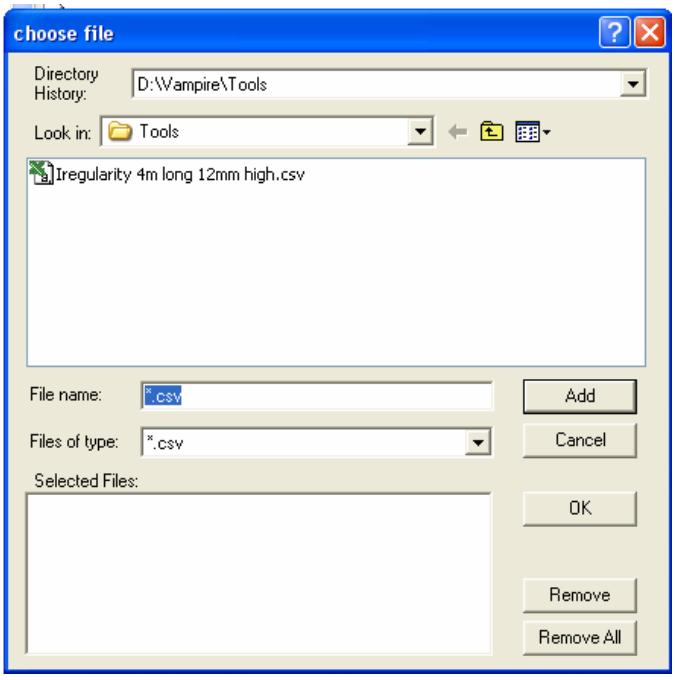

Figure 3-27: Excel to VAMPIRE File Converter Interface

4 WAGON MODEL VALIDATION

4.1. Introduction

Validating a mathematical model is necessary to ensure that it has the correct dynamic behaviour. Validation should be performed in the types of simulation that are of interest for the research that is being performed. It can never be certain that a complicated model such as a wagon model is valid on all domains. Therefore it can not be certain that the results produced for a given simulation are correct unless they are compared to experimental data (in similar modes of operation). To ensure that the results produced for this thesis are representative of rollingstock performance, the following validation tests were performed on the model:

1. Hunting test.
2. Comparison of wheel unloading due to steady lateral loads to the results published by (El-Sibaie, 1993).
3. Comparison of wheel unloading due to bogie pitch to the results published by (McClanachan *et al*, 2000).

4.2. Hunting Test

Railway vehicle hunting was briefly introduced in Section 2.4.2. The critical hunting speed is dependent on a large number of vehicle parameters. If a simulation of a vehicle model hunts at or near the known hunting speed for that vehicle, it is a good indication that the vehicle model parameters related to the wheel rail profiles and bogie steering are representative of that vehicle. An initial track irregularity was

used to laterally excite the vehicle. If the oscillations do not diminish and continue for 30 seconds on straight track it is considered hunting behaviour, (McClanachan and Roach, 2000).

4.2.1. Test Procedure

The track irregularity was a lateral cusp as shown in Figure 4-1. The irregularity was 4 metres long with a maximum lateral displacement of 12mm for both rails. A number of vehicle speeds were tested to determine the critical hunting speed. Speeds from 21m/s (75.6kph) to 30m/s (108kph) were tested in steps of 1.5m/s. The vehicle model validated for use in the thesis was the empty VAMB wagon with an empty mass of 15 tonnes, as discussed in Section 3.3.1.1 on page 36.

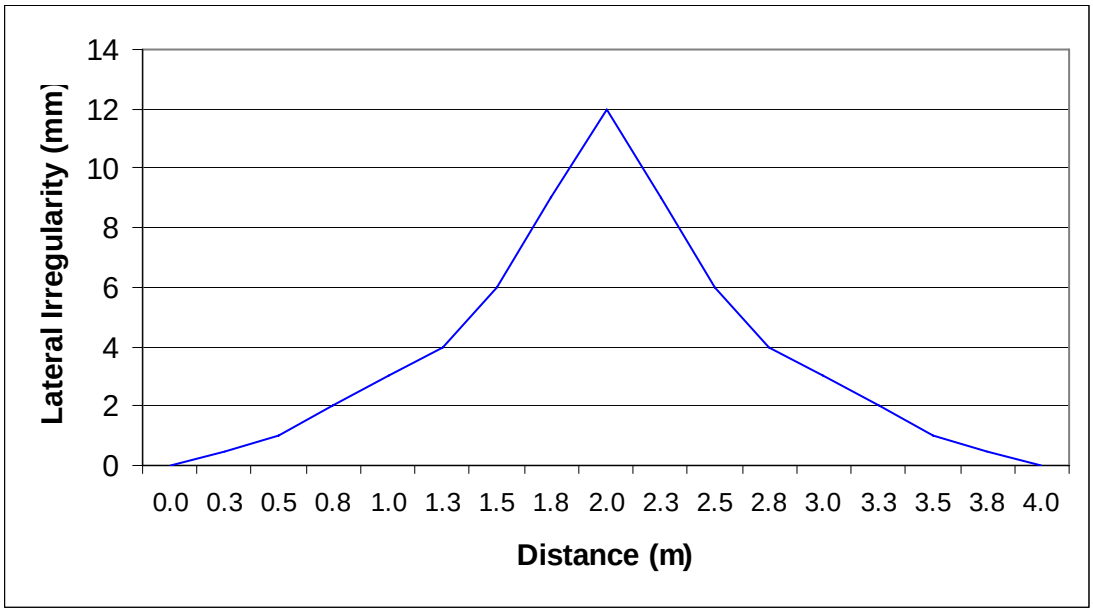

Figure 4-1: Lateral Track Irregularity

4.2.2. Discussion

Figure 4-2 was used to determine the approximate speed for when the vehicle began hunting. The results in Figure 4-2 show that at 28.5m/s hunting is present while at 27m/s no hunting was present. This verifies that the critical hunting speed is between 27 and 28.5m/s.

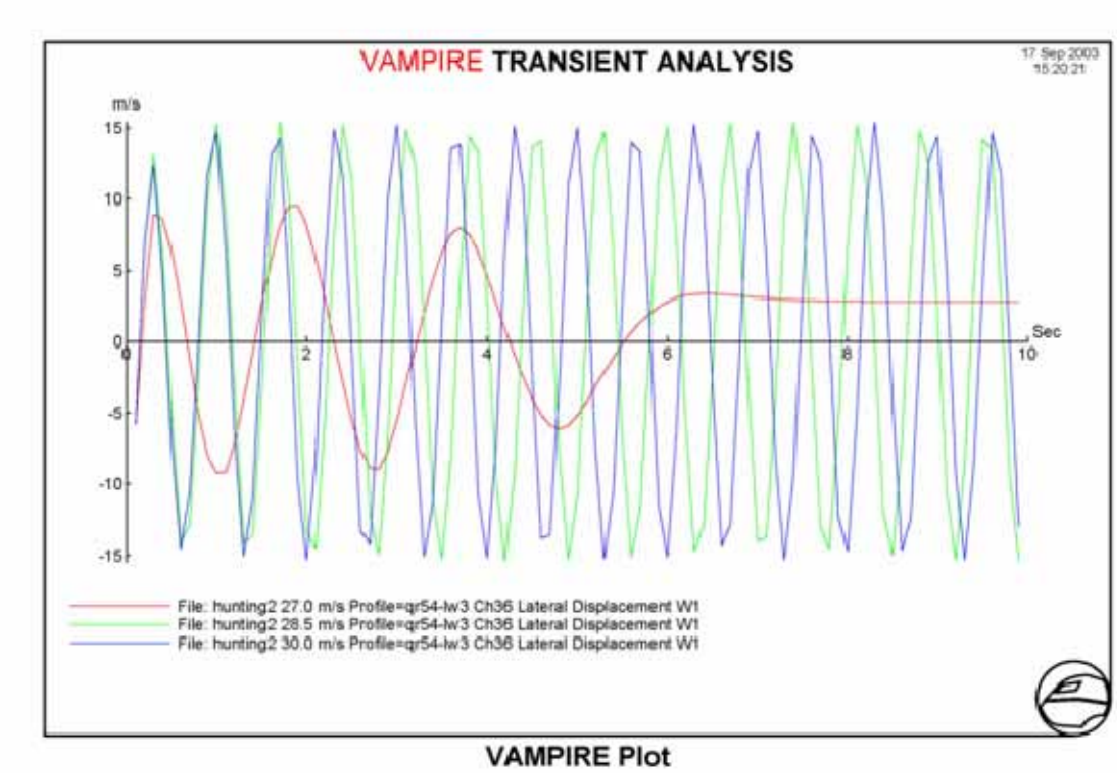

Figure 4-2: Hunting Behaviour of the Model

For vehicles of a typical three piece bogie arrangement hunting begins at approximately 80 kph, (McClanachan *et al*, 2000). The critical hunting speed simulated was slightly higher between 27m/s (97.2km/h) and 28.5m/s (102.6km/h). The hunting frequency obtained from simulation was 1.3Hz, which agrees with the data published by (McClanachan *et al*, 2000). The results produced in this

simulation are in the domain of a typical VAMB class wagon and are representative of the type of behaviour that would be expected.

4.3. Wheel Unloading due to Steady Lateral Components of In-train Forces

Another area of particular interest to this thesis is the effects of wheel unloading due to steady lateral forces of in-train forces. The paper published by (El-Sibaie, 1993) demonstrates the effects of lateral coupler forces generated by horizontal coupler angles. The paper reported the effects of steady lateral loads at the coupler pin on a vehicle travelling around a constant radius 175m radius curve. The work completed by (El-Sibaie, 1993) utilised experimental and simulation procedures where the load was varied from a negative load through to a positive lateral load at the coupler. Simulations were performed to compare the results from the VAMPIRE model with the results that were published by (El-Sibaie, 1993).

4.3.1. Test Procedure

The simulation procedure outlined in (El-Sibaie, 1993) was used. Unfortunately the wagon modelled by (El-Sibaie, 1993) is of little relevance to rollingstock used in Australian Mineral Trains which are the focus of this thesis. The model that was used by (El-Sibaie, 1993) was an empty 12.7 tonne 2-axle wagon with a coupler height of 810mm. The model used for this thesis was an empty four-axle wagon with three-piece bogies. The wagon had an empty mass of 15 tonne, a coupler height of 785mm and a track gauge of 1067mm. A track file with a curve radius of 175m

was created for the simulations to duplicate conditions published by (El-Sibaie, 1993). It was assumed that equilibrium cant was used. Simulations were completed at the same speed as (El-Sibaie, 1993) (i.e. 39kph).

Figure 4-3 gives a graphical representation of the VAMPIRE model used for simulations. Figure 4-4 shows a close-up of the front bogie arrangement and coupler pin mass. The wagon model was described in detail in Section 3.3.1.1 on page 36. Steady lateral loads were applied at the coupler pins to simulate the effects of in-train forces combined with coupler angling. The values of the lateral loads were varied from –13kN to 25kN during the simulation and the levels of wheel unloading and L/V ratio were recorded. The reduced negative force range (-13kN) was due to 100% wheel unloading being reached on one of the wheel sets. A positive force was taken as a force towards the centre of a positively curved track. A force of 25kN was required towards the centre of curvature to achieve 100% wheel unloading at one or more of the wheel sets. The greater positive lateral force required was due to the centripetal force required to hold the vehicle model body mass in circular motion.

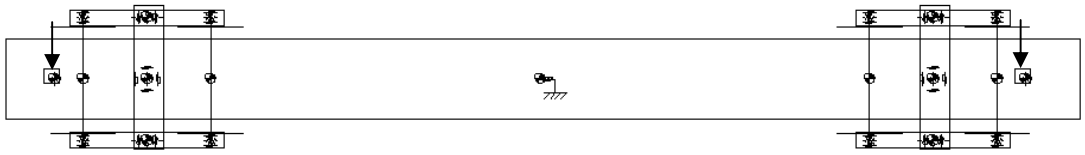

Figure 4-3: Top View of the Wagon Model

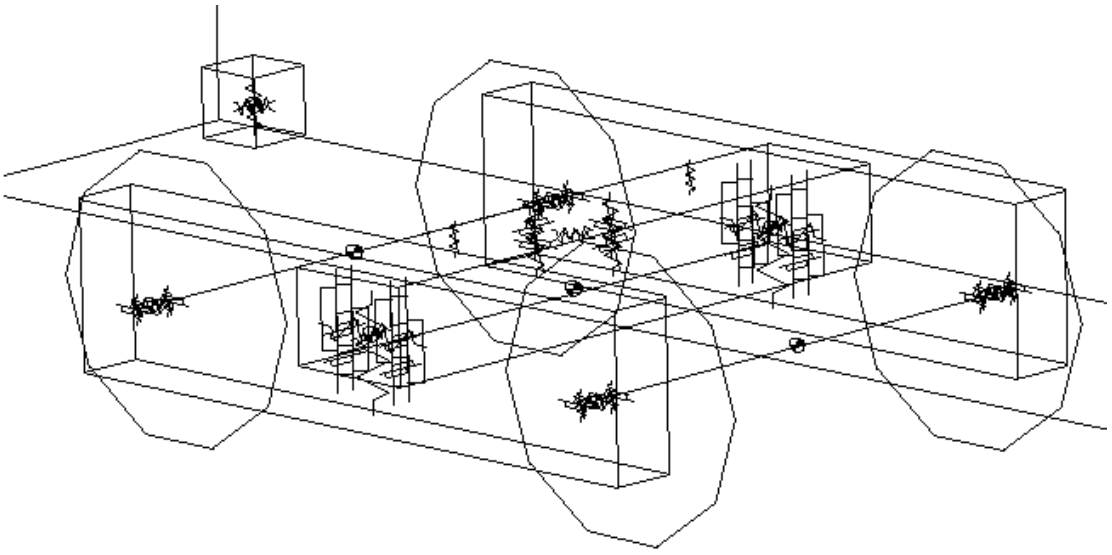

Figure 4-4: Bogie and Coupler Pin Elements

4.3.2. Results and Discussion

The results demonstrate similar behaviours to those in the paper published by (El-Sibaie, 1993). Figure 4-5 shows a comparison between the results published by (El-Sibaie, 1993) and the results obtained from the simulation. It should be noted that the left and right VAMPIRE plots are the sum of the left and right wheel reactions of each bogie to allow the comparison with a 2 axle wagon, (El-Sibaie, 1993). Although the two models are different, there is some similarity in the results shown in Figure 4-5. The plots of the left and right wheels both cross at approximately the same lateral coupler force for both models in Figure 4-5. The plots of the left and right wheels shown in Figure 4-5 do not cross at zero lateral force due to superelevation. The plots also have a similar gradient due to the similar combination of coupler height, mass, suspension, centre of gravity and track gauge. It can be seen that fluctuations became present on the VAMPIRE plot when a lateral force of approximately 18kN was reached. Examination of the simulation plots in detail

showed that the force fluctuations were due to the steering and flanging of the bogie on the lower rail of the curve. Fluctuations are therefore not expected in the single axle model in (El-Sibaie, 1993).

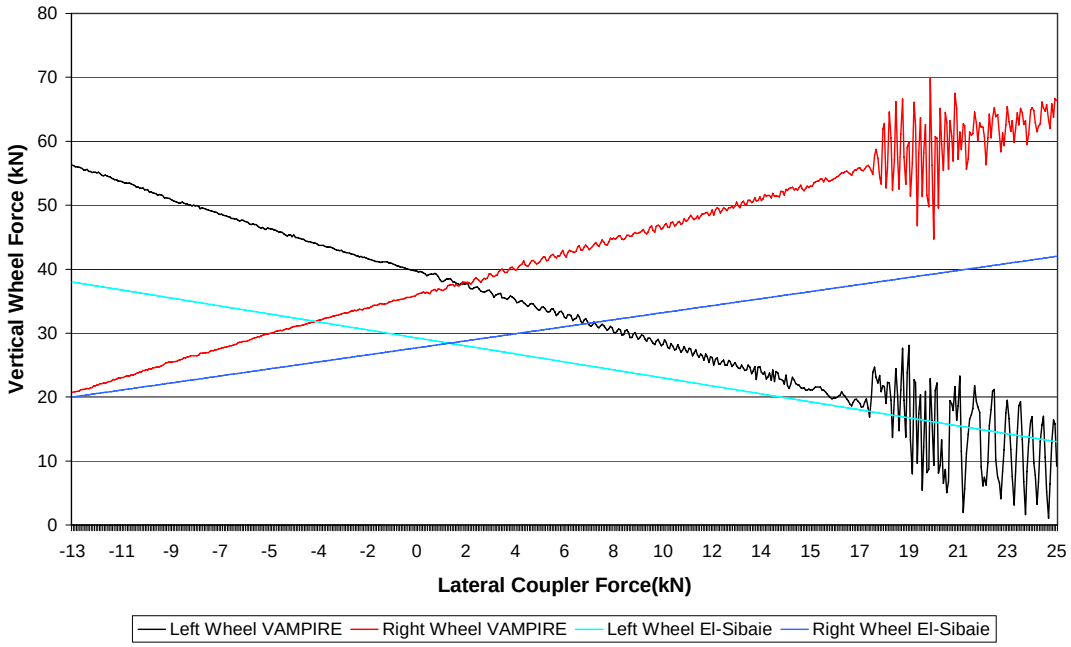

Figure 4-5: Comparison of Vertical Wheel Force vs Lateral Coupler Force

Figure 4-6 shows the force at each wheel in the bogie. It can be seen that the highest levels of wheel unloading fluctuation was on the front left wheel. This is due to the steering of the front wheelset combined with the right wheel lifting off the rail, the force was applied towards the centre of the curve. Fluctuations become present in Figure 4-6, Figure 4-7 and Figure 4-8. Figure 4-7 shows the effect of changing the lateral coupler force on lateral wheel force. Figure 4-8 displays the effects to the displacement and angle of the wheel.

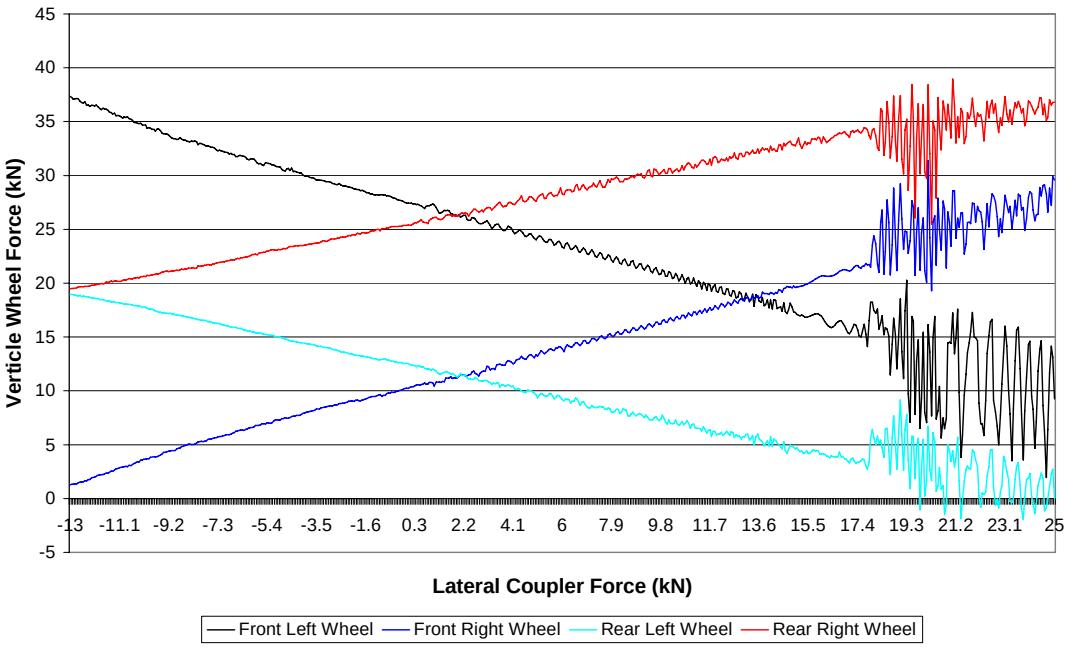

Figure 4-6: Vertical Wheel Force vs Lateral Coupler Force

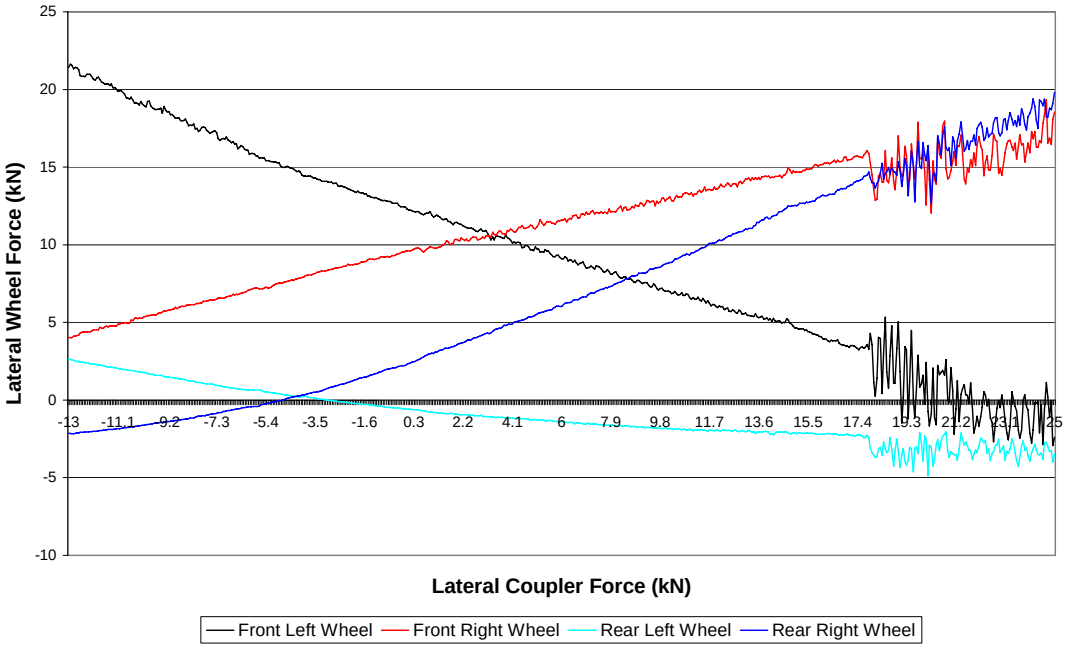

Figure 4-7: Lateral Wheel Force vs Lateral Coupler Force

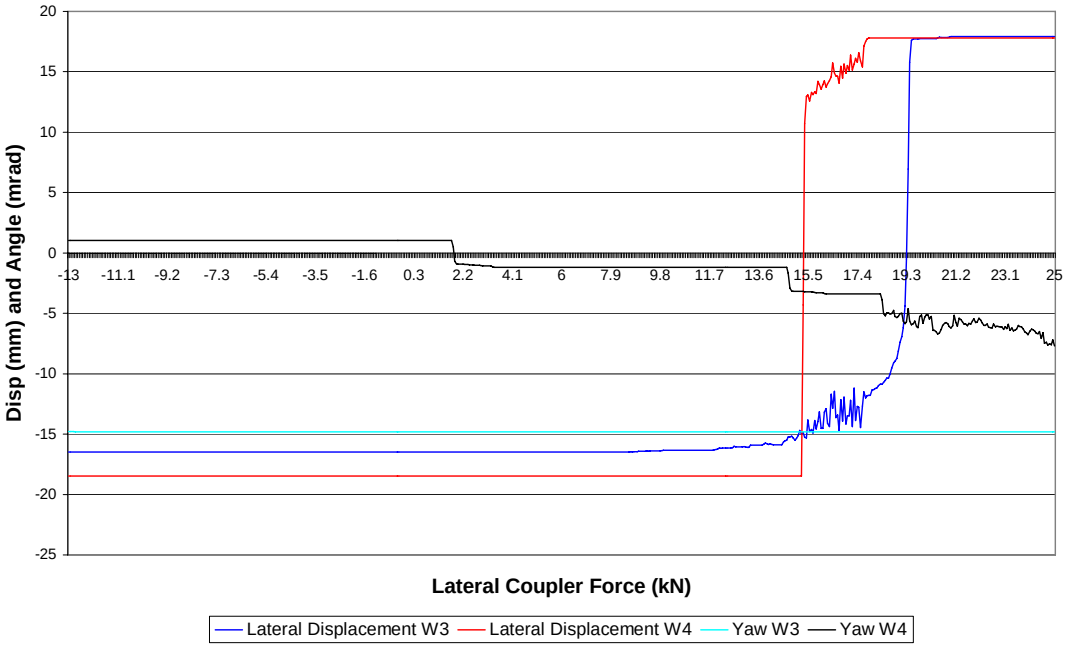

Figure 4-8: Lateral Displacement and Yaw vs Lateral Coupler Force

The differences produced in the simulations shown in Figure 4-5 to those published by (El-Sibaie, 1993) appear to be consistent with the differences expected between 2 and 4 axle wagons. The functionally of the VAMPIRE model created for this thesis was therefore accepted.

4.4. Bogie Pitch Test

Bogie pitch is caused due to the positioning of the connections between the bolster and the centreplate being above the centre of gravity of the bogie. When large in-train longitudinal accelerations occur it can cause the bogie to pitch about its centre of gravity, (i.e. rotating about its horizontal lateral axis, y axis). This creates wheel unloading on two wheelsets and overloading on the other two. Bogie pitch commonly occurs in empty or lightly loaded wagons.

It is important to validate the pitching behaviour of the vehicle model as it is another mechanism of wheel unloading related to longitudinal train dynamics. In an impact situation the levels of wheel unloading can change significantly due to bogie pitch. A paper published by (McClanachan *et al*, 2000) demonstrates the levels of wheel unloading experienced in the field. Simulations were also performed to simulate the experimental data.

The paper published by (McClanachan *et al*, 2000) was used as a guide to validate the model used in this thesis. The simulated data in this thesis was compared to the simulation results in the paper (McClanachan *et al*, 2000). The procedure and results from the simulations are outlined below.

4.4.1. Procedure

The procedure used was the same as outlined in (McClanachan *et al*, 2000). A sinusoidal force input with a similar magnitude and frequency as outlined in (McClanachan *et al*, 2000) was applied to the VAMPIRE model on a straight section of track and the levels of wheel unloading were recorded. The levels of wheel unloading that the vehicle experienced were then compared to the information published by (McClanachan *et al*, 2000).

The results published by (McClanachan *et al*, 2000) only had access to experimental data for the coupler force for the front coupler, so it is unknown what the force profile was on the rear coupler. It was decided that the wagon body accelerations published in the paper could be used to overcome the problem of not knowing the

force on the rear coupler. Some quick calculations were made to determine the maximum magnitude of the sum of coupler forces to get the desired wagon accelerations.

4.4.2. Results and Discussion

The model was tuned to the levels of wheel unloading found in the experimental data published by (McClanachan et al, 2000). The experimental data which was published by (McClanachan et al, 2000) can be seen in Figure 4-9. Comparison with Figure 4-10 and Figure 4-11 shows that the behaviour of the VAMPIRE model developed for this thesis gave similar outputs. Higher levels of wheel unloading can be seen in the experimental data in Figure 4-9. The tests performed in VAMPIRE were on perfect track so higher levels of wheel unloading would be likely in the experimental data due to the track irregularities. While not an exact match in bogie pitch response, the VAMPIRE model was considered representative of the VAMB rollingstock.

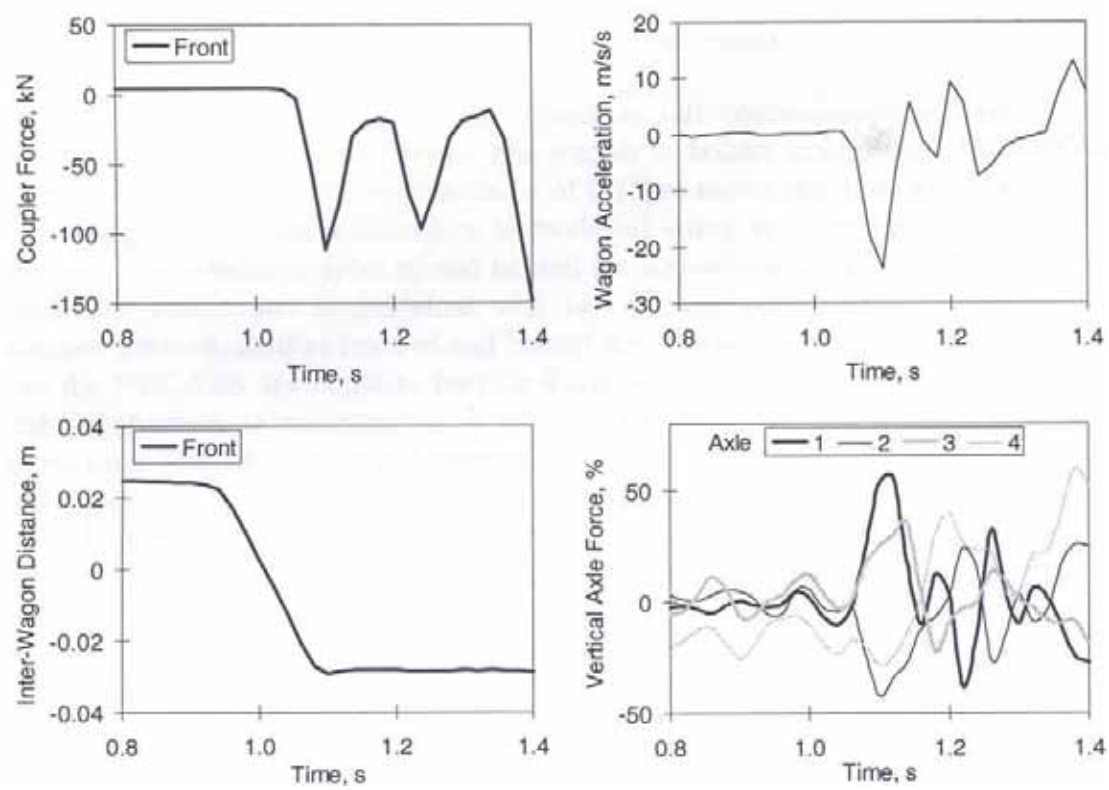

Figure 4-9: Experimental Data, (McClanachan *et al*, 2000)

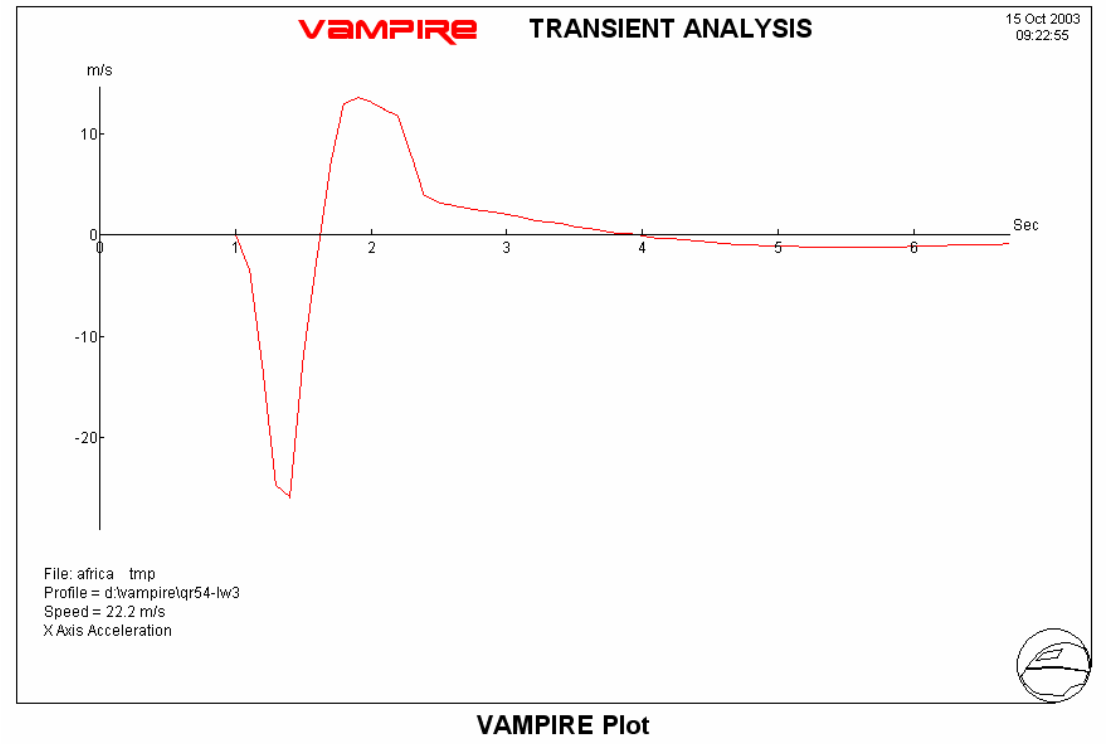

VAMPIRE Plot

Figure 4-10: VAMPIRE Model Acceleration

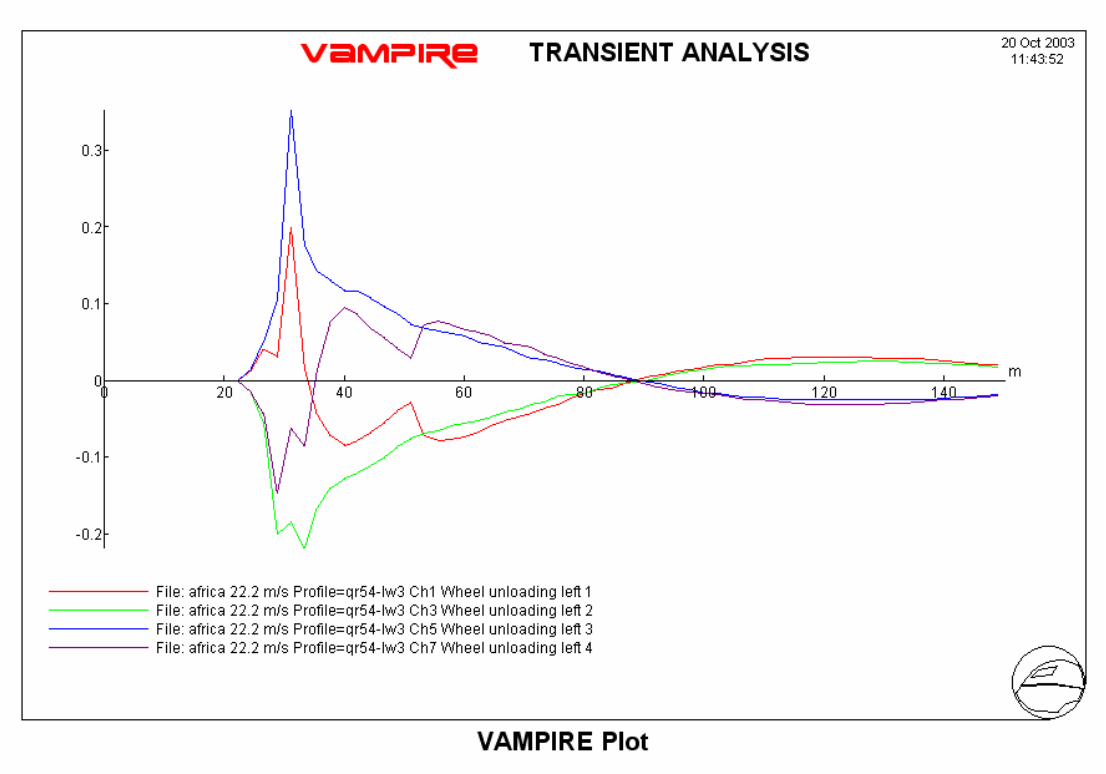

Figure 4-11: VAMPIRE Model Bogie Pitch Behaviour

5 STEADY FORCES ON CURVES AND CURVE TRANSITIONS

5.1. Introduction

The primary objective of this section of the thesis is to identify levels of wheel unloading and L/V ratio from different force magnitudes on a range of curve radii. By investigating key areas of derailment risk due to steady forces on curves, it is possible to determine if a given event will cause derailment. Detailed wagon dynamics simulation allows the identification of levels of wheel unloading and L/V ratio for a given event. VAMPIRE was used to simulate the dynamic behaviour of railway vehicles as they negotiated track geometry and experienced longitudinal steady forces. The process of determining an appropriate level of risk is covered in Chapter 8 - Derailment Risk Assessment starting on page 122.

Papers such as (El-Sibaie, 1993) demonstrate the effects of lateral coupler forces on tight curves (175m radius). This study differs from, (El-Sibaie, 1993) in that steady forces were applied to the model as it travelled along the track. The track sections consisted of a straight section of track, a transition, a constant radius curve and then an exit transition. The wagon model included dummy wagons either side of the detailed wagon model to allow the application of constant buff and draft forces. Using this type of VAMPIRE model allowed the forces to be applied to the detailed wagon model at the correct angle throughout the simulations. Maximum values of wheel unloading and L/V ratio were recorded for each simulation.

5.2. Procedure

The VAMPIRE model that was used for the simulations is shown schematically in Figure 5-1 and is discussed in detail in Section 3.3.1 on page 35. Longitudinal in-train force magnitudes of -1200kN to 1200kN in steps of 200kN were simulated on 200, 400, 600, 800 and 1000 metre radius curves. Steady forces were applied to the trailing dummy wagon while the leading dummy wagon was fixed to the reference point that sets the speed of the model in VAMPIRE. The connections between wagons were modelled as spring connections with a stiffness of 80MN/m.

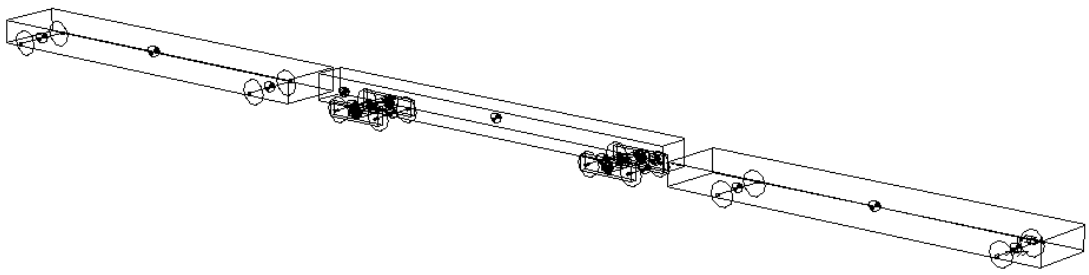

Figure 5-1: Isometric View of Wagon Model with Dummy Wagons

A cant of 2/3 equilibrium that changed at a linear rate was assumed typical of normal operation conditions. The transition curve was set at 40m in length and the simulated velocity of the vehicle was specified to the standards specified by Queensland Rail as shown in Table 5-1.

Table 5-1: Speed Settings for Curve Radius

Curve Radius (m)	Speed (kph)
1000	80
800	80
600	80
400	60
200	40

5.3. Results and Discussion

To provide a datum for comparison, the levels of wheel unloading and L/V ratio for the model travelling on a 800m radius curve with no force input are shown in Figure 5-2 and Figure 5-3. Figure 5-2 shows approximately 60% wheel unloading at the front right wheel at the exit point of the first transition. The wheel unloading fluctuations then reduce to become constant as the vehicle travels along the constant radius curve section of track. Figure 5-3 shows that the maximum level of L/V ratio of approximately 0.32 also occurs at the exit position of the first transition. Figure 5-2 and Figure 5-3 show that the maximum values for wheel unloading and L/V ratio are at simular positions along the track, they vary by only a few metres. The L/V ratio in Figure 5-3 remains at a high value along the constant radius section of the curve.

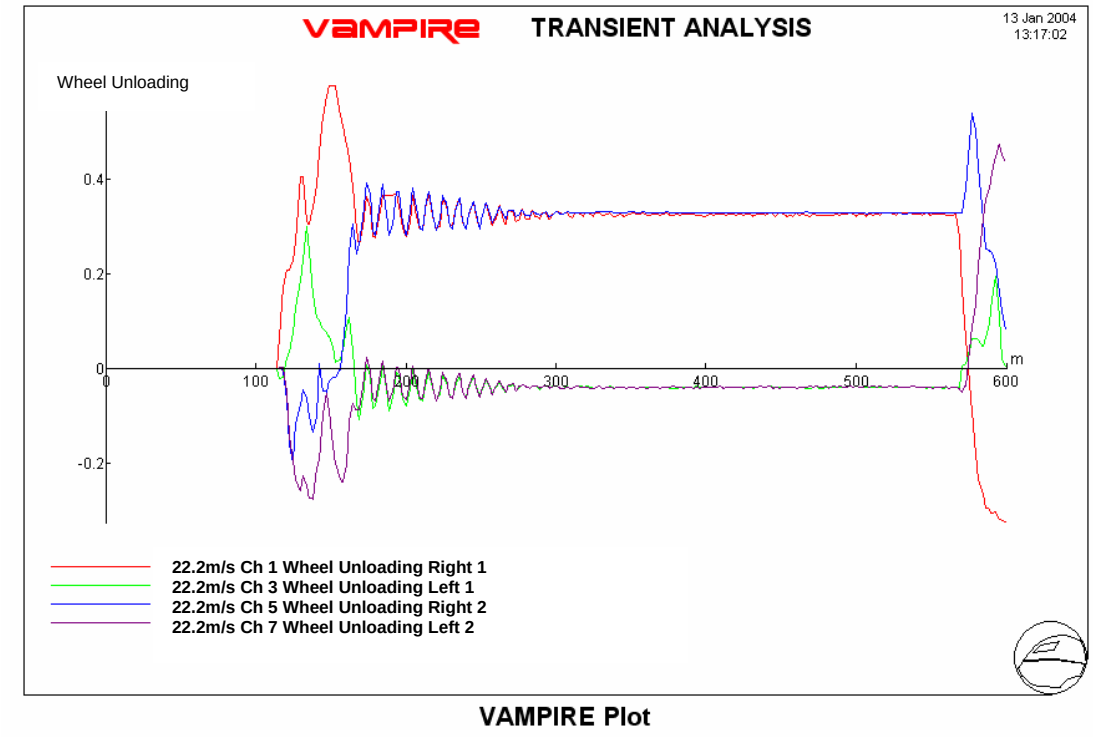

Figure 5-2: Wheel Unloading for 800m Radius Curve with no Force Input

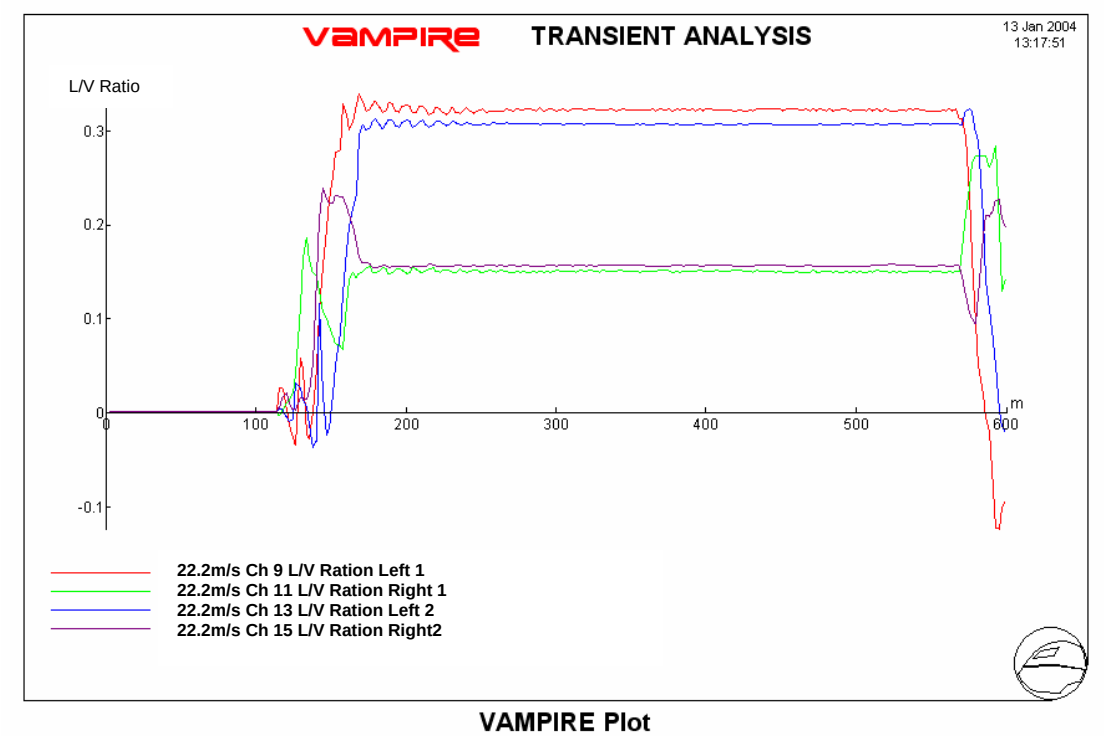

Figure 5-3: L/V Ratio for 800m Radius Curve with no Force Input

Figure 5-4 and Figure 5-5 shows the levels of wheel unloading and L/V ratio when a compressive load of 1MN is applied on an 800m radius curve. Figure 5-4 shows a maximum level of wheel unloading of approximately 90% on the exit point of the transition. The maximum level of L/V ratio is approximately 0.35. Again the maximum levels of wheel unloading and L/V ratio occur together. The close correspondence of maximum wheel unloading and L/V ratio was observed for all the transition studies performed.

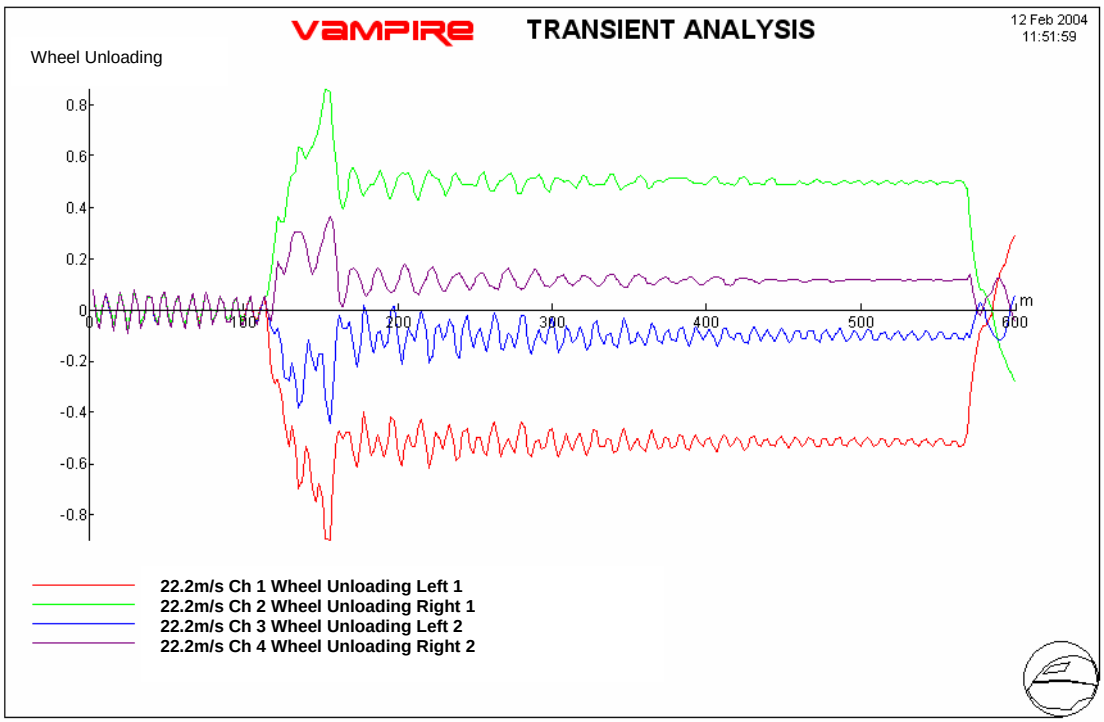

Figure 5-4: Wheel Unloading for 800m Radius Curve with 1000kN Compressive Force

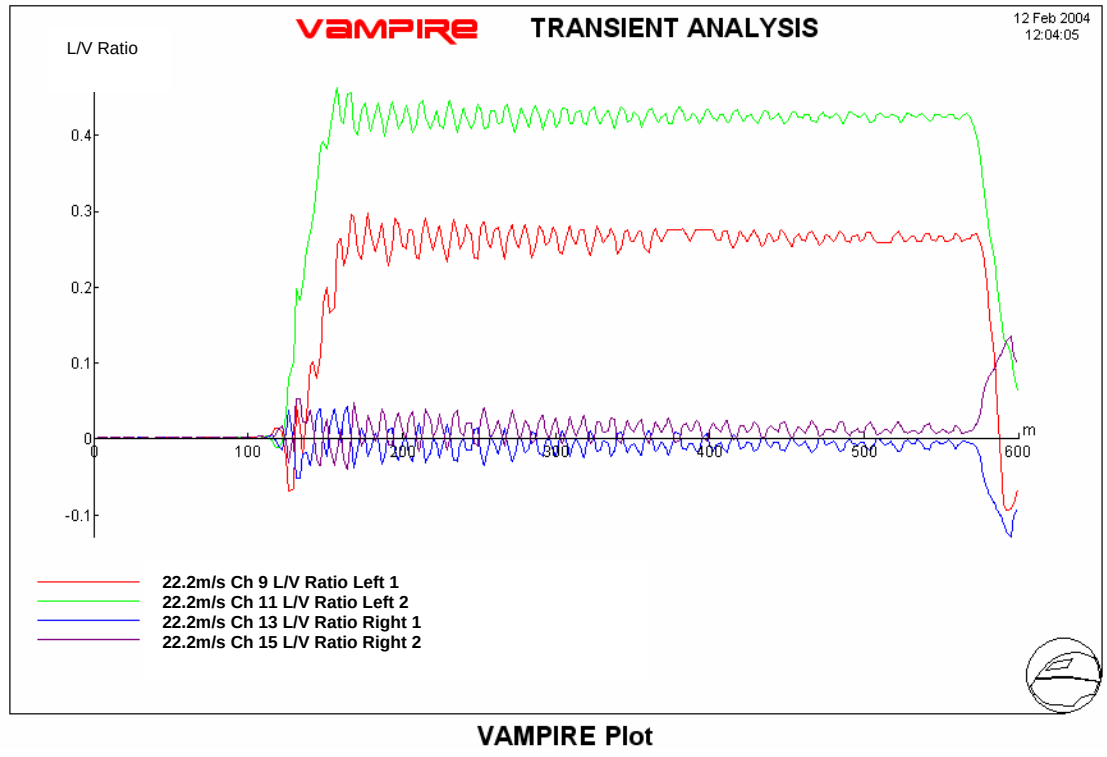

Figure 5-5: L/V Ratio for 800m Radius Curve with 1000kN Compressive Force

Figure 5-6 shows the relationship between levels of wheel unloading, tighter curve radii and larger draft force magnitudes. The buff forces produced the highest levels of wheel unloading due to the vehicle being forced onto the outer rail. It would be expected that the lowest levels of wheel unloading would be when no buff or draft forces were applied for a track configuration with equilibrium cant. Since the cant was set to 2/3 equilibrium cant this was not true. The levels of wheel unloading reduced as draft forces were increased. This was due to the effect of the 2/3 equilibrium cant. If the magnitude of draft force was increased further, the levels of wheel unloading would eventually begin to increase as the vehicle began to be pulled over the inner rail. The levels of wheel unloading reduced as the curve radius was increased due to the reduction in the lateral component produced from the coupler angles. As the curve radius was reduced it can be seen that the levels of wheel unloading vary more between the maximum and minimum values. This was due to the tighter curve radius producing proportionally larger coupler angles and lateral force components.

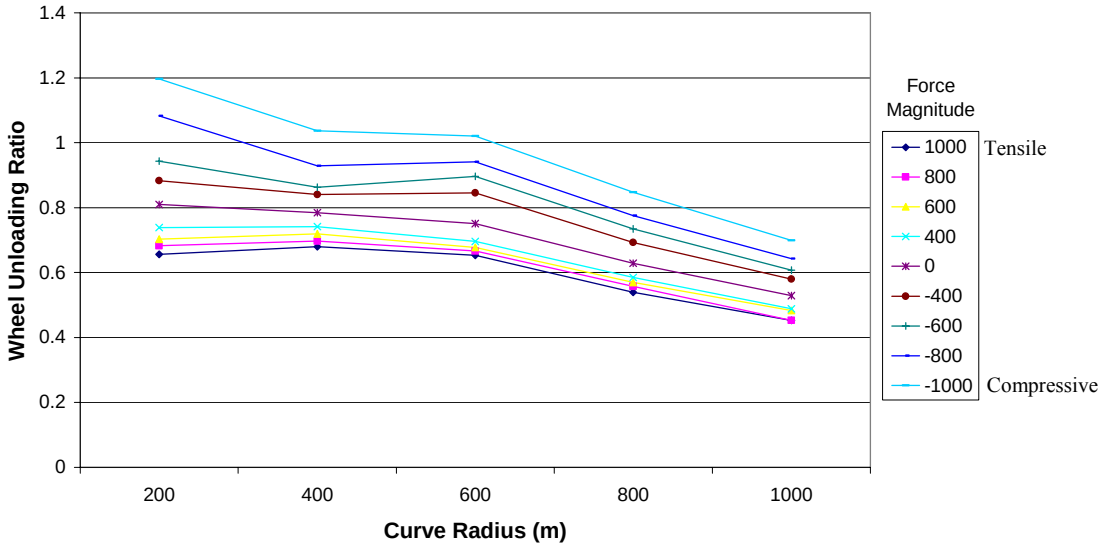

Figure 5-6: Maximum Wheel Unloading for VAMPIRE Wagon Model with Dummy Wagons

Similarly, the levels of L/V ratio are shown in Figure 5-7 for each curve radius and coupler force. The levels of L/V ratio showed similar trends to the levels of wheel unloading. The L/V ratio did not reach dangerous levels for the simulations completed.

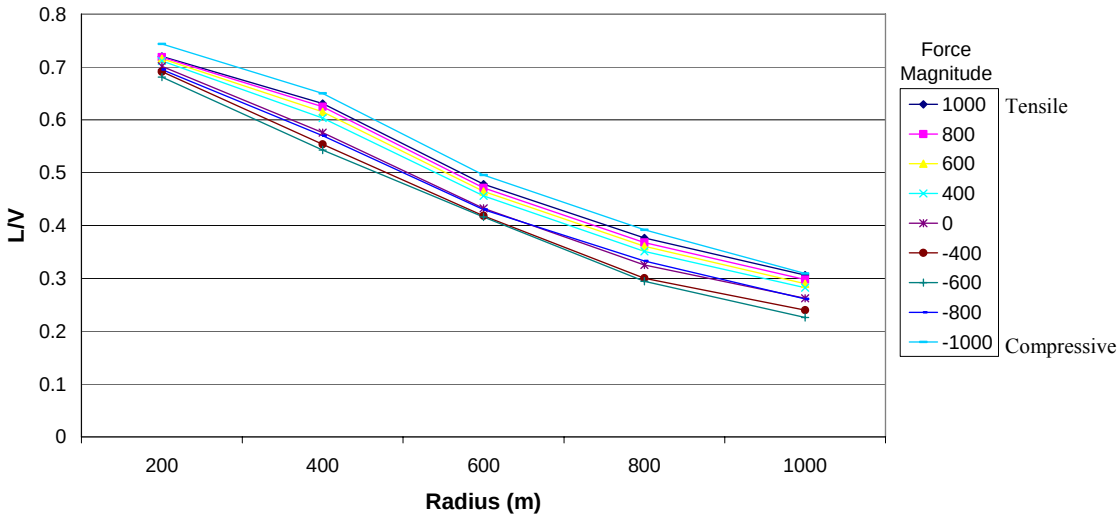

Figure 5-7: L/V Ratio for VAMPIRE Wagon Model with Dummy Wagons

As expected Figure 5-6 and Figure 5-7 show that levels of wheel unloading and L/V ratio increase as the curve radius is reduced. Figure 5-6 and Figure 5-7 show that under high compressive forces the levels of wheel unloading and L/V ratio are increased for all curve radii. A derailment criteria for wheel unloading was exceeded for a draft force of 1MN on a 200, 400 and 600 metre radius curve; and for a draft force of 800kN on a 200 metre radius curve, as shown in Figure 5-6. All L/V ratios are at safe levels (below a L/V ratio of 1.22).

6 IMPACTS ON CURVES AND CURVE TRANSITIONS

6.1. Introduction

A further issue of the interaction of train and wagon dynamics is the possibility of wheel unloading due to bogie or wagon body pitch. The worse case scenario is the combination of bogie or body pitch and lateral coupler components occurring on curves. Bogie and wagon pitch is generated due to longitudinal impact forces as demonstrated by (McClanachan *et al*, 2000). This section of the thesis is therefore focused on the study of impact forces on curve transitions.

6.2. Procedure

The procedure used to determine the effects of impact forces on transition curves consisted of firstly simulating impact forces in CRE-LTS and then applying these forces to the VAMPIRE vehicle model. The forces were applied as the vehicle was on the transition curve (i.e. to coincide with sites where the worse case wheel unloading and L/V ratio levels are known to occur). Levels of wheel unloading and L/V ratio were recorded throughout the simulation. The effects of impacts on transition curves were simulated for train configurations with a coupler slack of 25mm, 50mm and 75mm on 200, 400 and 600 metre radius curves.

The in-train forces were simulated in CRE-LTS using a severe driver control action. The driver action of sweeping from full throttle to full dynamic brake in forty seconds was used, as shown in Figure 6-1. The train simulated consisted of 107 vehicles with 4 locomotives placed in groups of two, at lead and mid train positions.

The simulated train was travelling at approximately 60km/h and the track had equilibrium cant. In-train force data was saved for all wagon connections. The worse case impact forces were extracted from the saved simulation output. The results are shown in Figure 6-2, Figure 6-3 and Figure 6-4.

Longitudinal wagon accelerations are proportional to the difference in coupler forces applied to the front and rear of the wagon. The most severe accelerations occur due to impacts where the coupler force changes sign. These can be due to the train bunching or stretching (i.e. run-ins, compressive or run-outs, tensile). Simulation outputs were searched for the worst cases. This allowed the maximum individual wagon acceleration to be found within the train and applied to the VAMPIRE wagon model. The maximum accelerations were found to be at position 18, 48 and 32 for coupler slacks 25, 50 and 75mm respectively, as shown in Figure 6-2, Figure 6-3 and Figure 6-4. The reason for the different maximum positions was not researched. It was assumed CRE-LTS modelling was reflective of real train operations.

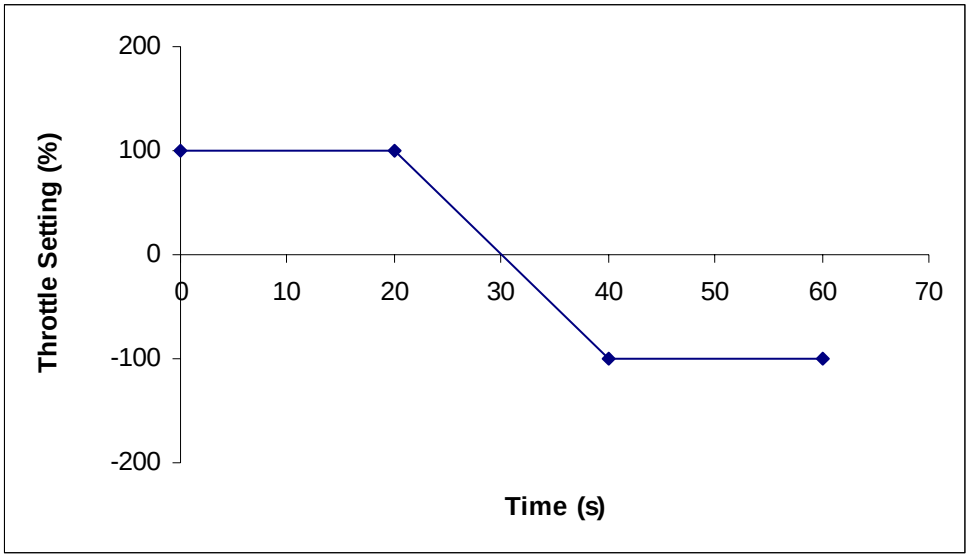

Figure 6-1: Driver Action

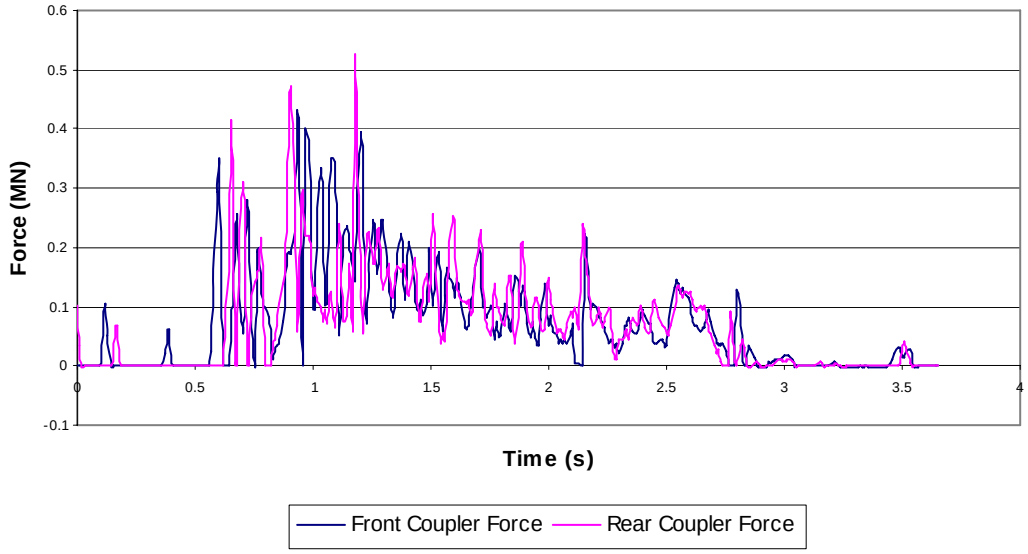

Figure 6-2: Force Profile 25mm Coupler Slack (Position 18)

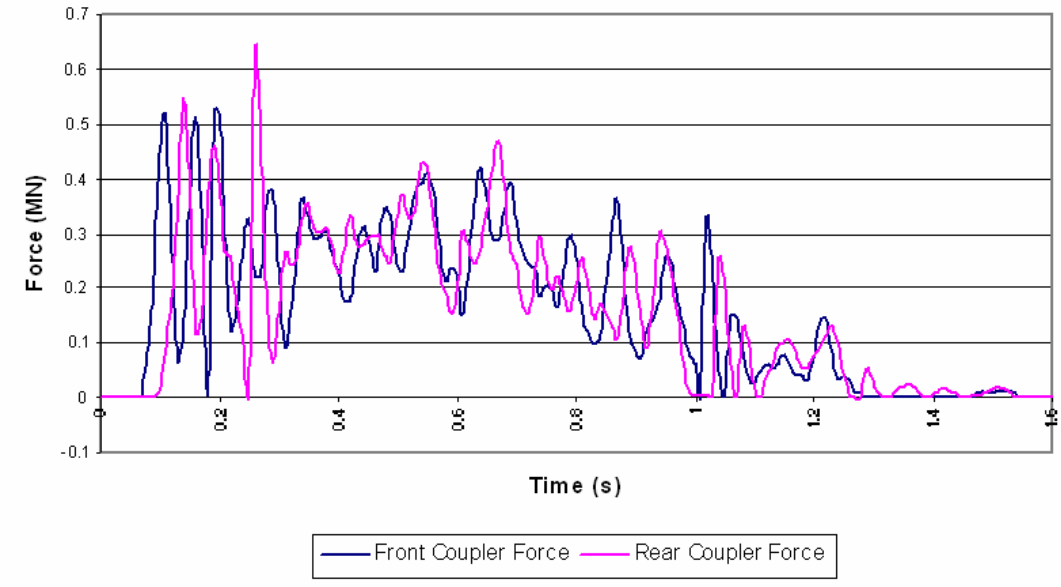

Figure 6-3: Force Profile 50mm Coupler Slack (Position 48)

Figure 6-4: Force Profile 75mm Coupler Slack (Position 32)

Using the code developed to calculate coupler angles in Section 3.3.3 on page 45, the simulations provided the angle between each vehicle as it negotiated the transition curve. The calculations assume vehicles stay laterally centred on the track. As the vehicle enters the curve transition the coupler angle increases until the vehicle enters the constant radius section of track. Table 6-1 gives approximate coupler angles for each curve radius.

Table 6-1: Approximate Coupler Angle for each Curve Radius

Curve Radius (m)	Approx Coupler Angle
Infinite	0°
800	0.0533°
600	0.39°
400	1.00°
300	1.50°
200	2.14°

Longitudinal and lateral in-train forces obtained were calculated for wagon connection coupler slacks of 25, 50 and 75mm for a train operating through 200, 400

and 600m radius curves. Appropriate speed settings were set for each curve radius, the speed settings are listed in Table 6-2.

Table 6-2: Speed Settings

Curve Radius (m)	Speed (kph)
1000	80
800	80
600	80
400	60
200	40

Longitudinal and lateral in-train forces were applied to the VAMPIRE model at the coupler pin position. For the first simulation the time series of force data was manually aligned so that impact forces were aligned with sites where maximum wheel unloading and L/V ratio were expected. The worst case position to align the data was at the end of the entry transition as noted in the previous chapter. The simulation was repeated for five positions either side of this position. The positions were selected in steps of 50 milliseconds, (i.e. @60km/h, steps of 0.83m). A total of nine sets of coupler forces were needed to perform the simulations. Each of these sets of coupler forces needed to have a longitudinal and lateral coupler force for each coupler, this came to a total of thirty-six force profiles. A total of one hundred and thirty two simulations were carried out using VAMPIRE with different coupler slack force profiles, curve radius and impact force positioning. The computations were automated using a batch file constructed using the macros in UltraEdit. After the simulations were performed the maximum levels of wheel unloading and L/V ratio were collated. The data was written to files and the worse cases pinpointed for each coupler slack and curve radius.

6.3. Results

Figure 6-5 and Figure 6-9 provide datum wagon responses with no impact force added to the model. L/V ratio for various impact conditions are shown in Figure 6-6 to Figure 6-8. Corresponding wheel unloading results are in Figure 6-10 to Figure 6-12. Wheel unloading and L/V ratio on the transition curve, as shown in Figure 6-5 to Figure 6-12 shows each scenario for wheel unloading and L/V ratio on a 400m radius curve. It can be seen that there is an increase in wheel unloading and L/V ratio as the coupler slack is increased. Figure 6-5 is the L/V ratio of a vehicle travelling around a 400m curve with no force input. It can be seen that the highest levels of L/V ratio are when the vehicle exits the transition and begins on the constant radius curve. Figure 6-9 shows wheel unloading for the model travelling around a 400m radius curve with no force input. It should be noted that the highest levels of wheel unloading are again at the end of the first transition. The worse case data was extracted from each simulation and plotted for comparison in Figure 6-13 and Figure 6-14.

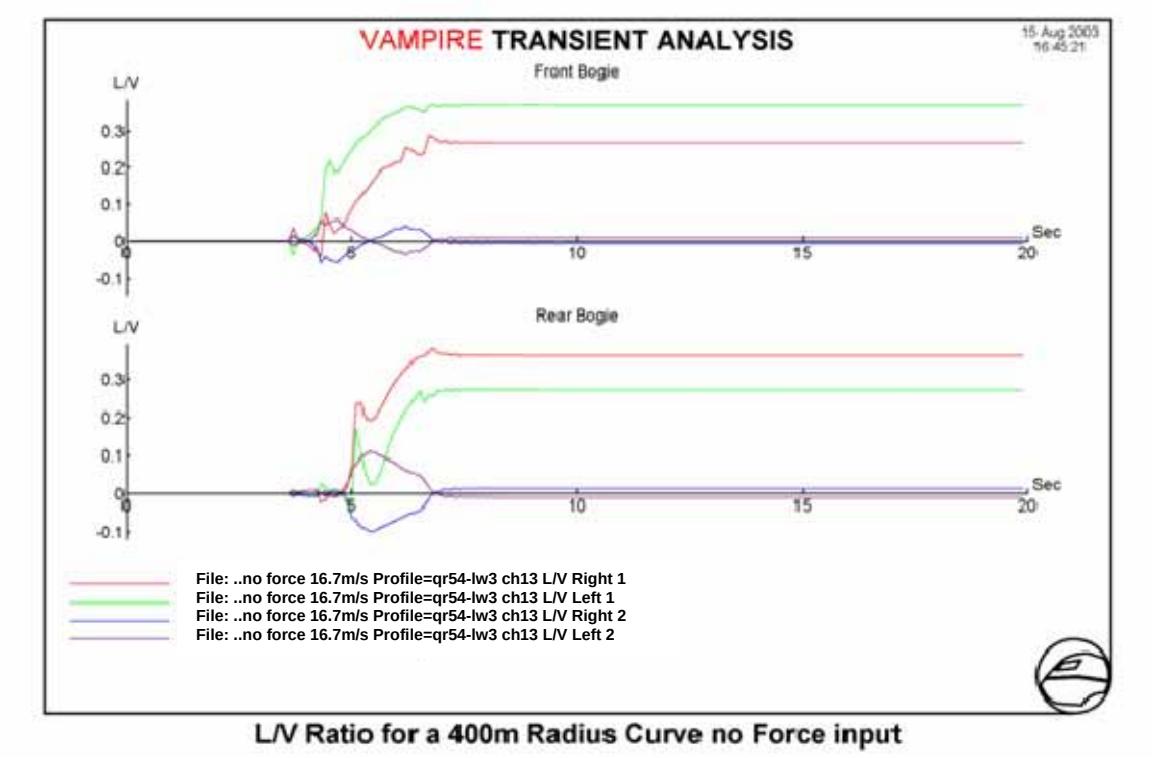

Figure 6-5: L/V Ratio for a 400m Radius Curve with No Force Input

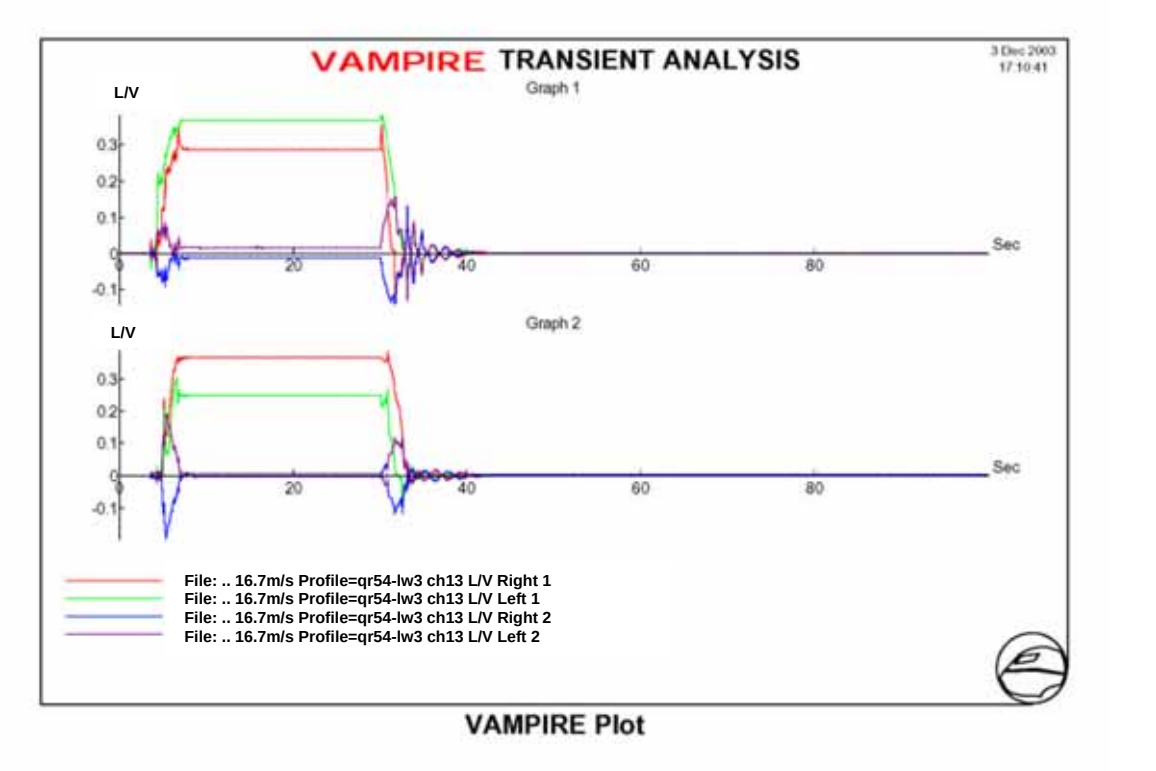

Figure 6-6: L/V Ratio for a 400m Radius Curve with 25mm Coupler Slack

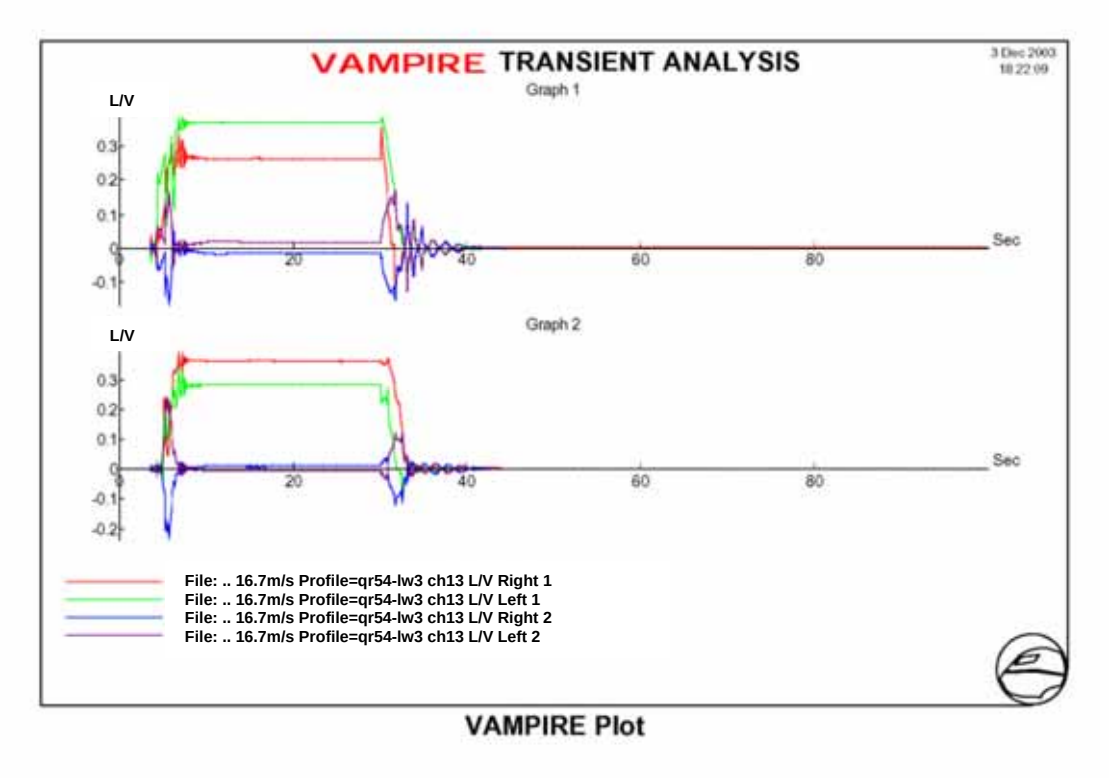

Figure 6-7: L/V Ratio for a 400m Radius Curve with 50mm Coupler Slack

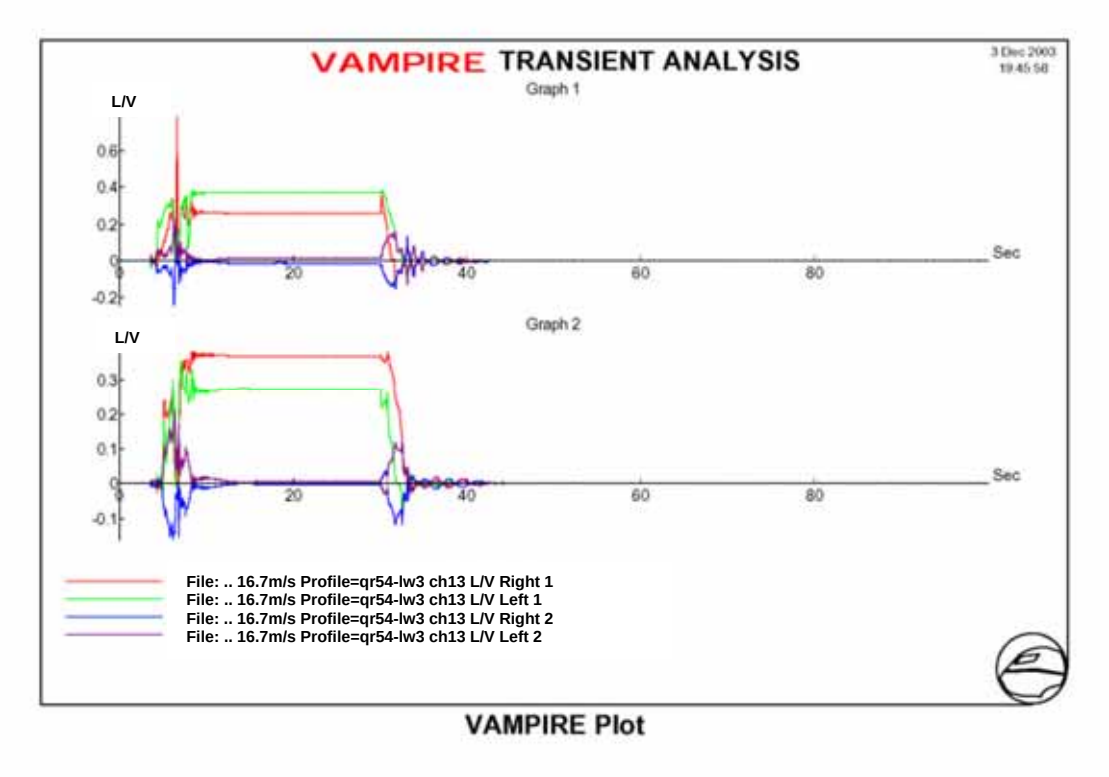

Figure 6-8: L/V Ratio for a 400m Radius Curve with 75mm Coupler Slack

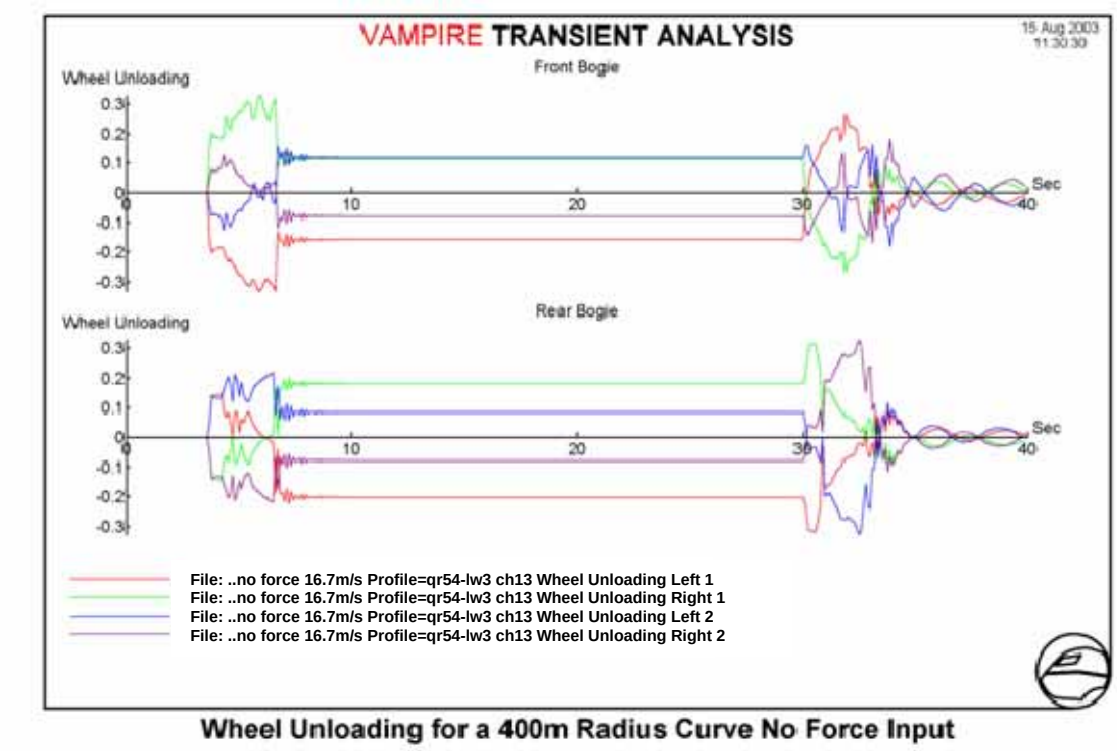

Figure 6-9: Wheel Unloading for a 400m Radius Curve with No Force Input

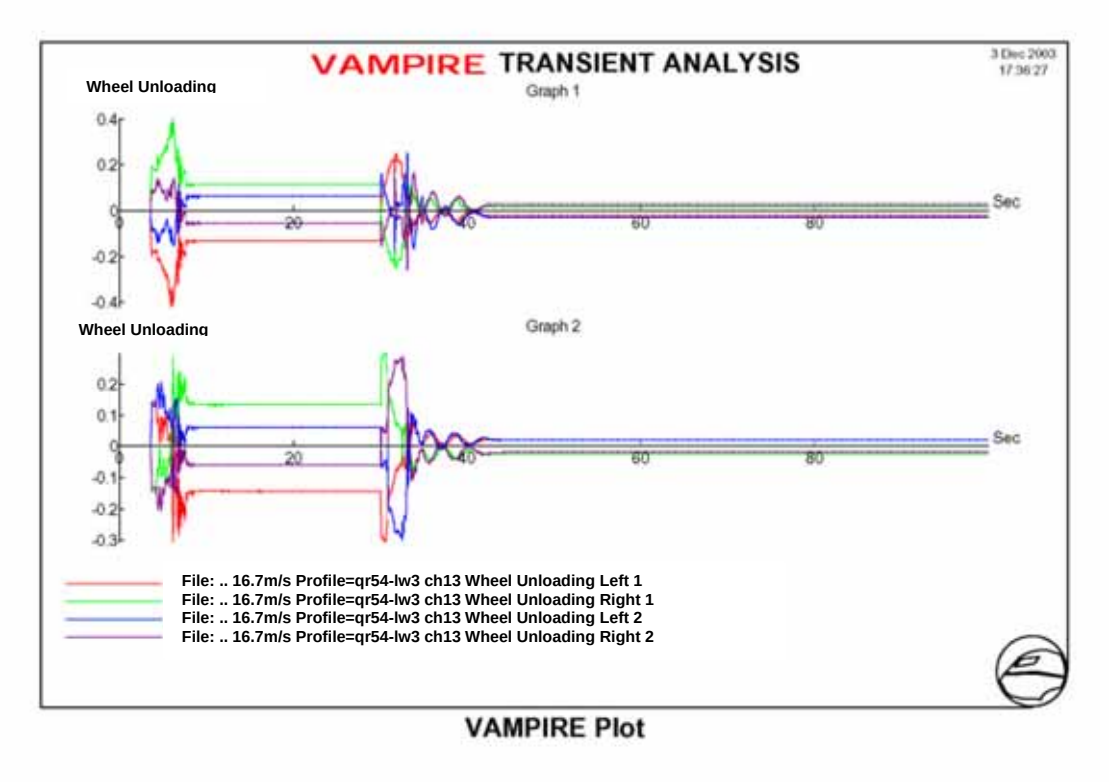

Figure 6-10: Wheel Unloading for a 400m Radius Curve with 25mm Coupler Slack

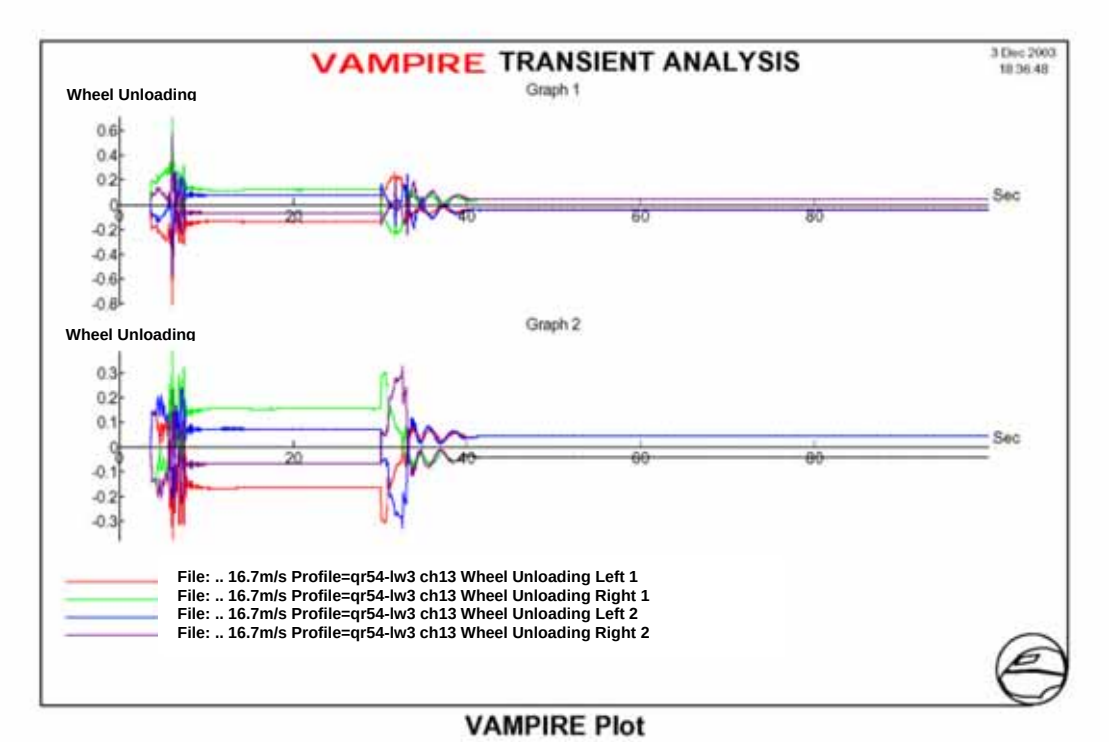

Figure 6-11: Wheel Unloading for a 400m Radius Curve with 50mm Coupler Slack

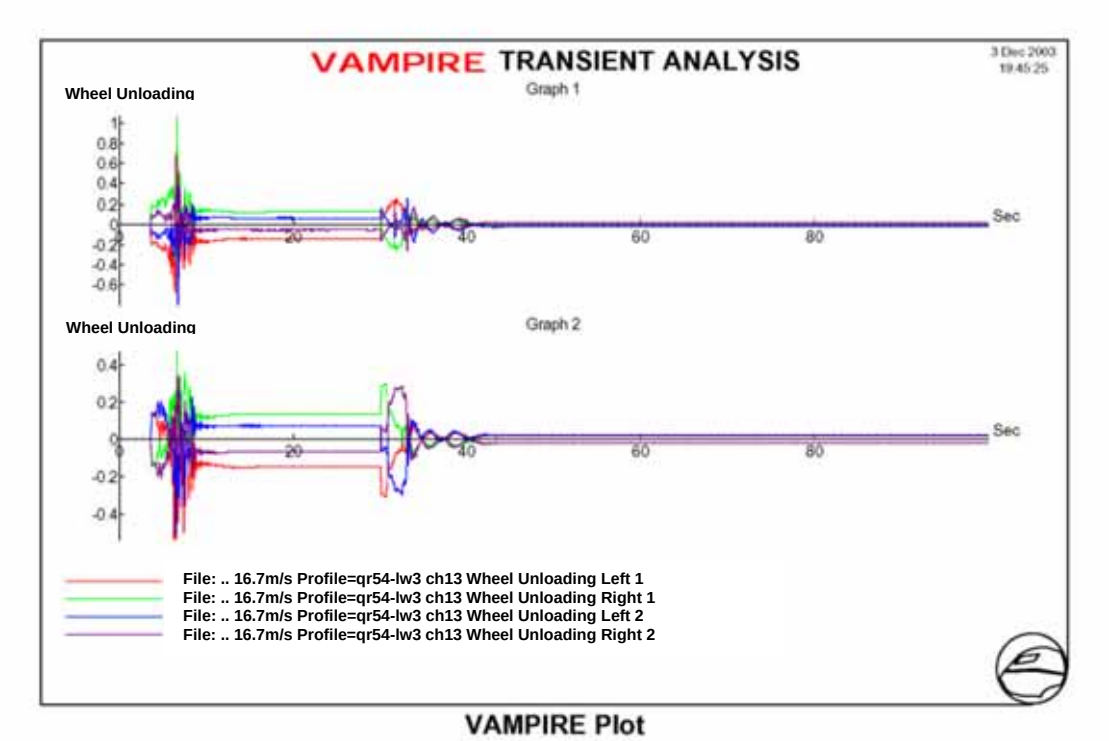

Figure 6-12: Wheel Unloading for a 400m Radius Curve with 75mm Coupler Slack

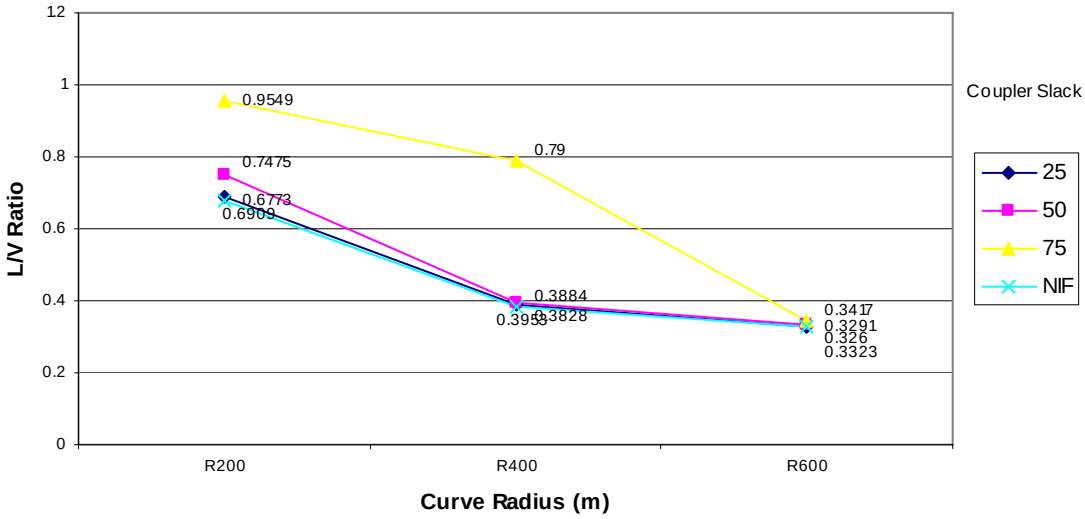

Figure 6-13: Worse Case Scenario of L/V Ratio vs Curve Radius

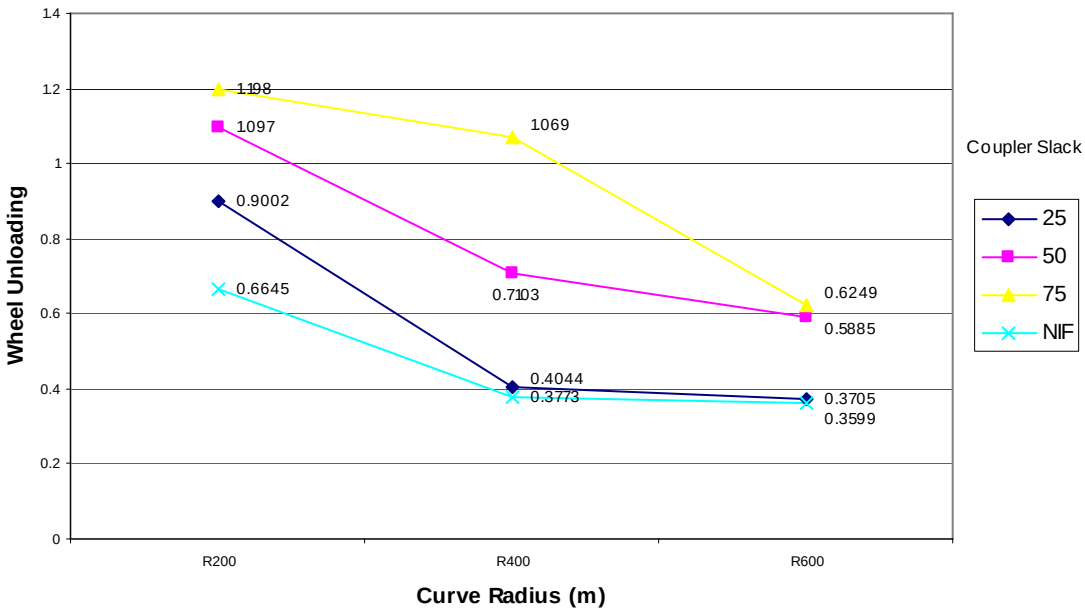

Figure 6-14: Worse Case Scenario of Wheel Unloading vs Curve Radius

*NIF - No Input Force. It represents a single vehicle travelling around a curve without disturbance.

6.4. Discussion

Figure 6-13 and Figure 6-14 shows increased levels of wheel unloading and L/V ratio and therefore imply an increased derailment risk as curve radius is reduced. There is a dramatic reduction in the maximum levels of wheel unloading and L/V ratio when the curve radius is increased to 600m in Figure 6-13 and Figure 6-14. By increasing the curve radius from 400m to 600m the maximum levels of wheel unloading is reduced by almost 40% for a coupler slack of 75mm. The coupler slack between vehicles is also identified as an important variable as this influences the levels of wheel unloading and L/V ratio experienced by vehicles. For a curve radius of 400m wheel unloading increases by approximately 30% when coupler slack increases from 25 to 50mm and a further 40% increase for further slack action increase from 50 to 75mm. To minimise the levels of wheel unloading the best combination would be to keep coupler slack below 25mm or remove sharp curves below 600m radius.

By decreasing the coupler slack to 25mm it can be seen that the levels of wheel unloading and L/V ratio are at a minimum for tests performed with force disturbance. For a 600m radius curve the levels of wheel unloading and L/V ratio vary less from coupler slack than on a 200m or 400m radius curve. This is because of the reduced lateral component due to small coupler angles.

The wheel unloading derailment criteria are reached for a coupler slack of 50mm on a 200m radius curve and for a coupler slack of 75mm on a curve radii of 200m and 400m. The L/V ratio remained at safe levels for all simulations (below a L/V ratio of

1.22). Larger radius curves were not simulated because an 800m curve has a coupler angle of approximately 0.05deg and 0.087% of in-train forces would be a lateral component. In-train forces would have to reach 20MN to give a significant lateral component of 17.4kN. A further reduction in wheel unloading and L/V ratio would therefore be expected by increasing the curve radius from 600m to 800m.

7 PROBABILITY DENSITY FUNCTIONS

7.1. Introduction

Probability density functions allow probability densities to be quantified. Plots of probability density functions allow a visual analysis of probability data. The data can be collected for several key parameters relating to track and simulation data. This section of the thesis focuses on constructing probability density functions from force and angling simulation data so that an analysis of train dynamics can be performed. Probability density functions are plotted for a number of longitudinal force components and coupler angles for a coupler slack of 25, 50 and 75mm for track sections on the Monto and North Coast Lines.

7.2. Procedure

Probability density functions were created from longitudinal train simulations performed in CRE-LTS. A probability density function is a specific type of probability distribution curve that consists of a number of intervals or densities, (Canavos, 1984; Devore, 1991). A probability density function is grouped together in a specific range to give a distribution curve. A probability density function relies on the theory that:

$$P(a \le X \le b) = \int_a^b f(x)dx \tag{7.1}$$

Where X is a random variable, a and b are constants. If the difference between a and b is reduced, then the function comes closer and closer to approximating a continuous probability distribution curve.

Longitudinal train simulations were performed using train control inputs from a fuzzy logic controller. The controller provided smooth driver actions as the train moved through different speed restrictions, track gradients and curve radii. The train configuration used in the simulations was a train consisting of 103 wagons and 4 locomotives with locomotives placed at lead and mid train positions. The wagon models within the train were based on a four-axle wagon with three-piece narrow (1067mm) gauge bogies. The wagon mass was 15 tonne (empty), the wagon length was 14,820mm and the coupler height was taken as 785mm.

The fuzzy logic control used for the simulations was designed to reduce in-train forces and energy usage. The fuzzy logic control determines appropriate throttle, dynamic brake and air brake setting from the grade, velocity and speed restrictions of the train, (Cole *et al*, 2001). The fuzzy control output is then filtered using the following rules to ensure good driving practices, (Cole, 2001):

- Traction application rates limited to 1.67%/second.
- Dynamic brake application rates limited to 5%/second.
- Interchange time between Traction and DB must be at least 10 seconds.
- All train brake applications with locomotive brakes fully bailed off.
- Speed restrictions set to QR curve speeds.
- Target running speed of 80km/h.
- Parallel control for distributed power simulation.
- Locomotive control actions, traction, dynamic brake and train brake were applied according to a rule based algorithm dependant on current speed, track topography and track speed restrictions.

Two different track sections were chosen for simulation. The first track section was on the North Coast Line in Central Queensland, Australia. The track section began at Callemondah (9,930 metres) and ended at 110,595 metres along the track. The second track section was on the Monto Line in Central Queensland. The simulations on the Monto Line began at Pilerwa at the 3,000 metre position and ended at 58,085 metres. Simulations were limited to the out-bound direction (increasing track position). A map of both track sections is shown in the Appendix II, Figure II-1 and Figure II-2. The track section at Callemondah consists of mainly straight track and moderate curves and grades while the track section at Monto has tight curves and steeper grades, as shown in Figure 7-1, Figure 7-2 and Figure 7-3. Both simulations lasted 5,500 seconds (1.52 hours). The track sections were plotted in approximately 50km lengths. The train travelling along the Monto track section travelled approximately half the distance of the train travelling along the Callemondah track section. The shorter run distance was due to the speed restrictions for the tight curves that exist on the Monto track section.

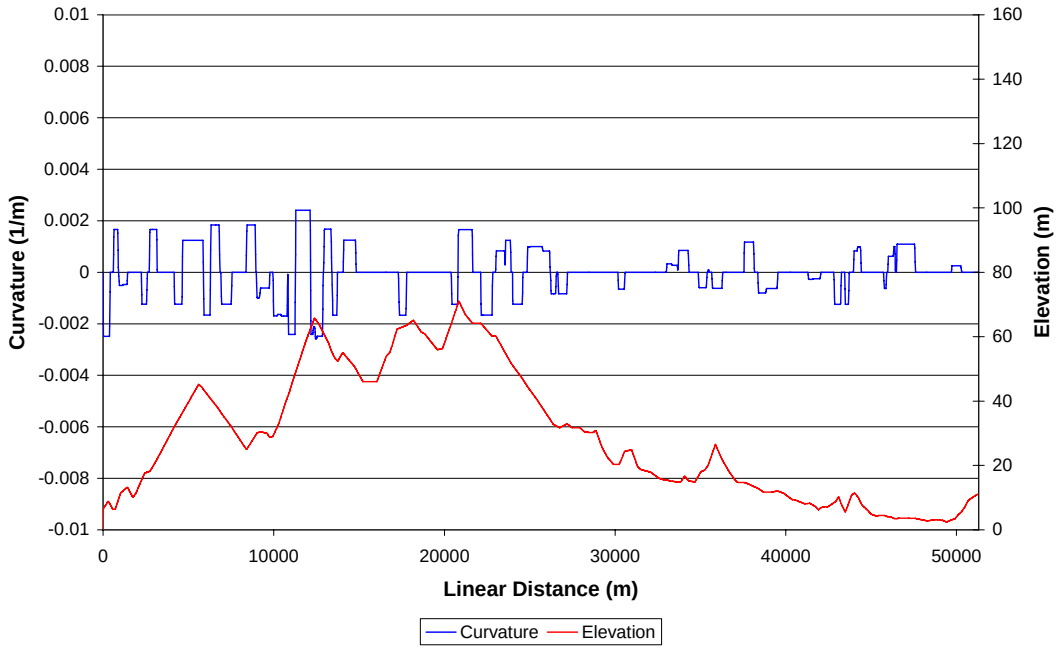

Figure 7-1: Callemondah Track Details 0 metres to 51,300 metres

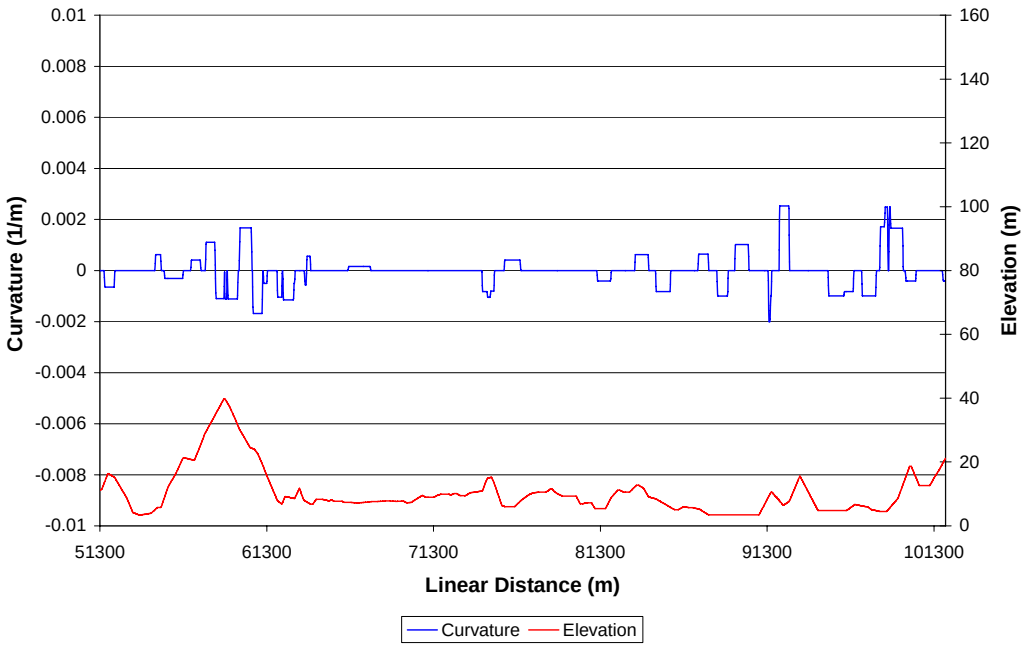

Figure 7-2: Callemondah Track Details 51,300 metres to 101,300 metres

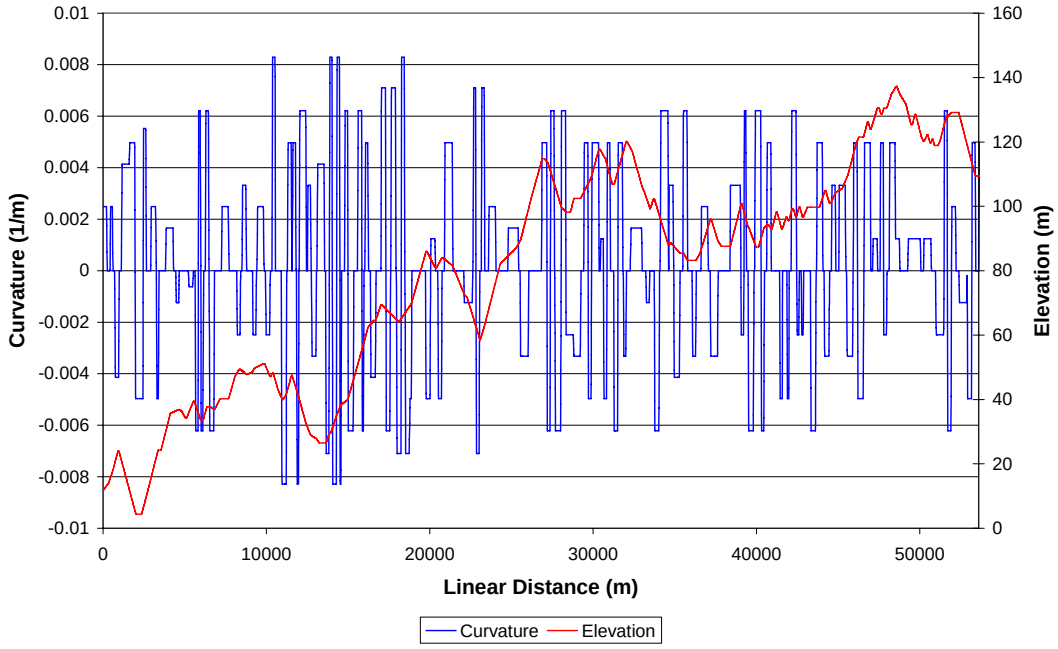

Figure 7-3: Monto Track Details

Simulations were performed for a coupler slack of 25mm, 50mm and 75mm for both track sections so that the influence of coupler slack could be investigated. This allows the effects of coupler slack, track details, track gradient and track topography to be investigated using probability density functions. It should be noted that defining the problem in this way constrains the analysis to track design, train configuration and train connection maintenance conditions.

7.3. Results

Probability density functions were constructed for coupler angles as shown in Figure 7-4. Coupler angle probability density functions were only constructed for the median coupler slack of 50mm. The maximum variation in coupler angle due to variation of coupler slack was less than 0.05 degrees. Probability density functions were constructed for longitudinal forces (Figure 7-5, Figure 7-6), impact forces (Figure 7-7, Figure 7-8) and the combination of steady forces, low frequency transients and high frequency transients (Figure 7-9, Figure 7-10) for a coupler slack of 25, 50 and 75mm on both track sections.

It was necessary to plot the data in Figure 7-4, Figure 7-5, Figure 7-6, Figure 7-7, Figure 7-8, Figure 7-9 and Figure 7-10 using a logarithmic scale so that the more extreme data that occurs less frequently on the outer regions could be viewed. Figure 7-4 shows the probability density functions of coupler angles within the train for the Monto and Callemondah track sections. The probability density functions shown in Figure 7-4 to Figure 7-10 only apply for the specific train configuration used for the

simulations performed in this thesis. Different train configurations, driver action strategies and wagon details will produce different probability density functions.

Figure 7-5 and Figure 7-6 show the probability density functions of longitudinal forces for the Callemondah and Monto track sections, respectively. Figure 7-7 and Figure 7-8 show the probability density functions of impact forces for the Callemondah and Monto track sections. Figure 7-9 and Figure 7-10 show the probability density functions of the combinations of non-impact forces consisting of steady, low frequency transients and high frequency transients for the Monto and Callemondah track sections. Steady forces, low frequency transients and high frequency transients force profiles that do not change the force state from tensile to compression or visa versa (i.e. no slack action, non-impact) do not cause bogie or wagon pitch. Bogie and wagon pitch require impact and rapid wagon accelerations as demonstrated by (McClanachan *et al*, 2000). Steady forces, low frequency transients and high frequency transients force profiles cause similar wagon dynamics to what is experienced during the study performed in Chapter 5 - Steady Forces on Curves and Curve Transitions on page 88. A more accurate definition of steady forces, low frequency transients and high frequency transient forces shown in Figure 7-9 and Figure 7-10 would be non-impact forces. Non-impact forces therefore can be defined as forces that do not meet the criteria of an impact outlined in section 3.4.2 on page 59.

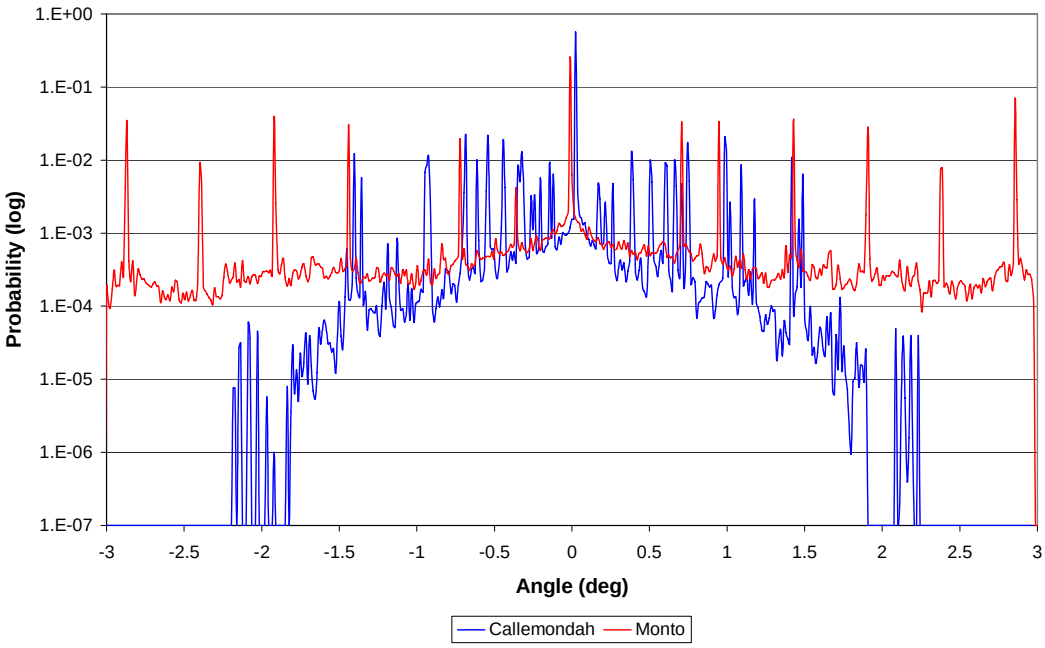

Figure 7-4: Coupler Angle Probability Distribution Curve – Callemondah and Monto

Longitudinal Forces (Steady, Transient and Impact Forces)

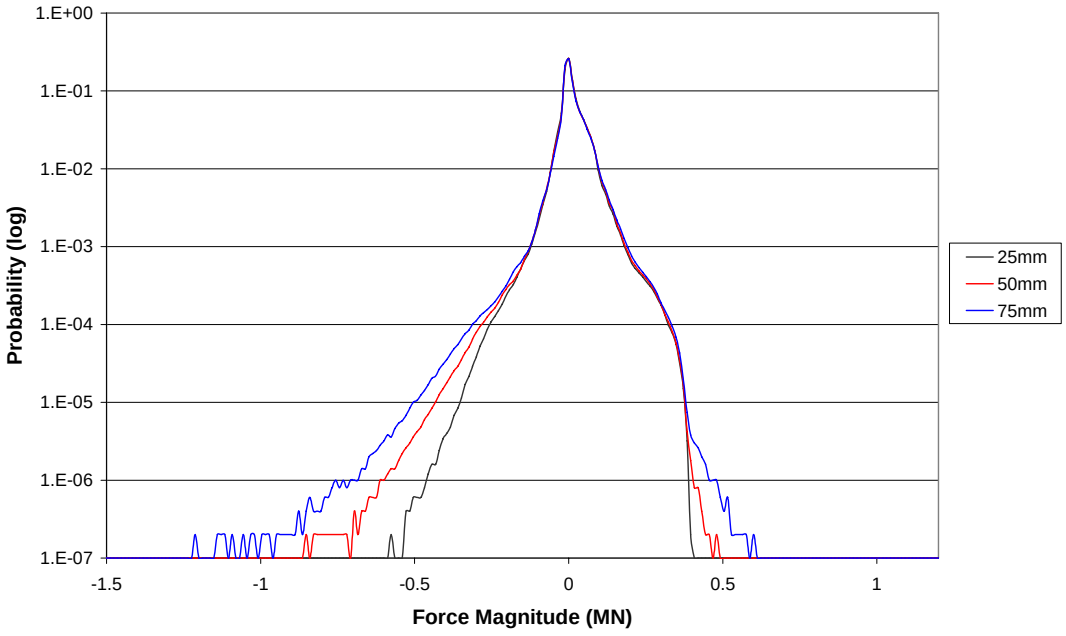

Figure 7-5: Longitudinal Force Probability Density Distribution Curve – Callemondah

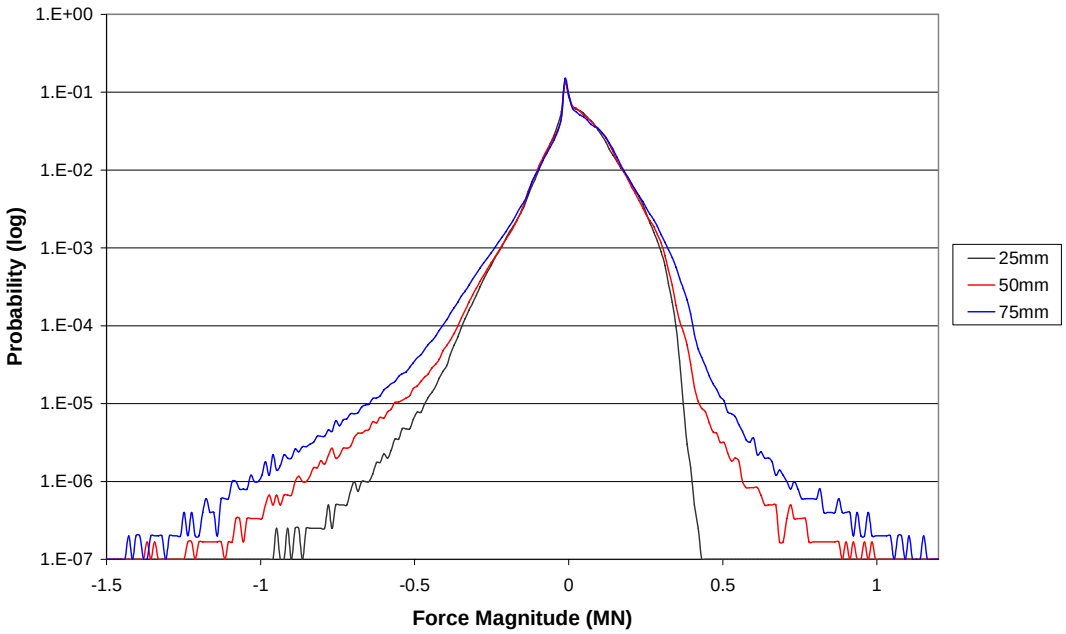

Figure 7-6: Longitudinal Force Probability Density Distribution Curve – Monto

Longitudinal Impact Forces

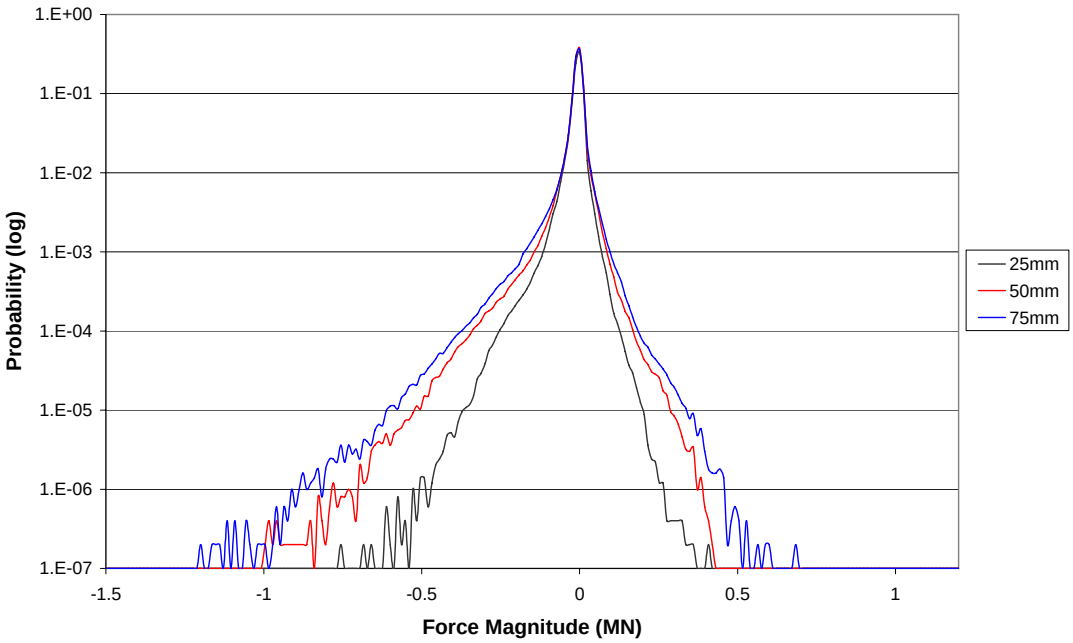

Figure 7-7: Impact Force Probability Density Distribution Curve –Callemondah

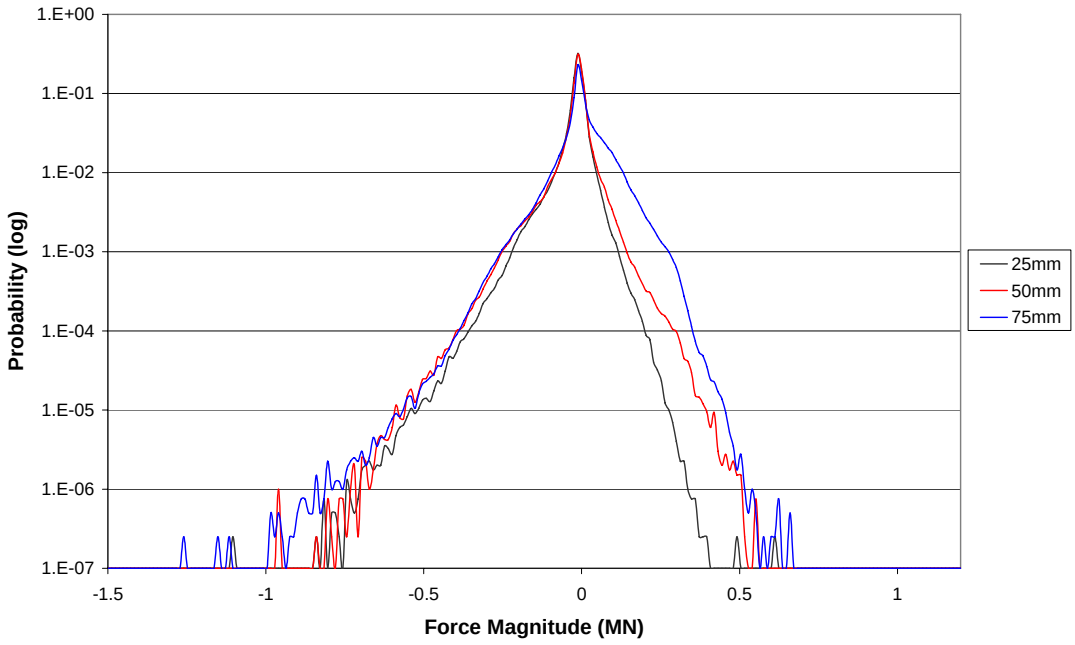

Figure 7-8: Impact Force Probability Density Distribution Curve – Monto

Longitudinal Non-impact Forces (Steady and Transient Forces)

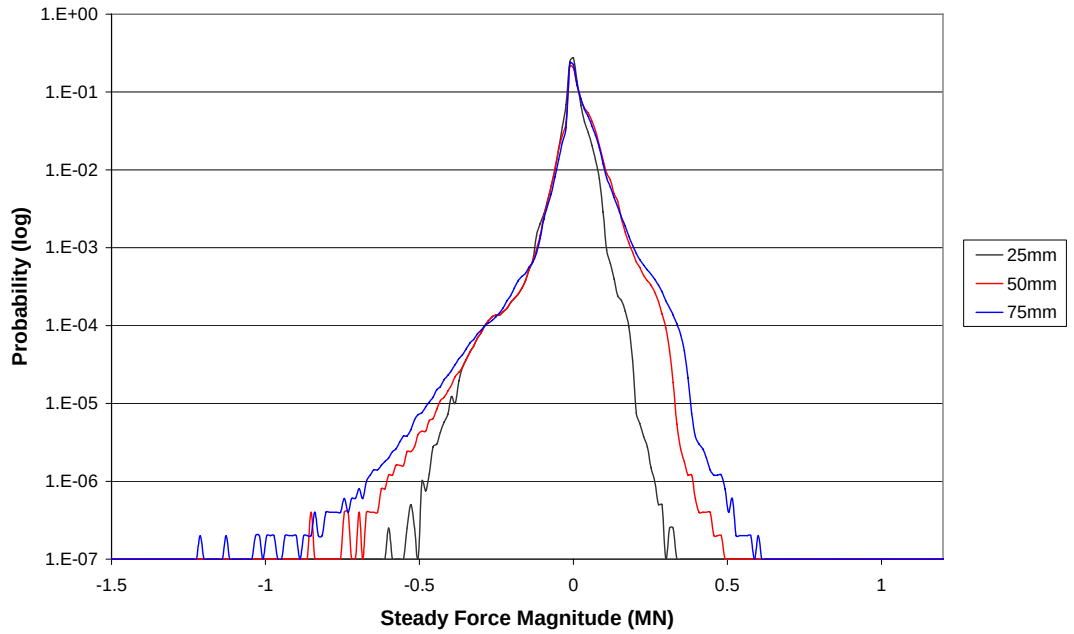

Figure 7-9: Longitudinal Non-Impact Probability Density Distribution Curve – Callemondah

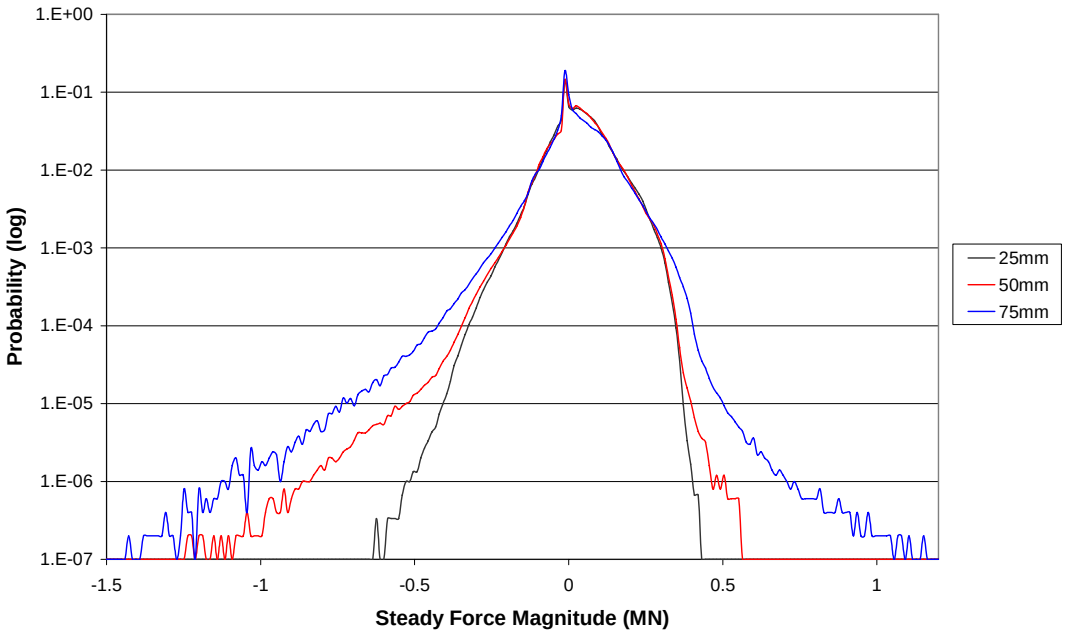

Figure 7-10: Longitudinal Non-Impact Force Probability Density Distribution Curve – Monto

7.4. Discussion

Figure 7-4 shows the probability density functions for coupler angles at the Monto and Callemondah region track sections. The coupler angling data was obtained using the coupler angling algorithm developed in Section 3.3.3 on page 45. The difference in the two track sections is illustrated by the increased probability of higher coupler angles at the Monto track section. The larger number of tight curves (125-300m radius, i.e. curvature of 0.008-0.003) on the Monto track section is shown in Figure 7-3. Conversely, there are no occurrences of coupler angles greater than approximately 2.2º (i.e. a curve of approximately 200m radius) on the North Coast Line.

A greater number of peaks can be seen in Figure 7-4 for the Monto area than the Callemondah line due to the selection of standard curve radii. Each wagon has similar dimensions and wagon properties so there is a similar coupler angle for each vehicle pair. Wider and shorter peaks would be expected if the same simulations were performed for a freight train made up of a mixture of wagons of different lengths and bogie overhang dimensions. Table 7-1 shows the coupler angle for two VAMB class wagons coupled together, so a corresponding curvature can be estimated in Figure 7-4. It is interesting to note that the peak values shown for the Callemondah area are for a coupler angle of approximately ±1.5º and ±1º which correspond to approximately 300 and 400 metre radius curves. As expected the highest probability peak is for a coupler angle of zero in Figure 7-4 for both track sections, corresponding to straight track. Although the peaks on the Callemondah track section shown in Figure 7-4 are not as definite and evenly spaced as the peaks for the Monto track section, a simular trend can be seen. This indicates that there is a greater variety of different curve radii on the Callemondah track section than the Monto track section.

Table 7-1: Approximate Coupler Angle for each Curve Radius

Curve Radius (m)	Approx Coupler Angle
Infinite	0.0000°
800	0.0533°
600	0.3900°
400	1.0000°
300	1.5000°

The trains travelling at the Monto area have an increased probability of high lateral force components being produced due to high coupler angles and an increased probability of events occurring on tight curves. This increases the probability of dangerous levels of wheel unloading and L/V ratio occurring as demonstrated by studies in Chapter 5 - Steady Forces on Curves and Curve Transitions on page 88 and Chapter 6 - Impacts on Curves and Curve Transition on page 95. Trains travelling along the Callemondah track section have a lower probability of lateral components being produced and events occurring on tight curves than on the Monto track section, as shown in Figure 7-1 to Figure 7-4.

The probabilities indicated from the probability density functions of a 1MN force or greater along the Callemondah track section are 0, 0 and 2.5E-7 for a coupler slack of 25, 50 and 75mm respectively, as shown in Figure 7-5. A 1MN force or greater was chosen as the force magnitude for comparison. When the probability is shown as zero it indicates that there were no occurrences during the simulations performed for this study. Event probabilities were determined by dividing the number of events that satisfies a given criteria by the total number of events. If longer simulations were performed and complete data was obtained, more accurate event probabilities could be calculated. The probability of a 1MN or greater longitudinal force along the Monto track section is 0, 5E-7 and 1E-6 for a coupler slack of 25, 50 and 75mm respectively, as shown in Figure 7-6. There is 4 times the probability of a 1MN or greater longitudinal force occurring along the Monto track section than the Callemondah track section for a 75mm coupler slack

Increased force magnitudes can be developed on grades due to the increased amount of tractive effort and braking needed. Forces from tractive effort and braking are passed through the train in the form of longitudinal buff (compressive) and draft (tensile) forces. As the track gradient increase so do the longitudinal forces within the train. There is a higher probability of increased force magnitudes in the Monto region than the force magnitudes in the Callemondah region, as shown in Figure 7-5 and Figure 7-6.

The probabilities indicated for a 1MN or greater non-impact force along the Callemondah track section are 0, 0 and 2.5E-7 for a coupler slack of 25, 50 and 75mm respectively, as shown in Figure 7-9. Corresponding probabilities indicated for the Monto track were 0, 3.3E-7 and 2.5E-6, as shown in Figure 7-10. There is 10 times the probability of a non-impact force with a magnitude of 1MN occurring on the Monto line than the Callemondah line for a coupler slack of 75mm. The non-impact force probability distribution curves are shown in Figure 7-9 and Figure 7-10. On the Monto track section a large percentage of the high magnitude longitudinal forces were non-impact forces. This was because the train spent a large amount of running time without changing from draft to buff or visa versa (i.e. no slack action) due to negotiating steep grades.

There is a higher probability of a vehicle experiencing positive (tensile) longitudinal forces than negative (compressive) forces in the 100kN to 400kN force region along the Monto track section in Figure 7-6. This is due to draft forces needed to increase the potential energy of the train. The majority of these forces are non-impact forces as shown in Figure 7-10. There is also a higher probability of a vehicle experiencing

positive longitudinal forces than negative forces in the 100kN to 400kN force region in the Callemondah area as shown in Figure 7-5. The increase in potential energy from starting point to ending point is less for the Callemondah region than the Monto region, as shown in Figure 7-1 and Figure 7-2. Therefore there is a lower probability of higher longitudinal forces and non-impact components in the 100kN to the 400kN region on the Callemondah section in Figure 7-5 and Figure 7-9. The probabilities of a 1MN or greater force along the Callemondah track section are 0, 0 and 2.5E-7 for a coupler slack of 25, 50 and 75mm respectively, as shown in Figure 7-7. No impacts occurred for a force magnitude of 1MN or greater along the Monto track section, as shown in Figure 7-8.

Impact forces are generated by run-ins and run-outs which are due to coupler slack, as discussed in Section 2.5 on page 24. The impact force probability density functions are shown in Figure 7-7 and Figure 7-8. The train simulated on the Monto area was under draft forces for a larger percentage of operating time than the train simulated on the Callemondah line. Conversely, trains on the Callemondah line are subjected to more parasitic slack action due to track undulations.

The results shown in the longitudinal forces (Figure 7-5, Figure 7-6) impact forces (Figure 7-7, Figure 7-8) and non-impact forces (Figure 7-9, Figure 7-10) probability density functions are conservative results due to the fuzzy driver control used to control the driver actions in CRE-LTS. The fuzzy logic driver control was designed specifically to reduce in-train forces and reduce energy usage. If actual driver actions were used it is expected that there would be an increase in the probability of larger magnitude in-train forces for both track sections.

8 DERAILMENT RISK ASSESSMENT

8.1. Introduction

Reductions in derailment risks improve the safety of train operations and reduce costs. If used properly, the risk management process can be a powerful tool that can be used to lower the derailment risks that a railway company experiences. This chapter presents a risk assessment that was performed on simulated data. The risk assessment process is covered in detail in Section 2.5 on page 24. In this chapter, risk assessment techniques were used in conjunction with simulation data and probability density functions to identify derailment risks.

8.2. Procedure

The data generated from CRE-LTS simulations in the procedure outlined in section 7.2 on page 108 was used for analysis. Computer code was written to calculate event probabilities and present the results as a table. A full list of the tables is shown in Appendix I on page 141.

Once the probability of each event was known, the likelihood of different combinations of events could be determined. It was decided that the existence of an event occurring would be based on the AAR 50ms criteria, (AAR, 1993). For example, for an event to be categorised as existent, an event must last for 50ms or more. The probabilities shown in Table 8-1 were calculated by Equation (8.1). The constants of 20, 60, 60, 24 and 365 are the number of 50ms time periods in one second, the number of seconds in a minute, the number of minutes in an hour, the

number of hours in a day and the number of days in a year respectively. This determines the probability of the number of events occurring per time frame in years.

$$P(Event) = \frac{N(Events)*100}{Ty*20*60*60*24*365*DutyCycle}$$

$$\therefore P(Event) = \frac{N(Events)}{Ty*6307200*DutyCycle} \quad (8.1)$$

Where P(Event) is the probability density (events per year) of a given event, Ty is the time in years, duty cycle is the time the train is operational as a percentage and N(event) is the number of events.

Table 8-1: Likelihood Probabilities

Definition	Likelihood	Probability Density
Almost certain	Will occur once a year or more frequently	1.585E-7
Likely	Will occur once every three years	5.285E-8
Moderate	Will occur once every ten years	1.585E-8
Unlikely	Will occur once every 30 years	5.285E-9
Rare	Will occur once every 100 years	1.585E-9
Very rare	Will occur once every 300 years	5.285E-10
Almost Incredible	Will occur once every 1000 years	1.585E-10

The probability of each event was calculated from the data produced in the simulations. A complete presentation of these calculations are given in the Appendix III, (Table III-1, Table III-2, Table III-3, Table III-4, Table III-6 and Table III-8 on

pages 148 to 152). Once the probability density of each event occurring was determined it is necessary to see if each event produces wheel unloading levels of 90% or more. If a given event produced 90% wheel unloading or more the derailment event probability was added to the likelihood table. Below 90% wheel unloading is an acceptance standard for road worthiness, (AAR, 1993). If the levels of wheel unloading are below 90% the likelihood was taken as zero. The levels of wheel unloading from Chapter 5 - Steady Forces on Curves and Curve Transitions on page 88 and Chapter 6 - Impacts on Curves and Curve Transitions on page 95 determined if a given event would cause derailment.

The L/V ratio was not used for analysis because the L/V ratio did not exceed the derailment criteria in Chapter 5 on page 88 and Chapter 6 on page 95. This was calculated by using Nadal's criteria which is covered in Section 2.3.2 on page 12. The acceptance standard calculated for the Queensland Rail wheel profile and rail profile was a L/V ratio of 1.22. It was assumed that a L/V ratio below this would not cause derailment.

The likelihood tables are shown in Table III-5, Table III-7 and Table III-9 on pages to 152. Due to the cost of the infrastructure and rollingstock assets often involved in a derailment, the consequences of a derailment are typically high. The consequences refer to how severe the outcome would be if the event occurred. The area of focus for derailments in this thesis has been derailment on curves and curve transitions. Derailments on curves at normal running speed are typically of high consequence involving multiple wagons. Due to the nature of derailment on curves it is assumed that all derailments would have major consequence in Table 8-2. Since the

likelihood and consequences of an event are known Table 8-3 can be used to determine the level of risk of an event. The definitions for each level of risk are listed in Table 8-4. These tables are also included in Section 2.5.3 on page 27.

Table 8-2: Consequences Definitions, (Standards Association of Australia, 1999)

Consequences	Definition
Catastrophic	The consequences would threaten the survival of not only the programme, but also the Organisation, possibly causing major problems for clients, the administration of the programme or for a large part of the Public Sector. Revenue loss greater than x% of total revenue being managed would have extreme consequences for the Organisation both financially and politically.
Major	The consequences would threaten the survival or continued effective function of the programme, or require the intervention of top level management or by the Elected Representatives. Revenue loss greater than y% of total revenue being managed would have very high consequences for the Organisation both financially and politically.
Moderate	The consequences would not threaten the programme, but would mean that the administration of the programme could be subject to significant review or changed ways of operating. Revenue loss greater than z% of total revenue being managed would have medium consequences for the Organisation both financially and politically.
Minor	The consequences would threaten the efficiency or effectiveness of some aspects of the programme, but would be dealt with internally. A loss of revenue below the tolerance level of 5% (Audit materiality) applied to clients would be of low consequence.
Insignificant	The consequences are dealt with by routine operations. A loss of revenue below the programme tolerance level of w% (less than Audit materiality) applied to clients would be of negligible consequence.

Table 8-3: Risk Assessment Table, (Standards Association of Australia, 1999)

Likelihood	Consequences				
	Insignificant	**Minor**	**Moderate**	**Major**	**Catastrophic**
Almost Certain	High Risk	High Risk	Extreme Risk	Extreme Risk	Extreme Risk
Likely	Moderate Risk	High Risk	High Risk	Extreme Risk	Extreme Risk
Moderate	Low Risk	Moderate Risk	High Risk	Extreme Risk	Extreme Risk
Unlikely	Low Risk	Low Risk	Moderate Risk	High Risk	Extreme Risk
Rare	Low Risk	Low Risk	Moderate Risk	High Risk	High Risk
Very rare	Trivial Risk	Trivial Risk	Low Risk	Moderate Risk	High Risk
Almost incredible	Trivial Risk	Trivial Risk	Low Risk	Moderate Risk	Moderate Risk

Table 8-4: Risk Definitions, (Standards Association of Australia, 1999)

Level of Risk	Impact and Action
Extreme Risk	Almost certain to threaten the survival of the program, its administration and the Organisation either financially or politically. Must be managed by senior management with a detailed plan
High Risk	Likely to cause some damage, disruption or breach of controls. Detailed research and management planning required at senior level
Moderate Risk	Unlikely to be a threat to the efficiency and effectiveness of the program. Manage by specific monitoring or response procedures
Low Risk	Unlikely to threaten some aspects of the program. Manage by routine procedures
Trivial Risk	Risks have negligible impact on the program. Unlikely to need specific application of resources

The following assumptions were made:

- Track sections are perfect. E.g. no track irregularities, smooth transitions and regular curves.
- Similar levels of wheel unloading and L/V ratio are experienced on the Callemondah and Monto track sections as the studies performed in Chapter 5 - Steady Forces on Curves and Curve Transitions and Chapter 6 - Impacts on Curves and Curve Transitions.
- All curves have a 40m curve transition.
- Any driver action can occur at any position along the track.

These assumptions were made to simplify the problem and because a train simulator which gives level of wheel unloading for each vehicle at each and every track position still does not exist. If a fully detailed train and vehicle simulator existed more accurate calculations could be made for probability densities taking into account driver actions for each track section. For example, the probability density of a 1MN force or greater on a 300m radius curve that causes derailment can be determined by scanning the data and finding the number of occurrences that fits the criteria.

8.3. Results

A derailment risk assessment was performed using the simulations in Chapter 5 - Steady Forces on Curves and Curve Transitions and Chapter 6 - Impacts on Curves and Curve Transitions and the probability density data from Chapter 7 - Probability Density Functions. Table 8-5 shows the derailment risks for non-impact forces from Section 5.3 on page 90 while Table 8-6 shows the derailment risks for impact forces from Section 6.3 on page 100. The events that resulted in a probability of zero were not listed in the results in Table 8-5 and Table 8-6. All probability calculation tables are included in Appendix III on page 141 in Table III-1 to Table III-13.

Table 8-5: Derailment Risk Assessment on Non-Impact Forces

Track Section	Coupler Slack	Curve Radius	Force Magnitude (MN)	Probability Density	Likelihood	Consequences	Risk
Monto	75mm	200	X<-0.40	6.975E-05	Almost Certain	Major	Extreme Risk
Monto	75mm	600	X<-0.60	1.6722E-05	Almost Certain	Major	Extreme Risk
Monto	75mm	400	X<-0.60	1.3695E-05	Almost Certain	Major	Extreme Risk
Monto	50mm	200	X<-0.60	1.0664E-06	Almost Certain	Major	Extreme Risk
Monto	75mm	200	X<-0.60	5.404E-06	Almost Certain	Major	Extreme Risk
Monto	75mm	600	X<-0.80	4.510E-06	Almost Certain	Major	Extreme Risk
Monto	75mm	400	X<-0.80	3.695E-06	Almost Certain	Major	Extreme Risk
Monto	75mm	200	X<-0.80	1.4574E-06	Almost Certain	Major	Extreme Risk
Monto	75mm	800	X<-1.00	1.3166E-06	Almost Certain	Major	Extreme Risk
Monto	75mm	600	X<-1.00	1.2101E-06	Almost Certain	Major	Extreme Risk
Monto	75mm	400	X<-1.00	9.912E-07	Almost Certain	Major	Extreme Risk
Monto	75mm	200	X<-1.00	3.910E-07	Almost Certain	Major	Extreme Risk
Monto	50mm	600	X<-0.60	3.300E-07	Almost Certain	Major	Extreme Risk
Monto	50mm	400	X<-0.60	2.703E-07	Almost Certain	Major	Extreme Risk
Monto	50mm	200	X<-0.60	2.703E-07	Almost Certain	Major	Extreme Risk
Callemondah	75mm	600	X<-0.60	6.111E-08	Likely	Major	Extreme Risk
Callemondah	75mm	400	X<-0.60	5.3466E-9	Likely	Major	Extreme Risk

Table 8-6: Derailment Risk Assessment on Impact Forces

Track Section	Coupler Slack	Curve Radius	Force Magnitude (MN)	Probability Density	Likelihood	Consequences	Risk
Monto	75mm	600	X>0.50	1.008E-08	Unlikely	Major	High Risk
Monto	75mm	600	X<-0.50	1.008E-08	Unlikely	Major	High Risk
Monto	75mm	400	X>0.50	8.259E-09	Unlikely	Major	High Risk
Monto	75mm	400	X<-0.50	8.259E-09	Unlikely	Major	High Risk
Monto	75mm	200	X>0.50	3.258E-09	Rare	Major	High Risk
Monto	75mm	200	X<-0.50	3.258E-09	Rare	Major	High Risk
Monto	75mm	600	X>0.62	2.428E-09	Rare	Major	High Risk
Monto	75mm	600	X<-0.62	2.428E-09	Rare	Major	High Risk
Monto	75mm	400	X>0.62	1.988E-09	Rare	Major	High Risk
Monto	75mm	400	X<-0.62	1.988E-09	Rare	Major	High Risk
Monto	75mm	200	X>0.62	7.844E-10	Very Rare	Major	Moderate Risk
Monto	75mm	200	X<-0.62	7.844E-10	Very Rare	Major	Moderate Risk
Callemondah	75mm	400	X<-0.50	4.375E-12	Almost Incredible	Major	Moderate Risk
Callemondah	75mm	400	X<0.50	4.375E-12	Almost Incredible	Major	Moderate Risk

8.4. Discussion

It should be noted that only compressive (negative) non-impact forces caused derailment, as shown in Table 8-5. This is because the study for steady forces in Chapter 5 was performed with 2/3 equilibrium cant. In Chapter 5, derailment only occurred for compressive forces for the force magnitude range specified. The study performed in Chapter 6 on impact forces had equilibrium cant. Both positive (tensile) and negative (compressive) forces are shown in Table 8-6.

The results demonstrate increased levels of risk associated with higher coupler slacks and increased levels of risk associated with the Monto track section. Almost all the identified risks were on the Monto track section, as shown in Table 8-5 and Table 8-6. The few identified risks on the Callemondah track section had a lower probability of occurring, as shown in Table 8-5 and Table 8-6. The results were as expected as the track topography and curvature of the two track sections are very different and were chosen to illustrate the different risk levels, see figures of track elevation and curvature (Figure 7-1, Figure 7-2 and Figure 7-3). The Monto track section consists of older infrastructure with steep grades and a high number of tight curves which increases the derailment risk for that track section. The Callemondah section consists of state-of-the-art modern track, optimised for heavy haul unit train operations. It should be noted that both tracks were assessed using simulations of the same state-of-the-art unit train.

By identifying high risk scenarios, it also allows the identification of strategies that can be field implemented to manage these risks. From the studies performed in this thesis, coupler slack is shown to have significant effects on the level of risk. No events were identified for a coupler slack of 25mm on either track. Lower coupler slack reduces the probability of higher magnitude forces occurring. This was true for all force probability studies performed in this thesis, as discussed in Chapter 7 - Probability Density Functions and is shown in Figure 7-5 to Figure 7-10 on page 114 to 117. The majority of events that were identified were for a coupler slack of 75mm. The derailment risk events that were identified with a coupler slack of 50mm were all on the Monto track section. Increased coupler slack increases the level of risk that is associated with a given event. No derailment risks were identified on the

Callemondah line with a coupler slack of 25mm or 50mm. No derailment risks were identified for a coupler slack of 25mm on both track sections.

From the studies performed in this thesis, reductions in derailment risk can be achieved on any track section by reducing coupler slack. This is supported by the results that the majority of the identified derailment events were for a coupler slack of 75mm, as shown in Table 8-5 and Table 8-6. It also implies that the risks are due to train slack action. It will be remembered that the train control was controlled by a optimised fuzzy logic driver system. The fuzzy logic system gives very smooth changes to control settings. It is probable that actual train control data would give worse slack action. Reductions in derailment risk can also be achieved by reducing the levels of curvature and gradient that a train experiences during simulations. Bad combinations exist where there are large in-train forces due to steep grade; combined with large coupler angles due to sharp curves and increased slack action due to track undulations. When comparing probability densities in Table 8-5 and Table 8-6, there is a higher chance of a high magnitude non-impact forces occurring than high magnitude impact forces. This is due the combination of the fuzzy logic driver system and the definition of an impact force (Section 3.4.2 on page 59) in this thesis.

The risk analysis in this section makes a number of assumptions. The study assumes that any force can occur at any position along the track which is similar to saying that driver controls have no connection to track geometry and that driver actions can occur any time at any place. This is not true as typically driver actions occur due to the driver responding to changes in curvature, grade and speed. An improved analysis could be achieved by a comprehensive train-wagon simulator. Simulating

packages for freight trains are still not available and were beyond the scope of this thesis to develop.

The steady components of non-impact forces are dependent on track topography and geometry. Changes in steady forces can be experienced as the potential energy of the train is changed. This is due to the tractive forces being transferred through the train. Impact forces are generated due to changes of grade and driver actions. Impact forces are typically generated when a wagon pair experiences slack action. An impact force can be developed due to changes in grade; some examples are a train travelling over a hill or through a dip. Impact forces can also be developed at any position on the track due to driver actions. An example of this occurring could be if a driver sees a cow on the track or a vehicle on a level crossing.

It should be noted that the two track sections used in the simulations are extremely different. The Monto track section is outdated for the type of train simulated, as it consists of wooden sleepers, tight curves and steep grades. When the Monto track section was built it was not designed to have long trains with powerful locomotives capable of hauling thousands of tonnes of coal operating on it. Increasing the train tonnage increases in-train forces. The results demonstrate that when a modern train operates on outdated track it increases the derailment risks.

When using Table 8-3 to determine the level of risk, the severity of the consequences means that high levels of risk are identified even if the likelihood is extremely low. If the consequences are classified as major, the lowest level of likelihood will still give an output of moderate risk, as shown in Table 8-3.

9 CONCLUSION

This thesis has demonstrated a method of quantifying derailment risks from the interaction of longitudinal train dynamics, lateral wagon dynamics and vertical wagon dynamics. Track irregularities were excluded to ensure that the study was focused on track design, train configuration and train connection maintenance.

Increased levels of risk were associated with higher coupler slack. Coupler slack increases the magnitude of both impact and non-impact forces. For a coupler slack of 25mm no derailment risks were identified, 50mm coupler slack derailment risks were only identified on the Monto track and the majority of derailment risks were identified for a 75mm coupler slack. Coupler slack maintenance was therefore identified as a key to reducing derailment risk.

Increased levels of risk were associated with sharp curves. The longitudinal impact force scenarios simulated showed that a reduction in maximum levels of wheel unloading of 40% can be achieved by increasing the curve radius from 400m to 600m. Further reductions in wheel unloading and L/V ratio can be achieved by further increasing the curve radii. If the minimum radius curve is increased to 800m, the lateral component at the coupler pin reduces to 0.087% of the longitudinal force. The benefits of progressively removing sharp curves from infrastructure can therefore be quantified in terms of reductions in derailment risk.

The maximum levels of wheel unloading experienced by a vehicle entering a constant radius curve is at a position close to the exit of the first transition. When a vehicle enters a curve, it must accelerate its lateral velocity to that of the constant radius curve. When the vehicle reaches the constant radius section of track there is a sudden change of acceleration, which causes body roll.

Probability density functions are useful in providing a visual comparison of simulation data. Probability density functions were also useful in identifying differences in coupler angles, longitudinal impact and non-impact forces for different track sections. The Monto track section was identified as having increased probabilities of higher coupler angles and higher magnitude longitudinal forces. The analysis of coupler angles can also be used to indicate the effect of long to short wagon combinations in mixed freight trains.

The derailment risk assessment technique outlined in this thesis categorises the levels of risk and allows the identification of operating scenarios with increased levels of risk. The studies performed in this thesis demonstrated that there is a relationship between coupler slack, minimum radius curve, track topography and gradient with the level of derailment risk experienced by a train.

The results obtained are limited in accuracy by the simulation tools available. Risk analyses of train-track system designs using simulated data require integrated train-wagon simulation. The fuzzy controller used to simulate driver actions was optimised to reduce in-train forces and will give an underestimate of in-train forces. Risks associated with non-impact forces are overestimated because the analysis

assumes any train force can be associated with any track site. Risks associated with impact forces are indicative as train control disturbances can occur at any track site. The levels of risk calculated in this thesis are therefore not exact, due to the restrictions and assumptions of simulation packages implicit in the method. The method is still useful for comparing the derailment risk of different train-track systems simulations.

A trade off exists between infrastructure and rollingstock maintenance. Derailment risk can be reduced by either or both increases in track curvature or reductions in coupler slack. It is conceivable that in some instances old infrastructure with sharp curves could be tolerated if coupler slack was reduced. Problems begin occurring when maintenance and design standards are not matched.

9.1. Suggestions for Further Work

Further studies would give an improved understanding of what influences derailment risk levels. In this thesis, a method of categorising events into different levels of risk has been shown. An investigation could be performed on a large range of maintenance, capital works and irregularity issues to determine how they affect derailment risks. Some other examples of studies which can be performed are different track sections, wheel profiles, driver actions, track cants, track gradients, train configurations, etc. Larger amounts of data would give more general event probabilities.

The level of risk associated with in-train vehicle positioning was not covered. This is because the focus was on developing a method of quantifying derailment risks and doing some fundamental research into steady and impact forces on curves and curve transitions. The method of quantifying derailment risks outlined in this thesis can be used to assess the level of risk associated with in-train vehicle positioning from simulated data.

Significant improvements to probability calculations could be achieved by a fully detailed train simulator which includes detailed wagon dynamics. This would match typical driver control actions with track topography and speed restrictions.

10 REFERENCES

Standards Association of Australia 1999, *Australian Standard: Risk Management*, (AS/NZS 4360-1999) Standards Australia, Strathfield.

AAR 1993, "Chapter 11", in *Manual of Standards and Recommended Practices*, AAR, Washington.

AEA-Technology 2002, *Vampire User Manual*, 2002, Derby.

Ahmadian, M. and Yang, S. 1998, "Effect of System Nonlinearities on Locomotive Bogie Hunting Stability", *Vehicle System Dynamics,* vol. 29.

Ahmed, M. E. and Bayoumi, M. N. 1983, "Simulation and Control of a Long Freight Train", in *Simulation in Engineering Sciences*, eds Burger, J. and Jarny, Y., Elsevier Sciences Publishers, Holland.

Anderson, K. and Francis, G. 2002, "Level Crossing Risk Management", *CORE 2002,* vol. 1, (ed.) 2002, C., RTSA, Wollongong.

ATSB 2003, Rail Safety in Australia, vol. 2003, no. 7 April, Available: http://www.atsb.gov.au/rail/rail_occurrences.cfm.

Canavos, G. 1984, *Applied Probability and Statistical Methods*, Little, Brown & Company (Canada) Limited, Canada.

Cole, C. 1996, "Dynamic Response of Coal Wagons During Normal Operation", *WCRR,* Centre for Railway Engineering, Colorado Springs, p. 9.

Cole, C. 1998a, "How Accurate Is Your Train Simulator? A Discussion of Simulation and Validation Techniques", *CORE 1998,* CORE 1998.

Cole, C. 1998b, "Improvements to Wagon Connection Modelling for Longitudinal Train Simulation", *Core 98*, pp. 187-194.

Cole, C. 1999, Longitudinal Train Dynamics. PhD Thesis, Central Queensland University.

Cole, C. 2001, "Heavy Haul Coal Train Dynamics Simulation Comparisons of the Coallink and Central Queensland Systems", *International Heavy Haul Conference*, vol. 7, pp. 217-230.

Cole, C. 2004, 50ms Criteria Approximation, (ed.) Wagner, S., Rockhampton.

Cole, C., McClanachan, M., Scown, B., Falwasser, N., Ashman, T. and Baguley, L. 2001, *Final Research Report-Stage a-Train Dynamics Management Project*, Centre for Railway Engineering, Central Queensland University, Rockhampton.

Devore, J. 1991, *Probability and Statistics for Engineering and the Sciences*, 3rd edn, R. R. Donnelley & Sons Company, California.

DiBartolomeis, M. J., Alexeeff, G. V., Fan, A. M. and Jackson, R. J. 1994, "Regulatory Approach to Assessing Health Risks of Toxic Chemical Releases Following Transportational Accidents", *Journal of Hazardous Materials*, vol. 39, pp. 193-210.

Duncan, I. B. and Webb, P. A. 1989, "The Longitudinal Behaviour of Heavy Haul Trains Using Remote Locomotives", *The Fourth International Heavy Haul Railway Conference 1989,* vol. 1, Brisbane, pp. 587-590.

El-Sibaie, M. 1990, "Coupler Angling under in-Train Loads: Modelling and Validation", *AREA/ASME Joint Railroad Conference,* Florida.

El-Sibaie, M. 1993, "Recent Advancements in Buff and Draft Testing Techniques", *Technical Papers - IEEE/ASME Joint Railroad Conference,* Publ by IEEE, Pittsburgh, PA.

Elkins, J. and Wu, H. 1999, *Investigation of Wheel Flange Climb Derailment*, Association of American Railroads, Washington.

Elkins, J. and Wu, H. 2000a, Angle of Attack and Distance-Based Criteria for Flange Climb Derailment In *Vehicle System Dynamics*
16th LAVSD Symposium 'The Dynamics of Vehicles on Roads and on Tracks',Aug 30-Sep 3 1999, vol. 33, Swets en Zeitlinger B.V.,Lisse,Netherlands, Pretoria,S Afr, pp. 293-305.

Elkins, J. and Wu, H. 2000b, "New Criteria for Flange Climb Derailment", *Proceedings of the IEEE/ASME Joint Railroad Conference*
The 2000 Spring ASME/IEEE Joint Rail Conference,Apr 4-Apr 6 2000, pp. 1-7.

Esveld, C. 1989, *Modern Railway Engineering*, Graphics Department of Thyssen Stahl AG, Duisburg.

Fukazawa, K. 1992, "Coupler Forces of 1000t Class Two-Axle Freight Trains", *RTRI,* vol. 33, RTRI.

Garg, V. and Dukkipati, R. 1984, *Dynamics of Railway Vehicle Systems*, Academic Press, New York.

Gilchrist, A. O. 1998, "The Long Road to Solution of the Railway Hunting and Curving Problems", *Journal of Rail and Rapid Transit*, vol. 212, no. F3**,** pp. 219-236.

Guangxiong, C. and Xincan, J. 2000, "A New Method for Evaluation of Wheel Climb Derailment", *Proceedings of the IEEE/ASME Joint Railroad Conference*
The 2000 Spring ASME/IEEE Joint Rail Conference,Apr 4-Apr 6 2000, pp. 9-18.

Guangxiong, C., Xincan, J. and Weiqian, B. 2000, Influence of Periodic Irregularities on Wheel Climb Derailment Safety of a Freight Car Running on a Transition Curve In *Proceedings of the IEEE/ASME Joint Railroad Conference*

The 2000 Spring ASME/IEEE Joint Rail Conference,Apr 4-Apr 6 2000, Institute of Electrical and Electronics Engineers Inc.,Piscataway,NJ,USA, Newark,NJ,USA, pp. 19-29.

Hay, W. 1982, *Railroad Engineering*, Second edn, John Wiley & Sons, New York.

Iwnicki, S. 2000, *An Intelligent Track Monitoring System*, Manchester Metropolitan University, Manchester.

Iwnicki, S. and Stow, J. 1999, "Assessing Railways Vehicles Derailment Potential Using Neural Networks", *International Conference on Fault-Free Infrastructure*.

Mayville, R. and Rancatore, R. 1999, "Investigation and Simulation of Lateral Buckling in Trains", *ASME/IEEE Joint Railroad Conference,* vol. 16, Texas.

McClanachan, M. and Cole, C. 1997, *Multi Wagon Test Program Report*, Centre for Railway Engineering, CQU, Rockhampton, Australia.

McClanachan, M., Cole, C., Roach, D. and Scown, B. 2000, "Investigation of the Effect of Bogie and Wagon Pitch Associated with Longitudinal Train Dynamics", *Vehicle System Dynamics*, vol. 33, no. SUPPL.**,** pp. 374-385.

McClanachan, M., Dhanasekar, M. and Skerman, D. 2002, "Monitoring the Dynamics of Freight Wagons", *CORE 2002,* Woolongong, pp. 213-222.

McClanachan, M. and Roach, D. 2000, "*Vertical Wheel Force Characteristics of a Coal Wagon Determined by Sideframe Strain Measurement*", *Conference on Railway Engineering,* (ed.) Roach, D., RTSA, Adelaide.

Meriam, J. L. and Kraige, L. G. 1993, *Dynamics*, Third edn, John Wiley & Sons, Inc, New York.

Miyamoto, M. 1996, "Mechanism of Derailment Phenomena of Railway Vehicles", *RTRI,* Fundamental Research Dept.

Miyamoto, M. and Fujimoto, H. 1990, "A Study of Lateral Dynamic Behaviour of Rail Vehicle in Curves by Measurement and Computer Simulation", *RTRI,* vol. 31, (ed.) RTRI, Fundamental Research Dept.

Muttram, R. I. 2002, "Railway Safety's Safety Risk Model", *Journal of Rail and Rapid Transit*, vol. 216, no. F2**,** pp. 71-79.

Nadal, M. J. 1960, *Theorie De La Stabilite Des Locomotives*, Annls Mines.

Novosyolov, A. 2002, *Risk Theory*, Institute of Computational Modelling, Krasnoyarsk, Russia.

Parena, D., Kuka, N., Masmoudi, W. and Kik, W. 2000, "Derailment Simulation, Parametric Study", *Vehicle System Dynamics*, vol. 33, no. SUPPL.**,** pp. 155-167.

Parkinson, H. 1999, *An Intelligent Track Monitoring System*, Kennedy and Donkin Ltd, Manchester.

Schupp, G. and Jaschinski, A. 1996, *Investigation of Running Behaviour and Derailment Criteria for Freight Cars by Dynamic Simulation*, Boston.

Sun, Y. Q. and Dhanasekar, M. 2000, "A Dynamic Model for the Vertical Interaction of the Rail Track and Wagon System", *International Journal of Solids and Structures*, vol. 39.

Takai, H., Muramatsu, H., Uchida, M. and Ishida, H. 2002, "Derailment Safety Evaluation by Analytic Equations", *RTRI,* (ed.) RTRI, RTRI.

Wagner, S. and Cole, C. 2003a, "Modelling Train-Wagon Interaction on Curves", *Proceedings of the 18th International Association of Vehicle System Dynamics Symposium,* Kanagawa Institute of Technology, Atsugi, Kanagawa, Japan.

Wagner, S. and Cole, C. 2003b, "Rollingstock Wheel Unloading Due to Coupler Impacts on Curve Transitions", *Central Region Engineering Conference,* (ed.) Wolfs, P., Central Queensland University, Rockhampton, Australia.

Waters, A., Fletcher, S., Karrasch, K., Sanderson, P., Humphreys, M., Horberry, T., Mabott, N., Simpson, S., Wilson, P. and McGraw, M. 2002, "Proceedings Qr Spad Conference", *QR SPAD Conference,* (ed.) Brand, K., Queensland Rail, Brisbane.

Wolf, G. 1998, *Best Practices for Derailment Prevention*, Rail Sciences.

Wu, P. and Zeng, J. 1998, Dynamic Analysis for Derailment Safety of Railway Vehicles In *Proceedings of the 1998 International Symposium on Safety Science and Technology, ISSST,Sep 1998*, Sci Press, Beijing,China, pp. 292-299.

Xiang, S. 1993, "On Low Dynamic Action in Heavy Haul Train", *International Heavy Haul Conference,* Beijing.

I APPENDIX

Table I-1: VAMPIRE Model Masses

Mass No	Mass Type	Mass Kg	Inertia X	Inertia Y	Inertia Z	Pos X	Pos Y	Pos Z
1	Body Mass Empty	8.1000	10.5760	79.3070	80.0170	0.000	0.000	1.000
1	Body Mass Full	66.1100	85.576	647.182	652.982	0.000	0.000	1.700
2	Bolster Mass F	0.4650	0.0175	0.0097	0.1760	5.181	0.000	0.453
3	Bolster Mass R	0.4650	0.0175	0.0097	0.1760	-5.181	0.000	0.453
4	Sideframe Mass FR	0.4475	0.1000	0.1156	0.1156	5.181	0.800	0.475
5	Sideframe Mass FL	0.4475	0.1000	0.1156	0.1156	5.181	-0.800	0.475
6	Sideframe Mass RR	0.4475	0.1000	0.1156	0.1156	-5.181	0.800	0.475
7	Sideframe Mass RL	0.4475	0.1000	0.1156	0.1156	-5.181	-0.800	0.475
8	Wheel sets 1	1.1200	0.0420		0.0420	6.019	0.000	0.425
9	Wheel sets 2	1.1200	0.0420		0.0420	4.434	0.000	0.425
10	Wheel sets 3	1.1200	0.0420		0.0420	-6.019	0.000	0.425
11	Wheel sets 4	1.1200	0.0420		0.0420	-4.434	0.000	0.425
12	Coupler Pin Mass F	0.0050	0.0010	0.0010	0.0010	6.397	0.000	0.785
13	Coupler Pin Mass R	0.0050	0.0010	0.0010	0.0010	-6.397	0.000	0.785

Table I-2: Spring Connections

No.	Connection	Stiffness	Pos X	Pos Y	Pos Z
1	Centre plate to Bolster Lateral	440.000	5.181	0.000	0.608
2	Centre plate to Bolster Lateral	440.000	-5.181	0.000	0.608
3	Centre plate to Bolster Longitudinal	440.000	5.181	0.000	0.608
4	Centre plate to Bolster Longitudinal	440.000	-5.181	0.000	0.608
5	Side Frame to Axle Box Lateral	40.000	6.019	0.800	0.425
6	Side Frame to Axle Box Lateral	40.000	6.019	-0.800	0.425
7	Side Frame to Axle Box Lateral	40.000	4.344	0.800	0.425
8	Side Frame to Axle Box Lateral	40.000	4.344	-0.800	0.425
9	Side Frame to Axle Box Lateral	40.000	-4.344	0.800	0.425
10	Side Frame to Axle Box Lateral	40.000	-4.344	-0.800	0.425
11	Side Frame to Axle Box Lateral	40.000	-6.019	0.800	0.425
12	Side Frame to Axle Box Lateral	40.000	-6.019	-0.800	0.425
13	Side Frame to Axle Box Longitudinal	440.000	6.019	0.800	0.425
14	Side Frame to Axle Box Longitudinal	440.000	6.019	-0.800	0.425
15	Side Frame to Axle Box Longitudinal	440.000	4.344	0.800	0.425
16	Side Frame to Axle Box Longitudinal	440.000	4.344	-0.800	0.425
17	Side Frame to Axle Box Longitudinal	440.000	-4.344	0.800	0.425
18	Side Frame to Axle Box Longitudinal	440.000	-4.344	-0.800	0.425
19	Side Frame to Axle Box Longitudinal	440.000	-6.019	0.800	0.425
20	Side Frame to Axle Box Longitudinal	440.000	-6.019	-0.800	0.425
21	Side Frame to Bolster Longitudinal	44.000	5.181	0.800	0.475
22	Side Frame to Bolster Longitudinal	44.000	5.181	-0.800	0.475
23	Side Frame to Bolster Longitudinal	44.000	-5.181	0.800	0.475
24	Side Frame to Bolster Longitudinal	44.000	-5.181	-0.800	0.475
25	Dummy Spring to Ground	0.010	0.000	0.000	1.700
26	Wagon Body to Coupler Pin	440.000	6.397	0.000	0.785
27	Wagon Body to Coupler Pin	440.000	6.397	0.000	0.785
28	Wagon Body to Coupler Pin	440.000	6.397	0.000	0.785
29	Wagon Body to Coupler Pin	440.000	6.397	0.000	0.785
30	Wagon Body to Coupler Pin	440.000	6.397	0.000	0.785
31	Wagon Body to Coupler Pin	440.000	6.397	0.000	0.785

Table I-3: Non-Linear Elements (Bumpstops)

No.	Connection	Pos X	Pos Y	Pos Z	Refer to
1	Centre Plate Vertical Front Right	5.180	0.15	0.608	Figure 3-6
2	Centre Plate Vertical Front Left	5.180	-0.15	0.608	Figure 3-6
3	Centre Plate Vertical Front Bottom	5.030	0	0.608	Figure 3-6
4	Centre Plate Vertical Front Top	5.330	0	0.608	Figure 3-6
5	Centre Plate Vertical Rear Right	-5.180	0.15	0.608	Figure 3-6
6	Centre Plate Vertical Rear Left	-5.180	-0.15	0.608	Figure 3-6
7	Centre Plate Vertical Rear Bottom	-5.030	0	0.608	Figure 3-6
8	Centre Plate Vertical Rear Top	-5.330	0	0.608	Figure 3-6
9	Vertical side bearing to Wagon Body FR	5.180	0.47	0.683	Figure 3-7
10	Vertical side bearing to Wagon Body FL	5.180	-0.47	0.683	Figure 3-7
11	Vertical side bearing to Wagon Body RR	-5.180	0.47	0.683	Figure 3-7
12	Vertical side bearing to Wagon Body RL	-5.180	-0.47	0.683	Figure 3-7
13	Side frame to axle box Vertical FR Ws1	6.018	0.74	0.425	Figure 3-8
14	Side frame to axle box Vertical FR Ws1	6.018	0.86	0.425	Figure 3-8
15	Side frame to axle box Vertical FL Ws1	6.018	-0.74	0.425	Figure 3-8
16	Side frame to axle box Vertical FL Ws1	6.018	-0.86	0.425	Figure 3-8
17	Side frame to axle box Vertical FR Ws2	4.342	0.74	0.425	Figure 3-8
18	Side frame to axle box Vertical FR Ws2	4.342	0.86	0.425	Figure 3-8
19	Side frame to axle box Vertical FL Ws2	4.342	-0.74	0.425	Figure 3-8
20	Side frame to axle box Vertical FL Ws2	4.342	-0.86	0.425	Figure 3-8
21	Side frame to axle box Vertical RR Ws3	-4.342	0.74	0.425	Figure 3-8
22	Side frame to axle box Vertical RR Ws3	-4.342	0.86	0.425	Figure 3-8
23	Side frame to axle box Vertical RL Ws3	-4.342	-0.74	0.425	Figure 3-8
24	Side frame to axle box Vertical RL Ws3	-4.342	-0.86	0.425	Figure 3-8
25	Side frame to axle box Vertical RR Ws4	-6.018	0.74	0.425	Figure 3-8
26	Side frame to axle box Vertical RR Ws4	-6.018	0.86	0.425	Figure 3-8
27	Side frame to axle box Vertical RL Ws4	-6.018	-0.74	0.425	Figure 3-8
28	Side frame to axle box Vertical RL Ws4	-6.018	-0.86	0.425	Figure 3-8
29	Lateral bolster to side frame FR	5.180	0.7	0.475	
30	Lateral bolster to side frame FL	5.180	-0.7	0.475	
31	Lateral bolster to side frame RR	-5.180	0.7	0.475	
32	Lateral bolster to side frame RL	-5.180	-0.7	0.475	

Table I-4: Spring Nest Bolster to Sideframe

Connection	X (MN/m)	Y (MN/m)	Z (MN/m)	Rotat X	Rotat Y	Rotat Z
Bolster to Side frame	4	4	6	0.4	0.4	2

Table I-5: Friction Elements

No.	Applied to	Friction Load E,F	Line	Rotational	Pos X	Pos Y	Pos Z
1	Bumpstop 1 Vertical	9.93, 81.06	0.26	0.26	5.181	0.15	0.608
2	Bumpstop 2 Vertical	9.93, 81.07	0.26	0.26	5.181	-0.15	0.608
3	Bumpstop 3 Vertical	9.93, 81.08	0.26	0.26	5.331	0	0.608
4	Bumpstop 4 Vertical	9.93, 81.09	0.26	0.26	5.031	0	0.608
5	Bumpstop 5 Vertical	9.93, 81.10	0.26	0.26	-5.181	0.15	0.608
6	Bumpstop 6 Vertical	9.93, 81.11	0.26	0.26	-5.181	-0.15	0.608
7	Bumpstop 7 Vertical	9.93, 81.12	0.26	0.26	-5.331	0	0.608
8	Bumpstop 8 Vertical	9.93, 81.13	0.26	0.26	-5.031	0	0.608
9	Spring Nest 1 Vertical	5.535, 41.15	0.2	0.13	5.077	0.77	0.475
10	Spring Nest 1 Vertical	5.535, 41.15	0.2	0.13	5.077	0.83	0.475
11	Spring Nest 1 Vertical	5.535, 41.15	0.2	0.13	5.285	0.77	0.475
12	Spring Nest 1 Vertical	5.535, 41.15	0.2	0.13	5.285	0.83	0.475
13	Spring Nest 2 Vertical	5.535, 41.15	0.2	0.13	5.077	-0.77	0.475
14	Spring Nest 2 Vertical	5.535, 41.15	0.2	0.13	5.077	-0.83	0.475
15	Spring Nest 2 Vertical	5.535, 41.15	0.2	0.13	5.285	-0.77	0.475
16	Spring Nest 2 Vertical	5.535, 41.15	0.2	0.13	5.285	-0.83	0.475
17	Spring Nest 3 Vertical	5.535, 41.15	0.2	0.13	-5.077	0.77	0.475
18	Spring Nest 3 Vertical	5.535, 41.15	0.2	0.13	-5.077	0.83	0.475
19	Spring Nest 3 Vertical	5.535, 41.15	0.2	0.13	-5.285	0.77	0.475
20	Spring Nest 3 Vertical	5.535, 41.15	0.2	0.13	-5.285	0.83	0.475
21	Spring Nest 4 Vertical	5.535, 41.15	0.2	0.13	-5.077	-0.77	0.475
22	Spring Nest 4 Vertical	5.535, 41.15	0.2	0.13	-5.077	-0.83	0.475
23	Spring Nest 4 Vertical	5.535, 41.15	0.2	0.13	-5.285	-0.77	0.475
24	Spring Nest 4 Vertical	5.535, 41.15	0.2	0.13	-5.285	-0.83	0.475
25	Spring Nest 1 Lateral	5.535, 41.16	0.2	0.13	5.077	0.8	0.465
26	Spring Nest 1 Lateral	5.535, 41.17	0.2	0.13	5.077	0.8	0.475
27	Spring Nest 2 Lateral	5.535, 41.18	0.2	0.13	5.285	0.8	0.465
28	Spring Nest 2 Lateral	5.535, 41.19	0.2	0.13	5.285	0.8	0.475
29	Spring Nest 3 Lateral	5.535, 41.20	0.2	0.13	5.077	0.8	0.465
30	Spring Nest 3 Lateral	5.535, 41.21	0.2	0.13	5.077	0.8	0.475
31	Spring Nest 4 Lateral	5.535, 41.22	0.2	0.13	5.285	0.8	0.465
32	Spring Nest 4 Lateral	5.535, 41.23	0.2	0.13	5.285	0.8	0.475
33	S.F to A.Box Long	6.635, 42.2	0.5	0.5	6.019	0.74	0.425
34	S.F to A.Box Long	6.635, 42.2	0.5	0.5	6.019	0.806	0.425
35	S.F to A.Box Long	6.635, 42.2	0.5	0.5	6.019	-0.74	0.425
36	S.F to A.Box Long	6.635, 42.2	0.5	0.5	6.019	-0.806	0.425
37	S.F to A.Box Long	6.635, 42.2	0.5	0.5	4.343	0.74	0.425
38	S.F to A.Box Long	6.635, 42.2	0.5	0.5	4.343	0.806	0.425
39	S.F to A.Box Long	6.635, 42.2	0.5	0.5	4.343	-0.74	0.425
40	S.F to A.Box Long	6.635, 42.2	0.5	0.5	4.343	-0.806	0.425
41	S.F to A.Box Long	6.635, 42.2	0.5	0.5	-4.343	0.74	0.425
42	S.F to A.Box Long	6.635, 42.2	0.5	0.5	-4.343	0.806	0.425
43	S.F to A.Box Long	6.635, 42.2	0.5	0.5	-4.343	-0.74	0.425
44	S.F to A.Box Long	6.635, 42.2	0.5	0.5	-4.343	-0.806	0.425
45	S.F to A.Box Long	6.635, 42.2	0.5	0.5	-6.019	0.74	0.425
46	S.F to A.Box Long	6.635, 42.2	0.5	0.5	-6.019	0.806	0.425
47	S.F to A.Box Long	6.635, 42.2	0.5	0.5	-6.019	-0.74	0.425
48	S.F to A.Box Long	6.635, 42.2	0.5	0.5	-6.019	-0.806	0.425

Table I-6: Damping Components

No.	Connection	Damping	Pos X	Pos Y	Pos Z
1	Side frame to axle box Lateral FR W1	0.33	6.018	0.74	0.425
2	Side frame to axle box Lateral FL W1	0.33	6.018	-0.74	0.425
3	Side frame to axle box Lateral FR W2	0.33	4.342	0.74	0.425
4	Side frame to axle box Lateral FL W2	0.33	4.342	-0.74	0.425
5	Side frame to axle box Lateral RR W3	0.33	-4.342	0.74	0.425
6	Side frame to axle box Lateral RL W3	0.33	-4.342	-0.74	0.425
7	Side frame to axle box Lateral RR W4	0.33	-6.018	0.74	0.425
8	Side frame to axle box Lateral RL W4	0.33	-6.018	-0.74	0.425

II APPENDIX

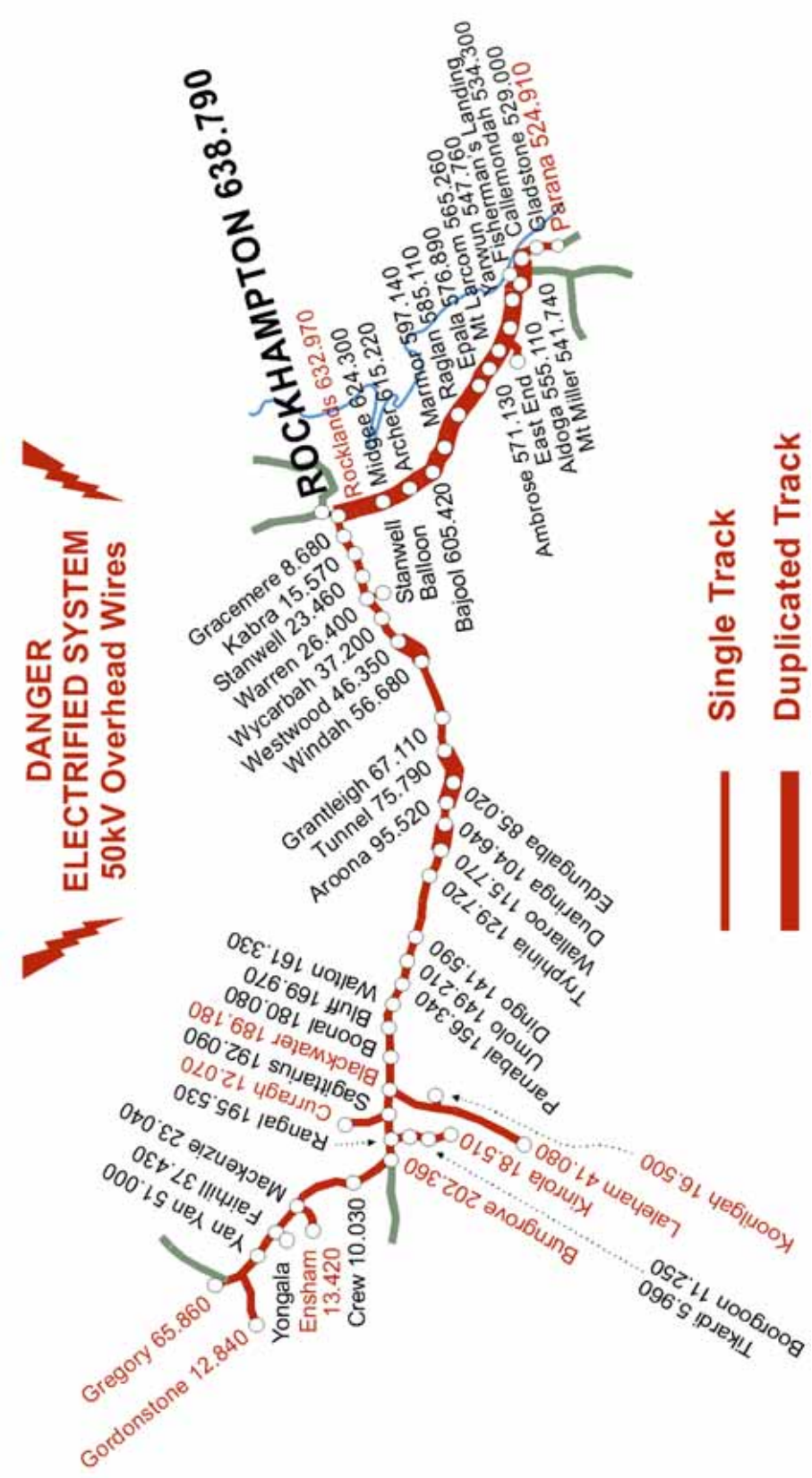

Figure II-1: Blackwater Line Track Kilometridge

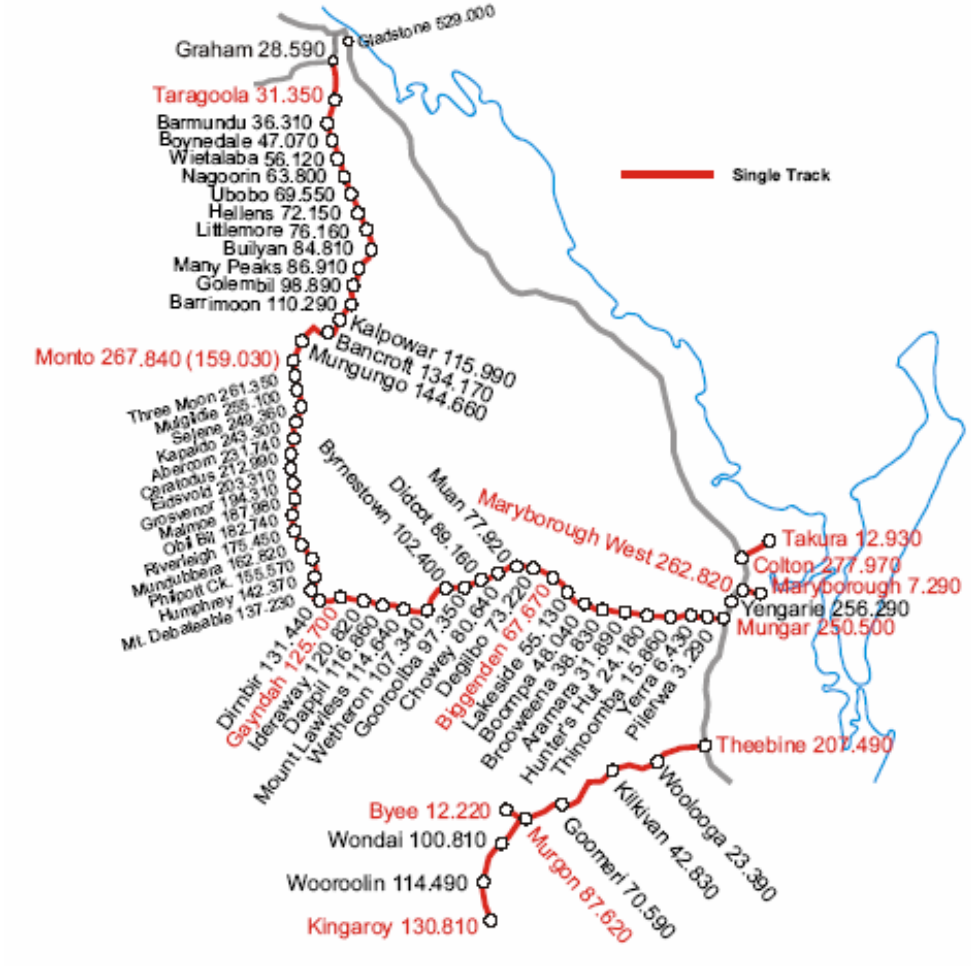

Figure II-2: Monto Line Track Kilometridge

III APPENDIX

Tables with only zeros are not included in this Appendix.

Table III-1: Callemondah 25mm Coupler Slack Probability Table

	Curve Radius									
Force Magnitude (MN)	**-1000**	**-800**	**-600**	**-400**	**-200**	**200**	**400**	**600**	**800**	**1000**
<-1.00	0.00	0	0	0	0	0	0	0	0	0
<-0.80	0.00	0	0	0	0	0	0	0	0	0
<-0.60	0.00	0	0	0	0	0	0	0	0	0
<-0.40	2.00E-07	2.27E-08	1.27E-08	9.04E-09	2.58E-10	0	0	1.52E-09	1.13E-08	1.63E-08
<0.00	6.41E-01	7.28E-02	4.07E-02	2.90E-02	8.26E-04	0	0	4.88E-03	3.63E-02	5.21E-02
>0.00	2.19E-01	2.48E-02	1.39E-02	9.88E-03	2.82E-04	0	0	1.67E-03	1.24E-02	1.78E-02
>0.40	8.40E-06	9.55E-07	5.33E-07	3.80E-07	1.08E-08	0	0	6.40E-08	4.76E-07	6.83E-07
>0.60	0	0	0	0	0	0	0	0	0	0
>0.80	0	0	0	0	0	0	0	0	0	0
>1.00	0	0	0	0	0	0	0	0	0	0
>1.20	0	0	0	0	0	0	0	0	0	0

Table III-2: Monto 25mm Coupler Slack Probability Table

	Curve Radius									
Force Magnitude (MN)	**-1000**	**-800**	**-600**	**-400**	**-200**	**200**	**400**	**600**	**800**	**1000**
<-1.00	0	0	0	0	0	0	0	0	0	0
<-0.80	0	0	0	0	0	0	0	0	0	0
<-0.60	0	0	0	0	0	0	0	0	0	0
<-0.40	8.696 E-07	7.913 E-07	7.732 E-07	6.324 E-07	2.685 E-07	2.647 E-07	7.191 E-07	8.770 E-07	1.004 E-06	1.128 E-06
<0.00	1.790 E-01	1.629 E-01	1.592 E-01	1.302 E-01	5.527 E-02	5.449 E-02	1.480 E-01	1.805 E-01	2.067 E-01	2.323 E-01
>0.00	7.599 E-02	6.915 E-02	6.757 E-02	5.526 E-02	2.346 E-02	2.313 E-02	6.284 E-02	7.664 E-02	8.773 E-02	9.861 E-02
>0.40	1.015 E-05	9.232 E-06	9.021 E-06	7.378 E-06	3.132 E-06	3.088 E-06	8.390 E-06	1.023 E-05	1.171 E-05	1.317 E-05
>0.60	2.899 E-07	2.638 E-07	2.577 E-07	2.108 E-07	8.949 E-08	8.824 E-08	2.397 E-07	2.923 E-07	3.347 E-07	3.762 E-07
>0.80	0	0	0	0	0	0	0	0	0	0
>1.00	0	0	0	0	0	0	0	0	0	0
>1.20	0	0	0	0	0	0	0	0	0	0

Table III-3: Callemondah 50mm Coupler Slack Event Probability Table

	Curve Radius									
Force Magnitude (MN)	**-1000**	**-800**	**-600**	**-400**	**-200**	**200**	**400**	**600**	**800**	**1000**
<-1.00	0	0	0	0	0	0	0	0	0	0
<-0.80	0	0	0	0	0	0	0	0	0	0
<-0.60	0	0	0	0	0	0	0	0	0	0
<-0.40	5.684 E-07	3.175 E-07	2.260 E-07	6.447 E-09	0	0	3.811 E-08	2.833 E-07	4.068 E-07	6.375 E-07
<0.00	7.240 E-02	4.044 E-02	2.879 E-02	8.212 E-04	0	0	4.854 E-03	3.608 E-02	5.182 E-02	8.120 E-02
>0.00	2.278 E-02	1.272 E-02	9.057 E-03	2.584 E-04	0	0	1.527 E-03	1.135 E-02	1.630 E-02	2.555 E-02
>0.40	6.025 E-06	3.366 E-06	2.396 E-06	6.834 E-08	0	0	4.040 E-07	3.002 E-06	4.312 E-06	6.757 E-06
>0.60	3.865 E-07	2.159 E-07	1.537 E-07	4.384 E-09	0	0	2.591 E-08	1.926 E-07	2.766 E-07	4.335 E-07
>0.80	6.821 E-08	3.810 E-08	2.712 E-08	7.736 E-10	0	0	4.573 E-09	3.399 E-08	4.882 E-08	7.650 E-08
>1.00	2.274 E-08	1.270 E-08	9.040 E-09	2.579 E-10	0	0	1.524 E-09	1.133 E-08	1.627 E-08	2.550 E-08
>1.20	0	0	0	0	0	0	0	0	0	0

Table III-4: Monto 50mm Coupler Slack Event Probability Table

	Curve Radius									
Force (MN)	**-1000**	**-800**	**-600**	**-400**	**-200**	**200**	**400**	**600**	**800**	**1000**
<-1.00	0	0	0	0	0	0	0	0	0	0
<-0.80	0	0	0	0	0	0	0	0	0	0
<-0.60	1.739 E-07	1.583 E-07	1.546 E-07	1.265 E-07	5.370 E-08	5.294 E-08	1.438 E-07	1.754 E-07	2.008 E-07	2.257 E-07
<-0.40	8.812 E-06	8.019 E-06	7.835 E-06	6.408 E-06	2.721 E-06	2.683 E-06	7.287 E-06	8.887 E-06	1.017 E-05	1.144 E-05
<0.00	1.835 E-01	1.670 E-01	1.631 E-01	1.334 E-01	5.664 E-02	5.585 E-02	1.517 E-01	1.850 E-01	2.118 E-01	2.381 E-01
>0.00	6.790 E-02	6.179 E-02	6.037 E-02	4.938 E-02	2.096 E-02	2.067 E-02	5.615 E-02	6.848 E-02	7.839 E-02	8.811 E-02
>0.40	7.925 E-05	7.212 E-05	7.047 E-05	5.763 E-05	2.447 E-05	2.412 E-05	6.554 E-05	7.992 E-05	9.150 E-05	1.028 E-04
>0.60	1.826 E-05	1.662 E-05	1.624 E-05	1.328 E-05	5.638 E-06	5.559 E-06	1.510 E-05	1.842 E-05	2.108 E-05	2.370 E-05
>0.80	4.058 E-06	3.693 E-06	3.608 E-06	2.951 E-06	1.253 E-06	1.235 E-06	3.356 E-06	4.093 E-06	4.685 E-06	5.266 E-06
>1.00	9.275 E-07	8.441 E-07	8.248 E-07	6.746 E-07	2.864 E-07	2.824 E-07	7.671 E-07	9.355 E-07	1.071 E-06	1.204 E-06
>1.20	2.899 E-07	2.638 E-07	2.577 E-07	2.108 E-07	8.949 E-08	8.824 E-08	2.397 E-07	2.923 E-07	3.347 E-07	3.762 E-07

Table III-5: Monto 50mm Coupler Slack Event Likelihood

	Curve Radius									
Force (MN)	**-1000**	**-800**	**-600**	**-400**	**-200**	**200**	**400**	**600**	**800**	**1000**
<-1.00	0	0	0	0	0	0	0	0	0	0
<-0.80	0	0	0	0	0	0	0	0	0	0
<-0.60	0	0	1.546E-07	1.265E-07	5.370 E-08	5.294 E-08	1.438E-07	1.754E-07	0	0
<-0.40	0	0	0	0	2.721 E-06	2.683 E-06	0	0	0	0
<0.00	0	0	0	0	0	0	0	0	0	0
>0.00	0	0	0	0	0	0	0	0	0	0
>0.40	0	0	0	0	0	0	0	0	0	0
>0.60	0	0	0	0	0	0	0	0	0	0
>0.80	0	0	0	0	0	0	0	0	0	0
>1.00	0	0	0	0	0	0	0	0	0	0
>1.20	0	0	0	0	0	0	0	0	0	0

Table III-6: Callemondah 75mm Coupler Slack Event Probability Table

	Curve Radius									
Force (MN)	**-1000**	**-800**	**-600**	**-400**	**-200**	**200**	**400**	**600**	**800**	**1000**
<-1.00	0	0	0	0	0	0	0	0	0	0
<-0.80	0	0	0	0	0	0	0	0	0	0
<-0.60	6.821E-08	3.810E-08	2.712E-08	7.736E-10	0	0	4.573E-09	3.399 E-08	4.882 E-08	7.650E-08
<-0.40	1.523E-06	8.509E-07	6.057E-07	1.728E-08	0	0	1.021E-07	7.591 E-07	1.090 E-06	1.708E-06
<0.00	7.157E-02	3.998E-02	2.846E-02	8.118E-04	0	0	4.799E-03	3.567 E-02	5.123 E-02	8.027E-02
>0.00	2.333E-02	1.303E-02	9.278E-03	2.647E-04	0	0	1.564E-03	1.163 E-02	1.670 E-02	2.617E-02
>0.40	2.269E-05	1.267E-05	9.022E-06	2.574E-07	0	0	1.521E-06	1.131 E-05	1.624 E-05	2.545E-05
>0.60	2.978E-06	1.664E-06	1.184E-06	3.378E-08	0	0	1.997E-07	1.484 E-06	2.132 E-06	3.340E-06
>0.80	7.275E-07	4.064E-07	2.893E-07	8.252E-09	0	0	4.878E-08	3.626 E-07	5.207 E-07	8.160E-07
>1.00	2.728E-07	1.524E-07	1.085E-07	3.095E-09	0	0	1.829E-08	1.360 E-07	1.953 E-07	3.060E-07
>1.20	9.094E-08	5.080E-08	3.616E-08	1.032E-09	0	0	6.097E-09	4.532 E-08	6.509 E-08	1.020E-07

Table III-7: Callemondah 75mm Coupler Slack Event Likelihood

	Curve Radius									
Force Magnitude (MN)	**-1000**	**-800**	**-600**	**-400**	**-200**	**200**	**400**	**600**	**800**	**1000**
<-1.00	0	0	0	0	0	0	0	0	0	0
<-0.80	0	0	0	0	0	0	0	0	0	0
<-0.60	0	0	2.712E-08	7.736E-10	0	0	4.573E-09	3.399E-08	0	0
<-0.40	0	0	0	0	0	0	0	0	0	0
<0.00	0	0	0	0	0	0	0	0	0	0
>0.00	0	0	0	0	0	0	0	0	0	0
>0.40	0	0	0	0	0	0	0	0	0	0
>0.60	0	0	0	0	0	0	0	0	0	0
>0.80	0	0	0	0	0	0	0	0	0	0
>1.00	0	0	0	0	0	0	0	0	0	0
>1.20	0	0	0	0	0	0	0	0	0	0

Table III-8: Monto 75mm Coupler Slack Event Probability Table

	Curve Radius									
Force (MN)	**-1000**	**-800**	**-600**	**-400**	**-200**	**200**	**400**	**600**	**800**	**1000**
<-1.00	6.377E-07	5.803E-07	5.670E-07	4.638E-07	1.969 E-07	1.941 E-07	5.274 E-07	6.431 E-07	7.363 E-07	8.275 E-07
<-0.80	2.377E-06	2.163E-06	2.113E-06	1.729E-06	7.338 E-07	7.236 E-07	1.966 E-06	2.397 E-06	2.744 E-06	3.084 E-06
<-0.60	8.812E-06	8.019E-06	7.835E-06	6.408E-06	2.721 E-06	2.683 E-06	7.287 E-06	8.887 E-06	1.017 E-05	1.144 E-05
<-0.40	1.137E-04	1.035E-04	1.011E-04	8.272E-05	3.512 E-05	3.463 E-05	9.406 E-05	1.147 E-04	1.313 E-04	1.476 E-04
<0.00	1.829E-01	1.665E-01	1.627E-01	1.330E-01	5.648 E-02	5.569 E-02	1.513 E-01	1.845 E-01	2.112 E-01	2.374 E-01
>0.00	6.470E-02	5.888E-02	5.753E-02	4.705E-02	1.998 E-02	1.970 E-02	5.351 E-02	6.525 E-02	7.470 E-02	8.396 E-02
>0.40	1.587E-04	1.444E-04	1.411E-04	1.154E-04	4.901 E-05	4.832 E-05	1.313 E-04	1.601 E-04	1.833 E-04	2.060 E-04
>0.60	3.183E-05	2.896E-05	2.830E-05	2.315E-05	9.826 E-06	9.689 E-06	2.632 E-05	3.210 E-05	3.675 E-05	4.130 E-05
>0.80	1.020E-05	9.285E-06	9.073E-06	7.420E-06	3.150 E-06	3.106 E-06	8.438 E-06	1.029 E-05	1.178 E-05	1.324 E-05
>1.00	3.304E-06	3.007E-06	2.938E-06	2.403E-06	1.020 E-06	1.006 E-06	2.733 E-06	3.333 E-06	3.815 E-06	4.288 E-06
>1.20	1.217E-06	1.108E-06	1.083E-06	8.854E-07	3.759 E-07	3.706 E-07	1.007 E-06	1.228 E-06	1.406 E-06	1.580 E-06

Table III-9: Monto 75mm Coupler Slack Event Likelihood

	Curve Radius									
Force Magnitude (MN)	**-1000**	**-800**	**-600**	**-400**	**-200**	**200**	**400**	**600**	**800**	**1000**
<-1.00	0	5.803 E-07	5.670 E-07	4.638E-07	1.969 E-07	1.941 E-07	5.274 E-07	6.431 E-07	7.363 E-07	0
<-0.80	0	0	2.113 E-06	1.729E-06	7.338 E-07	7.236 E-07	1.966 E-06	2.397 E-06	0	0
<-0.60	0	0	7.835 E-06	6.408E-06	2.721 E-06	2.683 E-06	7.287 E-06	8.887 E-06	0	0
<-0.40	0	0	0	0	3.512 E-05	3.463 E-05	0	0	0	0
<0.00	0	0	0	0	0	0	0	0	0	0
>0.00	0	0	0	0	0	0	0	0	0	0
>0.40	0	0	0	0	0	0	0	0	0	0
>0.60	0	0	0	0	0	0	0	0	0	0
>0.80	0	0	0	0	0	0	0	0	0	0
>1.00	0	0	0	0	0	0	0	0	0	0
>1.20	0	0	0	0	0	0	0	0	0	0

Table III-10: Event Probabilities of Impacts on the Monto Line 75mm Coupler Slack

	Curve Radius					
Force Magnitude (MN)	**-600**	**-400**	**-200**	**200**	**400**	**600**
X>1.42	0	0	0	0	0	0
X>0.62	2.761E-08	2.258E-08	9.587E-09	9.45231E-09	2.56784E-08	3.131E-08
X>0.5	1.147E-07	9.380E-08	3.982E-08	3.92634E-08	1.06664E-07	1.301E-07
X<-0.5	1.147E-07	9.380E-08	3.982E-08	3.92634E-08	1.06664E-07	1.301E-07
X<-0.62	2.761E-08	2.258E-08	9.587E-09	9.45231E-09	2.56784E-08	3.131E-08
X<-1.42	0	0	0	0	0	0

Table III-11: Event Likelihood of Impacts on the Monto Line 75mm Coupler Slack

	Curve Radius					
Force Magnitude (MN)	**-600**	**-400**	**-200**	**200**	**400**	**600**
X>1.42	0	0	0	0	0	0
X>0.62	0	2.258E-08	9.587E-09	9.45231E-09	2.56784E-08	0
X>0.5	0	9.380E-08	3.982E-08	3.92634E-08	1.06664E-07	0
X<-0.5	0	9.380E-08	3.982E-08	3.92634E-08	1.06664E-07	0
X<-0.62	0	2.258E-08	9.587E-09	9.45231E-09	2.56784E-08	0
X<-1.42	0	0	0	0	0	0

Table III-12: Event Probabilities of Impacts on the Callemondah Line 75mm Coupler Slack

	Curve Radius					
Force Magnitude (MN)	**-600**	**-400**	**-200**	**200**	**400**	**600**
X>1.42	0	0	0	0	0	0
X>0.62	0	0	0	0	0	0
X>0.5	1.862E-09	5.312E-11	0	0	3.140E-10	2.334E-09
X<-0.5	1.862E-09	5.312E-11	0	0	3.140E-10	2.334E-09
X<-0.62	0	0	0	0	0	0
X<-1.42	0	0	0	0	0	0

Table III-13: Event Likelihood of Impacts on the Callemondah Line 75mm Coupler Slack

	Curve Radius					
Force Magnitude (MN)	**-600**	**-400**	**-200**	**200**	**400**	**600**
X>1.42	0	0	0	0	0	0
X>0.62	0	0	0	0	0	0
X>0.5	0	5.312E-11	0	0	3.140E-10	0
X<-0.5	0	5.312E-11	0	0	3.140E-10	0
X<-0.62	0	0	0	0	0	0
X<-1.42	0	0	0	0	0	0